TG
400
.D47
1989

DEVELOP AND FABRICATE A PROTOTYPE NONDESTRUCTIVE

TION AND MONITORING SYSTEM FOR STRUCTURAL CABLES

RANDS OF SUSPENSION BRIDGES, VOLUME I

Research, Development,
and Technology

Turner-Fairbank Highway
Research Center
6300 Georgetown Pike
McLean, Virginia 22101-2296

Report No.
FHWA/RD-89/158

U.S. Department
of Transportation

**Federal Highway
Administration**

Final Report
May 1989

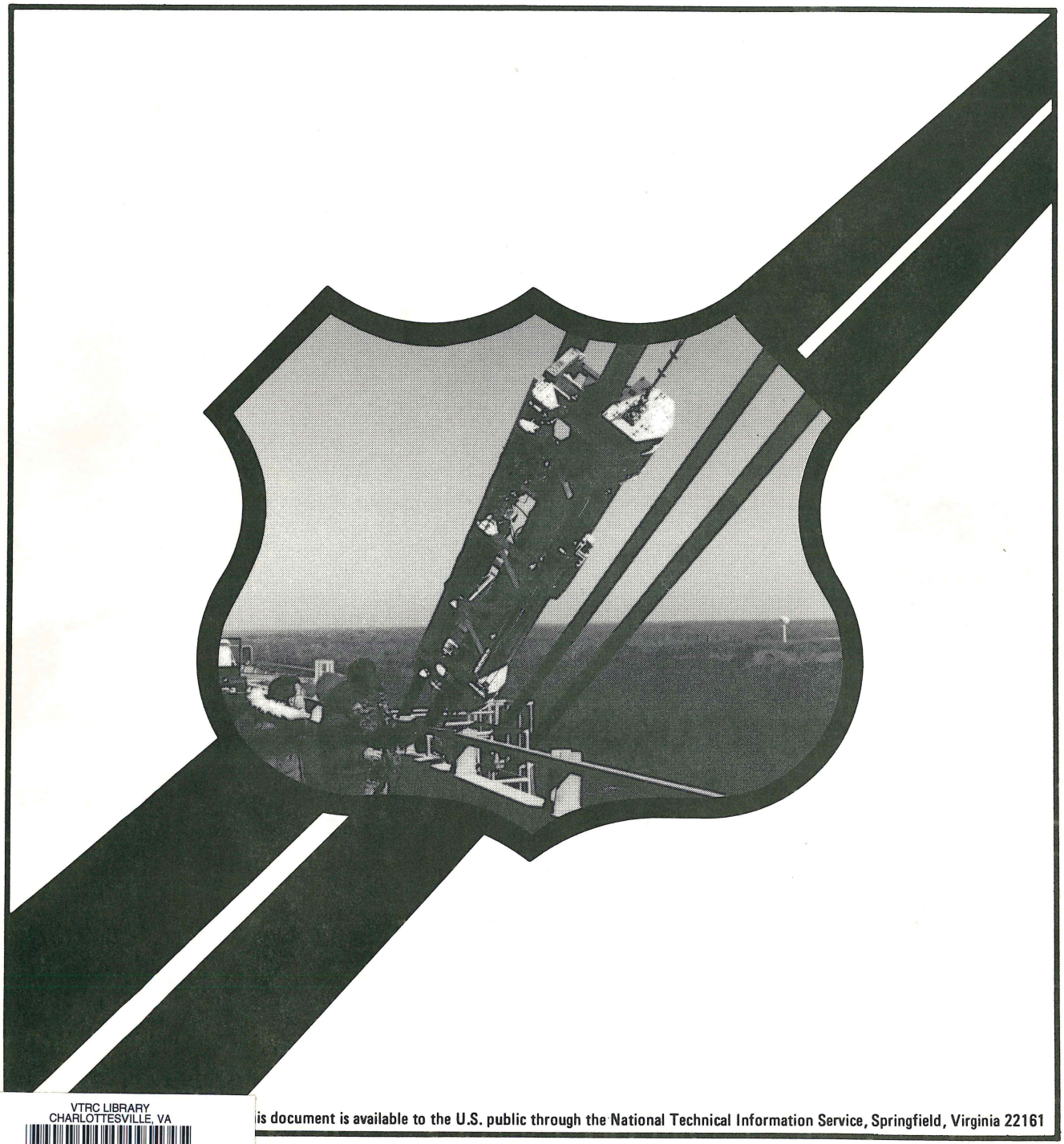

is document is available to the U.S. public through the National Technical Information Service, Springfield, Virginia 22161

VTRC LIBRARY
CHARLOTTESVILLE, VA
I 0029941

FOREWORD

This report will be of interest to bridge design, maintenance and inspection engineers, in particular those persons concerned with the degradation and damage of structural cables and strands.

Results are represented of the design, development and fabrication of a computer-integrated, self-propelled, remotely-controlled, automated system for nondestructive evaluation (inspection and long term monitoring) of the main structural cables of long span suspension bridges. The Magnetic Perturbation NDE Cable System (MPC) requires no surface preparation nor removal of protective coatings, and provides high resolution, quantitative NDE data essential for assessing the structural integrity of suspension bridge cables. Field trials conducted on the Luling Bridge in Louisiana demonstrated the usefulness of the MPC for inspecting stay cables under realistic field conditions. Additional work is recommended to modify the MPC for use on a larger variety of cable diameters and types.

Thomas J. Pasko
Director, Office of Engineering
and Highway Operations
Research and Development

NOTICE

This document is disseminated under the sponsorship of the Department of Transportation in the interest of information exchange. The United States Government assumes no liability for its contents or use thereof. The contents of this report reflect the views of the contractor, who is responsible for the accuracy of the data presented herein. The contents do not necessarily reflect the official policy of the Department of Transportation. This report does not constitute a standard, specification, or regulation.

The United States Government does not endorse product or manufacturers. Trade or manufacturers' names appear herein only because they are considered essential to the object of this document.

Technical Report Documentation Page

1. Report No.	2. Government Accession No.	3. Recipient's Catalog No.
FHWA-RD-89-158		

4. Title and Subtitle	5. Report Date
Design, Develop and Fabricate a Prototype Nondestructive Inspection and Monitoring System for Structural Cables and Strands of Suspension Bridges, Volume I: Final Report	May 1989
	6. Performing Organization Code
7. Author(s) John R. Barton, Cecil M. Teller, Sidney A. Suhler	8. Performing Organization Report No. 86211
9. Performing Organization Name and Address Texas Research Institute Austin, Inc. 9063 Bee Caves Road Austin, TX 78733-6201	10. Work Unit No. (TRAIS)
	11. Contract or Grant No. DTFH61-87-C-00090
12. Sponsoring Agency Name and Address Office of Engineering and Highway Operations R & D Federal Highway Administration 6300 Georgetown Pike McLean, VA 22101-2296	13. Type of Report and Period Covered Final Report
	14. Sponsoring Agency Code

15. Supplementary Notes FHWA Contract Manager: Charles McGogney, HNR-10; Assistance for field demonstration provided by Louisiana Department of Transportation and Research (LADOTR); Public Works Journal Corporation hereby grants to Texas Research Institute Austin, Inc. and to the United States Government a royalty-free, nonexclusive, irrevocable right to use, reproduce, distribute, and sell pages 44 through 48 of Public Works, January 1989, throughout the world.

16. Abstract

This report describes the development of a prototype magnetic perturbation NDE system for inspecting and monitoring structural cables and strands of suspension bridges. Although this method had been applied successfully to a variety of NDE problems, including small diameter cables, the application to larger diameter cables was an extremely difficult endeavor. A limited parametric laboratory investigation was conducted using a rudimentary system consisting of a 200-lb (91 kg) electromagnet with an attached Hall probe to measure the magnetic perturbations as a simulated cable was scanned. The first specimen consisted of 370 steel rods (0.25-in (6.4-mm) diameter by 20-ft (6.1-m) long) enclosed by a 6.0-in (15.2-cm) I. D. by 0.28-in (7.1 mm) wall thickness steel pipe 20-ft (6.1 m) long that supported the rods and also simulated the 0.2-in (5.1 mm) diameter soft steel spiral protective wrap used on some main cables. Magnetic anomalies in the steel pipe obscured flaw signals except for very large flaws. After many changes in the experimental arrangement which included replacing the steel pipe with an aluminum pipe, detection of a 0.27 percent cross-sectional area flaw at a depth of 1.9 in (4.8 cm) was achieved. Subsequently, a prototype Magnetic Perturbation Cable (MPC) NDE system was constructed and field demonstrations were successfully conducted on the 6.3-in diameter (16-cm) Luling Bridge stay cables (12 through 15 December 1988). Approximately 420 data scans (each 100 in (2.5 m) long) were recorded. Comprehensive analyses disclosed the possibility that grouting was so thin in several regions on top of a cable that segments of wires were moved by the magnetic attractive forces at each poleface.

The MPC incorporates the high sensitivity, excellent resolution, long-term stability, etc. of the magnetic perturbation method with modern microprocessor control, digital communication, computer archival storage, digital signal analyses routines, etc. into an integrated, state-of-the-art, automated NDE system that now makes it possible to apply modern quantitative structural lifetime assurance strategies to suspension bridge cables.

17. Key Words	18. Distribution Statement
Magnetic Perturbation, Leakage Flux, Nondestructive Inspection, Bridge Cables, Stay Cables, Automated Inspection	This document is available to the U.S. public through the National Technical Information Service, Springfield, VA 22161

19. Security Classif. (of this report)	20. Security Classif. (of this page)	21. No. of Pages	22. Price
Unclassified	Unclassified	133	

Form DOT F 1700.7 (8-72) Reproduction of completed page authorized

METRIC CONVERSION FACTORS

APPROXIMATE CONVERSIONS FROM METRIC MEASURES

SYMBOL	WHEN YOU KNOW	MULTIPLY BY	TO FIND	SYMBOL
	LENGTH			
in	inches	2.5	centimeters	cm
ft	feet	30	centimeters	cm
yd	yards	0.9	meters	m
mi	miles	1.6	kilometers	km
	AREA			
in^2	square inches	6.5	square centimeters	cm^2
ft^2	square feet	0.09	square meters	m^2
yd^2	square yards	0.6	square meters	m^2
mi^2	square miles	2.6	square kilometers	km^2
	acres	0.4	hectares	ha
	MASS (weight)			
oz	ounces	28	grams	g
lb	pounds	0.45	kilograms	kg
	short tons(2000 lb)	0.9	tonnes	t
	VOLUME			
tsp	teaspoons	5	milliliters	ml
tbsp	tablespoons	15	milliliters	ml
fl oz	fluid ounces	30	milliliters	ml
c	cups	0.24	liters	l
pt	pints	0.47	liters	l
qt	quarts	0.95	liters	l
gal	gallons	3.8	liters	l
ft^3	cubic feet	0.03	cubic meters	m^3
yd^3	cubic yards	0.76	cubic meters	m^3
	TEMPERATURE (exact)			
°F	Fahrenheit temperature	5/9 (after subtracting 32)	Celsius temperature	°C

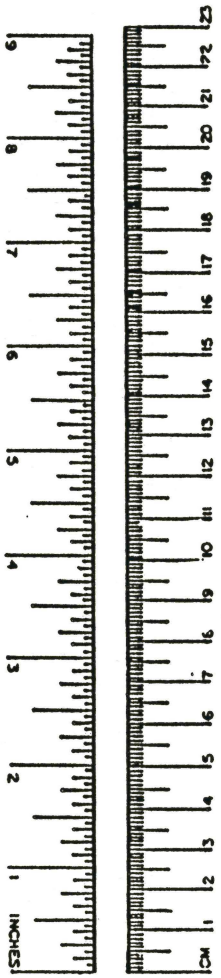

APPROXIMATE CONVERSIONS FROM METRIC MEASURES

SYMBOL	WHEN YOU KNOW	MULTIPLY BY	TO FIND	SYMBOL
	LENGTH			
mm	millimeters	0.04	inches	in
cm	centimeters	0.4	inches	in
m	meters	3.3	feet	ft
m	meters	1.1	yards	yd
km	kilometers	0.6	miles	mi
	AREA			
cm^2	square centimeters	0.16	square inches	in^2
m^2	square meters	1.2	square yards	yd^2
km^2	square kilometers	0.4	square miles	mi^2
ha	hectares(10,000 m^2)	2.5	acres	
	MASS (weight)			
g	grams	0.035	ounces	oz
kg	kilograms	2.2	pounds	lb
t	tonnes (1000 kg)	1.1	short tons	
	VOLUME			
ml	milliliters	8.03	fluid ounces	fl oz
l	liters	2.1	pints	pt
l	liters	1.06	quarts	qt
l	liters	0.26	gallons	gal
m^3	cubic meters	36	cubic feet	ft^3
m^3	cubic meters	1.3	cubic yards	yd^3
	TEMPERATURE (exact)			
°C	Celsius temperature	9/5 (then add 32)	Fahrenheit temperature	°F

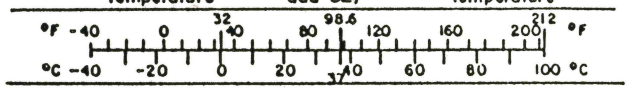

TABLE OF CONTENTS

LIST OF FIGURES iii

LIST OF TABLES ix

I. INTRODUCTION 1

A. Background 1
B. Summary of Phase I Program - Prototype Development 11
C. Summary of Phase II - Field Demonstration 22

II. PARAMETRIC INVESTIGATION 33

A. Specimens 33
B. Rudimentary Scanning Assembly 39
C. Data System 39
D. Experimental Results 45

III. PROTOTYPE MAGNETIC PERTURBATION NDE CABLE SYSTEM (MPC) 54

A. Equipment Description and Operation 54
1. Overall System 54
2. Mechanical System 54
3. Electrical and Electronic Subsystem 56
4. Attachment and Removal 59
B. Performance Verification 59
1. Specimen 59
2. Calibration and Reference Data 61
3. Data Analyses and Flaw Detection Forecasts 64

IV. FIELD DEMONSTRATION, CABLE-STAYED BRIDGE ACROSS THE MISSISSIPPI RIVER 66

A. Preparation and Team Training 66
B. Site Demonstration 66
1. Equipment Setup, Check-out and Installation 66
2. Data Acquisition and Field Analyses 67
3. Comprehensive Analyses 69
4. Summary of Results 75
C. Assessment of Field Performance 78

V. COMPREHENSIVE ASSESSMENT OF MAGNETIC METHODS AND MPC PROTOTYPE SYSTEM....80

VI. DISCUSSION OF INSPECTION RATES....87

VII. EVOLUTION OF MPC PROTOTYPE SYSTEMS AND FUTURE POSSIBILITIES....89

VIII. CONCLUSIONS AND RECOMMENDATIONS....91

A. Conclusions....91
B. Recommendations....92

APPENDIX A Inspecting and Evaluating New York's East River Suspension Bridge Cables....93

APPENDIX B NDE of Bridges....98

APPENDIX C The Magnetic Field Perturbation Method....106

APPENDIX D Results of Signal Analysis Investigations....116

APPENDIX E Potential MPC System Improvements....128

REFERENCES....131

LIST OF FIGURES

Figure 1 The George Washington Bridge....2

Figure 2 Views of the Golden Gate Bridge between San Francisco and Marin County (Opened 1937)....3

Figure 3 The Pasco-Kennewick Bridge....4

Figure 4 Views of the cable stayed Luling Bridge on I-310 across the Mississippi River near New Orleans, LA....5

Figure 5 Main suspension cables and information indicating the immensity of the inspection problem....7

Figure 6 Williamsburg Bridge main suspension cables....8

Figure 7 Inspection of the Williamsburg Bridge main cables in 1988 *(Upper, segment of cable with paint flaking; middle, spiral wrap removed; lower, temporary protective covering - two lane roadway at left)*....9

Figure 8 Prototype magnetic perturbation NDE cable system *(MPC)*....13

Figure 9 System flaw detection verification specimen *(271 rods 1/4-in diameter by 20 ft with 1/4-in diameter spiral cable wrap before insertion into black polyethylene tubing 6.30-in O.D. by 5.62-in I.D. simulating stay cable of Luling Bridge)*....13

Figure 10 Magnetic perturbation signature features and magnetizing method....15

Figure 11 Signatures from flaw *(0.25-in gap in 0.25-in diameter rods)* at three depths *(Luling Bridge specimen)* obtained with prototype MPC....16

Figure 12 Signature from flaw *(0.5-in gap in four 0.25-in diameter rods)* at depth of 1.69 in *(bottom record flaw S/N ratio > 24/1)*....18

Figure 13 Signatures from flaw *(0.5-in gap in four 0.25-in diameter rods)* at depth of 1.90 in *(bottom record flaw S/N ratio > 24/1)*....19

Figure 14 Views of MPC system inspection module attachment to Luling Bridge cable LN 3 on 12/13/88 for first field demonstrations ever conducted *(upper, support arms and clamp chains "open"; middle, "secured" and lifting fixture removal; lower, attachment "complete")* 24

Figure 15 Views of data logging activities on Luling Bridge *(Clockwise from upper left, inspection module in 0° position or Track 3 on 525 ft long stay cable LN 3; Track 2 or -72° position; Track 1 or -144° position; operators command, data acquisition-storage-processing-display computer)* 25

Figure 16 Data acquisition at approximately 70 ft, 0° position, Track 3 *(Upper)* and 130 ft, 288° position, Track 2 *(Lower)* cable LN 3, 12/14/88 26

Figure 17 Typical analog records obtained during one scan of the Luling Bridge cable *(1/4-in diameter wire rope spiral wrap signals indicated by broken lines 1, 2, 3; other features occur simultaneously at solid lines A, B, C; note three reference signals on CH3)* 27

Figure 18 Typical analog records computer "reconstructed" after digital subtraction of CH 6 data from CH 1 thru CH 5. Note prominence of spiral wrap signals *(broken lines 1, 2, 3)*, artifacts caused by subtraction *(Solid vertical lines)*, and CH 3 reference signal separation *(Upper value from magnetic record and lower value tape measurement)* 29

Figure 19 Array of records around circumference illustrating possible variation of grout coverage 30

Figure 20 Sequence of records selected to illustrate the possibility of grout coverage variation on 0° or top region of cable *(Note: major background excursions and also prominence of spiral wrap signals for records @ 1420 in; background excursions, all records track 3; data sequence @ 1220 in not included)* 32

Figure 21 Steel pipe 20 ft by 6.0-in I.D. by 0.28-in wall; 20 ft by 0.25-in diameter cold drawn ASTM 1018 steel rods 35

Figure 22 Steel pipe-parallel wire *(rod)* specimen for parametric investigation 35

Figure 23 Views of steel pipe-parallel wire specimen with flaw bundle only *(Upper)* and with 370 rods *(Lower)* 36

Figure 24 Views of aluminum pipe *(20 ft by 6.0-in I.D. by 0.28-in wall)* parallel wire *(rod)* specimen 37

Figure 25 Aluminum pipe-suspender rope specimen *(Upper, 2 11/16-in diameter suspender rope with socket removed from the Golden Gate Bridge; lower broken wire 0.14-in diameter with missing segment 2 3/4-in long detected during magnetic experiments)* 38

Figure 26 Flaw configurations used in steel pipe *(upper two sketches and Figure 31 records)* and aluminum pipe *(lower sketch and Figure 32 records)* 41

Figure 27 Several views of laboratory scanning equipment 42

Figure 28 Photographs of the laboratory scanner and computer controls 43

Figure 29 Data collection system 44

Figure 30 Records selected to illustrate flaw signatures and influence of flux density *(Steel pipe-parallel wire specimen; 10 amp. mag current; cross-sectional area of pipe 5.52 in^2; 2.2-gauss signature expected at 36-in position)* 46

Figure 31 Complex effects of flux density and filtering on flaw signature characteristics *(Steel pipe-parallel wire specimen + one 7 wire by 1/2-in diameter strand)* 48

Figure 32 Decreased magnetic background and improved flaw detection with aluminum pipe-parallel wire specimen and increased magnetizing current of 20 amps *(Flaws 0.5-in gaps in four 0.25-in diameter rods, 370 rods total)* 50

Figure 33 Improved flaw detection with differential Hall probes and no filtering *(Front to back Hall element spacing - 1.0 in, 20 amp magnetizing current)* 51

Figure 34 Records obtained during detection experiments on Golden Gate suspender rope specimen shown in Figure 25 *(Flaw signal @ 54 in from 2 3/4-in long missing segment of 0.14-in diameter broken wire; flaw signal @ 80 in from 0.5-in gap in 4 rods 1/4-in diameter at depth of 0.65 in; 14 rods + suspender rope in aluminum pipe; magnetizing current 14 amps, upper, 20 amps, lower; filter used to minimize signals from wire rope lay)* 52

Figure 35 Schematic illustration of mechanical system 55

Figure 36 Electronic and electrical block diagram 57

Figure 37 System lifting harness 60

Figure 38 Records from laboratory specimen cable obtained with MPC system after field demonstration *(records in right column obtained after digital subtraction of CH2)* 62

Figure 39 Comparison of data sets obtained on two different days from the same regions 70

Figure 40 Overlay of two data sets indicating excellent repeatability and potential for long term monitoring (*First set obtained, system rotated to obtain Track 3 data, then back to Track 2. Signal @ 34 in caused by 1/8-in diameter wire taped transverse to cable. Data from cable LN 1 Track 2 after subtracting CH 6)* 72

Figure 41 Overlay with horizontal offset of two data sets indicating excellent repeatability and potential for long term monitoring *(First set obtained, system rotated to obtain Track 3 data, then back to Track 2. Signal @ 34 in caused by 1/8-in diameter wire taped transverse to cable. Data from cable LN 1 Track 2 after subtracting CH 6)* 73

Figure 42 Comparison of anomalous background signals (undulations) in Luling Bridge stay cable and laboratory specimen cable 74

Figure 43 Major improvement in flaw signal amplitude at higher flux density 81

Figure 44 Prominent signatures from all flaws after subtracting CH3, modified laboratory specimen cable *(25 amp. 8500-9500 gauss; CH3 subtraction produces 3 reference signals which inverted polarity on all channels, also since CH2 was inoperative second record from bottom becomes inverted CH3, compare with CH3 lower records of Figure 43)*.....82

Figure 45 Correlation results using data from modified laboratory specimen after subtracting CH6 from all other channels; correlation parameters: 75 data points *(7.5 in)*; peak to peak separation 1.0 in *(Negative correlations obtained for flaws in CH1 2, 3 because subtraction of CH 6 inverted flaw signals; negative correlations for three reference signals on CH3 because the signals have polarity opposite to flaws, see Figure 43)*.....85

Figure 46 Sketch of spherical void or hole in an infinite magnetized ferromagnetic matrix and the resulting magnetic field perturbation in the Y direction.....107

Figure 47 Graphs of magnetic perturbation signals.....110

Figure 48 Magnetic modeling of flaw detection in main suspension cables.....112

Figure 49 Reconstructed digitized magnetic signatures before and after enhancement and correlation for strand with medium flaw in first row, near stirrup *(B = 16)*.....118

Figure 50 Reconstructed display of digitized magnetic signatures before and after enhancement and correlation for strand with medium flaw in first row, near stirrup *(B=16)*.....119

Figure 51 Goodness of fit between a typical strand flaw and the algorithm based on a theoretical model.....120

Figure 52 Graph of correlation value between algorithm and typical flaws in strand and bar as a function of B *(peak separation)*.....122

Figure 53 Reconstructed display of digitized magnetic signatures before and after enhancement and correlation for surface artifact *(B=8, 16, 32)*.....123

Figure 54 Reconstructed display of digitized magnetic signatures before and after enhancement and correlation for strand with small flaw in first row, over stirrup *(B=16)*.....125

Figure 55 Reconstructed display of digitized magnetic signatures before and after enhancement and correlation for strand with small flaw in first row, between stirrups *(B=16)*.....126

Figure 56 Reconstructed display of digitized magnetic signatures before and after enhancement and correlation for strand with medium flaw in first row, between stirrups *(B=16)*.....127

LIST OF TABLES

Table 1 Estimated capabilities of magnetic method.....21

Table 2 Flaw schedule.....40

Table 3 Equipment physical parameters.....55

Table 4 Survey of Luling Bridge stay cable LN3 records for background undulations.....76

Table 5 Estimated detection limits of magnetic method.....114

Table 6 Significant attributes of the magnetic field perturbation NDE method.....115

I. INTRODUCTION

A. Background

Main cables and suspender cables of suspension bridges and the stays of cable-stayed bridges are primary structural elements, and deterioration (corrosion and fracture) of the individual wires comprising these elements is a continuing structural integrity concern of bridge engineers.

Historically, suspension bridges are among the oldest steel bridges in this country and throughout the world. The George Washington Bridge, figure 1, built in the early 1930's across the Hudson River between New York City and New Jersey is a classic example; while the Golden Gate Bridge, shown in figure 2, between San Francisco and Marin County across the Golden Gate has the longest center span which is 4200 ft. Although completed in 1937 it is still ranked as an outstanding engineering achievement of this century.

Typical design features of suspension bridges consist of: two steel towers with "saddles" which support two to four parallel main cables that are continuous between massive anchorages at each end of the bridge; the steel truss "deck" that carries the roadway is suspended from the main cables by multiple vertical wire ropes, "suspender ropes"; the suspender ropes extend from the deck and usually are looped across and stably positioned on a main cable by cast steel "cable bands" or clamps contoured to match the main cable and with grooves angled to accommodate the suspender ropes; each end of a suspender rope terminates in a socket, and a bracket attached to the steel truss transmits the bridge load to the upper surface of each socket thereby loading the suspender ropes.

Other types of bridges that use cables as primary structural elements are cable stayed bridges. Historically, first used in Europe in the early 1800's, development was halted by two serious accidents; the collapse of the Pryburg bridge in 1818 (Great Britain) and the collapse of the Saale River bridge in 1824 (Germany). After studying these accidents, the French scientist Navier recommended suspension bridges rather than cable stayed bridges, and for about 100 years only a few stayed bridges were built in the U.S. The technology of cable stayed bridges was revived in Europe after World War II because of the need to rebuild many destroyed bridges. The first modern cable stayed bridge is now recognized to be the Strömsund Bridge built in Sweden in 1955. In the U.S., two major cable stayed steel bridges erected in the past few years are: the Pasco-Kennewick Bridge, shown in figure 3, across the Columbia River in Washington, and the Luling Bridge across the Mississippi River in Louisiana shown in figure 4. In addition to these there are several segmental concrete cable stayed major bridges under construction or recently completed. An example is the Sunshine Skyway Bridge across Tampa Bay Florida.



Figure 1. The George Washington Bridge.

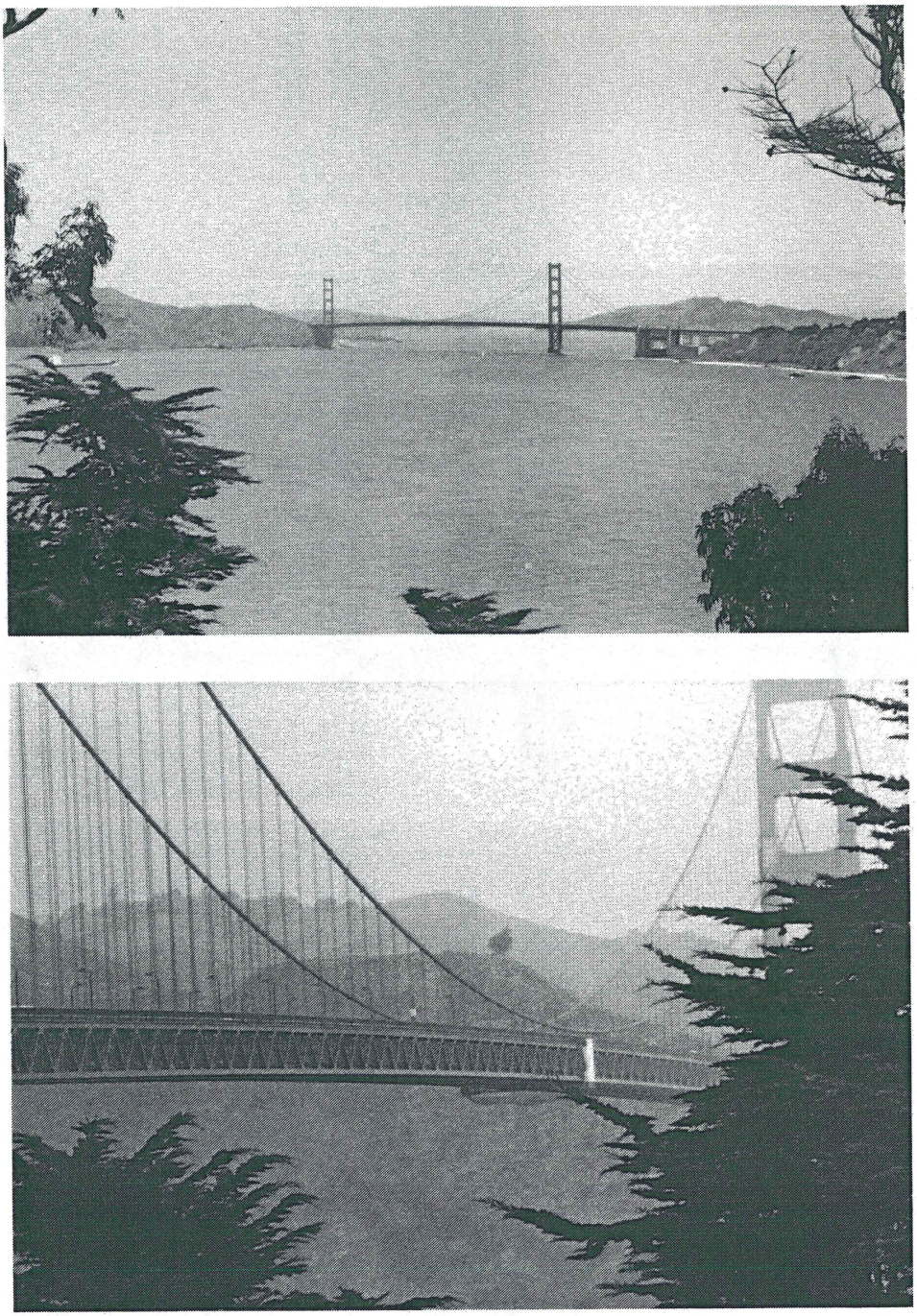

Figure 2. Views of the Golden Gate Bridge between San Francisco and Marin County *(Opened 1937).*

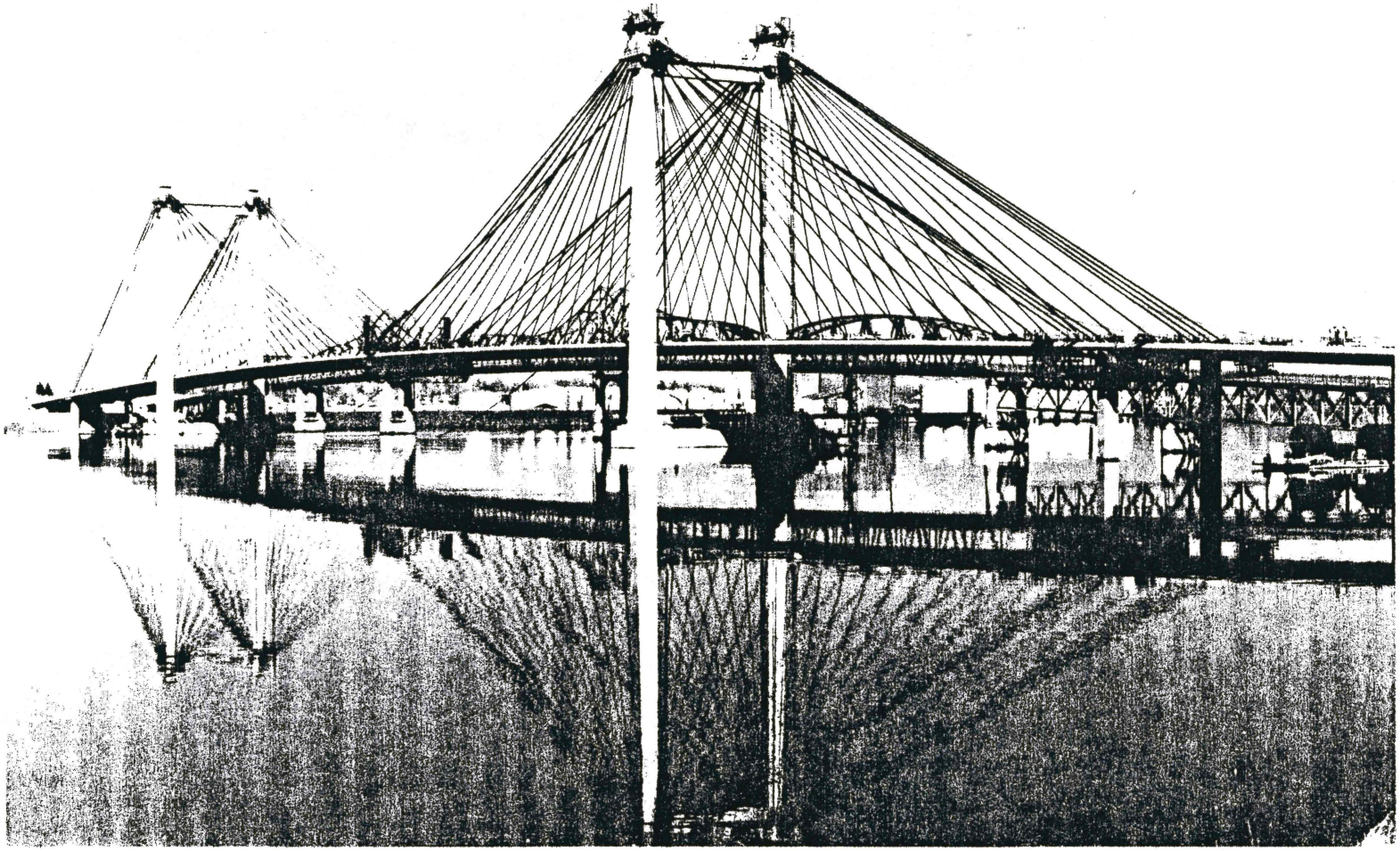

Figure 3. The Pasco-Kennewick Bridge.

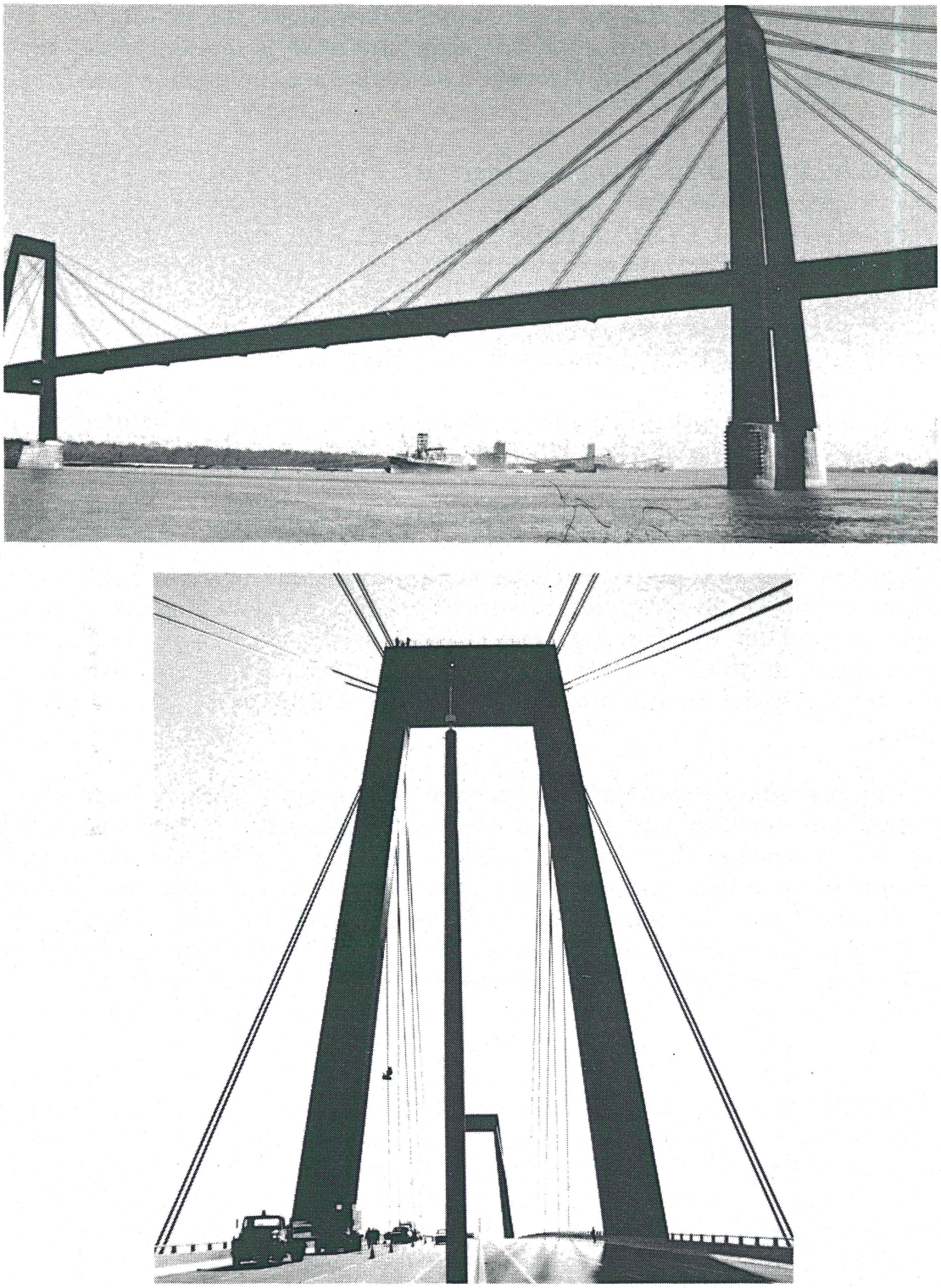

Figure 4. Views of the cable stayed Luling Bridge on I-310 across the Mississippi River near New Orleans LA. *(Opened 1983).*

In February 1989 during a program review at the FHWA Turner Fairbank Research Center, it was indicated that there are now 12 modern long-span cable stayed bridges in the U.S., and that this type bridge will be used for most long-span bridges in the future.

Main cable and stay cable designs and fabrication details vary from bridge to bridge. In general individual wires are cold drawn and range up to 0.25-in diameter for main cables and 0.6-in diameter for stay cables. In many long-span suspension bridges the individual wires are continuous and are "spun-in-place" from anchorage to anchorage over the two towers; several hundred wires are collected into a "strand" and when the required number of strands have been completed the bundle of several thousand parallel wires is compressed into a circular cross-section. Diameter may range from approximately 5 in to 36 in and length may extend to nearly 8000 ft. In other cases the main cables may consist of one or more wire ropes fabricated off-site and shipped to the bridge site.

Protection of the steel wires from the environment is a significant factor influencing life, and a variety of approaches have been used. Wire may be galvanized or bare; cables may be coated with red lead or zinc paste and covered with a tightly wound spiral wrapping of soft iron wire and several coats of paint or in some cases a rubber, overlapping, wrap is used instead of the wire. Stay cables have been encased in thick polyethylene or steel pipes, and after installation and tensioning the space surrounding the steel wires is filled with cement grout under pressure.

The preceding provides a perspective on the difficulties and complexities of the inspection problem and these are further emphasized by the photographs of figure 5. It is obvious that visual inspections of cables can not be used to determine the condition of wires with the confidence warranted for such critical elements. Nevertheless, this is the primary method used, in 1987 and early 1988, for a major critical inspection of the heavily traveled, 85-year old, Williamsburg Bridge over the East River in New York City because no proven nondestructive evaluation (NDE) method (other than visual inspection) has been developed (see figure 6; Related information is described in a 1989 Public Works article included in appendix A). Visual access, even for the exterior of wires on the surface, required complete removal of the spiral wire wrappings as shown in figure 7; interior wires could only be examined wire by wire after gingerly forcing apart overlaying and adjacent wires by wooden wedges forced into the 18-in diameter bundle. This is a time consuming, expensive, and not entirely satisfactory process and was applied, only, to very limited segments of these cables. ("Hardwood wedges were driven deep into the cable, which allowed for about 15 percent of the cable wires to be viewed directly." See page 96, Public Works article, appendix A.) Visual inspection after removal of protective coverings was used, also, on the Portsmouth Bridge.[1,2]



Figure 5. Main suspension cables and information indicating the immensity of the inspection problem.

Inspecting and Evaluating New York's East River Suspension Bridge Cables

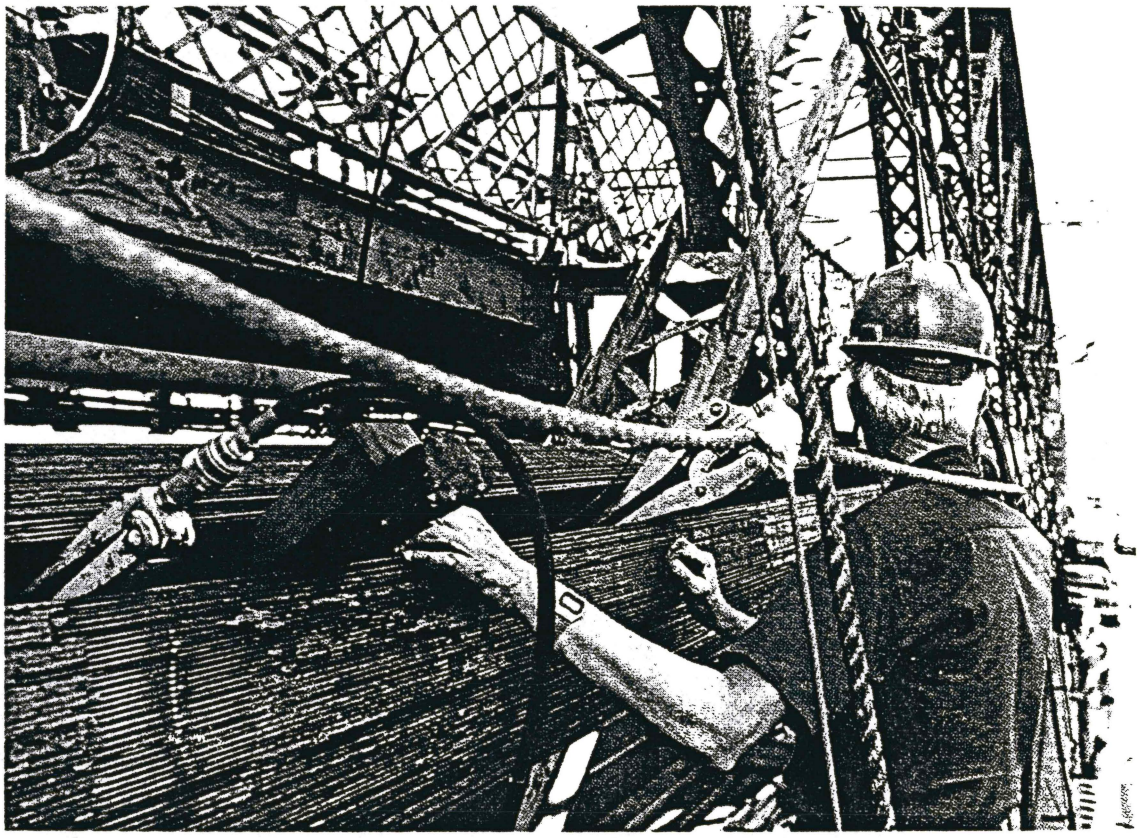

■ GROOVE is opened in the main cable of the Williamsburg Bridge to allow inspection of the interior wires.

Figure 6. Williamsburg Bridge main suspension cables.

(Reprinted from Public Works. Used by permission.)

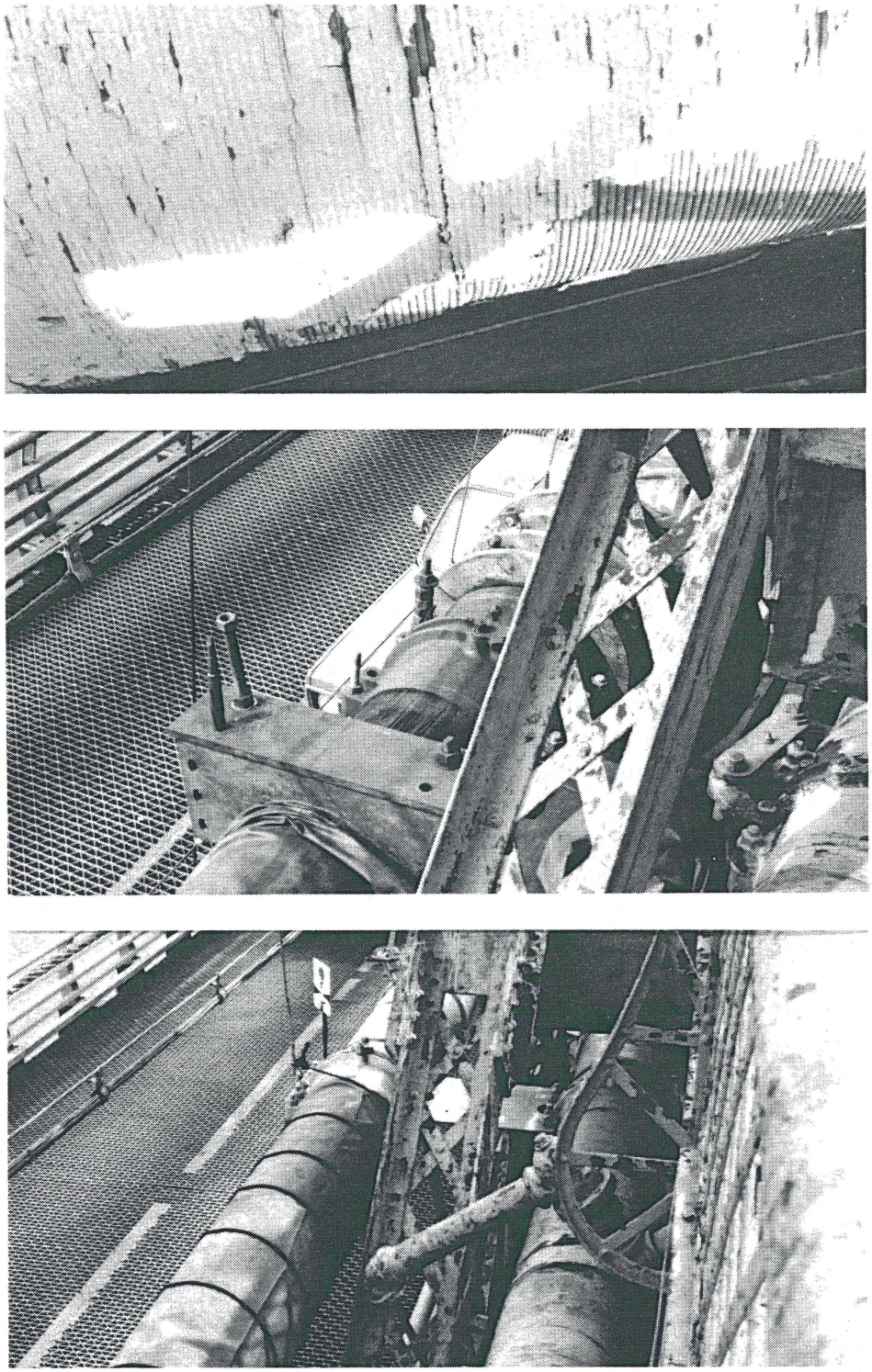

Figure 7. Inspection of the Williamsburg Bridge main cables in 1988 *(Upper, segment of cable with paint flaking; middle, spiral wrap removed; lower, temporary protective covering - two lane roadway at left).*

Because of the increasing requirement for more effective NDE methods, the FHWA has undertaken a program for the development of a prototype nondestructive inspection and monitoring system for structural cables and strands of suspension bridges. The prototype system is based on using the magnetic field perturbation method, and although no funding was provided in this contract for methods applicability assessments, a brief review of candidate methods follows. (See appendix B for a more comprehensive review.)

Methods that were considered include:

- Radiography
- Ultrasonics
- Acoustic emission
- Magnetics

Because of the penetrating power of gamma and X-radiation; both film and real-time radiography have potential for the inspection of small to intermediate diameter cables containing bundles of strands for detection of broken wires, thinning, corrosion and other anomalies. However, cost, safety, speed, sensitivity (under favorable conditions approximately 1 percent), and resolution constraints must be considered serious disadvantages. Computerized photon tomography also shows potential for inspecting wires, especially at end-fitting locations, but development costs would be very high (approaching $1 million) and essentially the same safety and speed constraints apply as for conventional radiography. (Because of the very high sensitivity, better than 0.1 percent, excellent resolution, cross-sectional imaging, and other features, tomography could be an important method for verfiying conditions at local "suspect" positions.)

Ultrasonic testing of wires using rod waves generated by magnetostriction excitation and pulse-echo testing using angle probes on accessible wires are both possible. However, past attempts to apply ultrasonic pulse-echo techniques transverse to and along a wire rope were not successful.[3] The sound pulses were reflected (and also mode conversion would occur) at each wire, and it was not possible to distinguish between broken and intact wires. No reports of reliable velocity and attenuation measurements on cables and wires (other than the 1 to 5 db/in along individual wires and 20 db from wire to wire) have been found in the NDE literature.[4] The high attenuation from wire to wire limits the transverse techniques to less than 2-in diameter ropes or cables, and even for exterior wires propagation along the wire would be limited to less than approximately 5 ft.

Acoustic emission (AE) testing has been used to monitor cables on a lift bridge in California and also has been employed in wire rope tests; however, attenuation was a serious problem.[3,4] Recent field work has demonstrated the potential of acoustic emission techniques for detecting cracking in steel girders in areas of high background noise.[5] This work has shown that acoustic emission may also be

applicable to cable locations difficult to monitor by visual examination, e.g., main cables under bands and on suspender ropes at end fittings. However, for general applicability to main cables and stays, an unacceptably high number of transducers and cabling runs would be required, even if an adequate method of coupling through the protective coverings could be developed.

Magnetic field perturbation methods have been used effectively to detect cracks and other damage in, for example, mine and elevator wire rope.[6] Equipment of this type has been used for many years and may be of interest for tests of newly fabricated wires and structural strands and also for suspender strands and ropes. Typically, it has been limited to cable diameters less than 2 to 3 in, but for sizes representative of main cables new equipment concepts are required. As further evidence supporting applicability of the magnetic field perturbation method, a prototype magnetic instrument designed specifically for inspecting parallel wire suspender ropes (75 wires each 0.2 inches in diameter arranged in a hexagon with a 1.97-in maximum, diagonal, dimension) was recently described, 1985, and results of actual use presented.[7] This magnetic instrument used direct current in an electromagnet and two encircling arrays of 36 Hall elements for high resolution sensing of corrosion and other deficiencies. Importantly, the new magnetic field disturbance (MFD) system previously developed under FHWA funding has demonstrated the potential of magnetic methods to detect fatigue failure separations of wires in the reinforcing steel strands of a concrete beam at distances slightly greater than 2 1/2 in, and this successful development opens many possibilities for application to main cables.[8,9,10]

B. Summary of Phase I Program - Prototype Development

Although the magnetic field perturbation method is well understood and has been incorporated in a variety of applications, the problem of inspecting main cables for deterioration and broken wires in the interior regions is formidable and warranted a full-scale parametric investigation. Nevertheless, because the contract funding and time did not allow such a full-scale investigation, it was necessary to undertake a higher risk more limited parametric investigation. The rudimentary system used for the parametric investigation was conceptually simple, and consisted of a 200-lb electromagnet with an attached Hall effect sensor which was moved along the specimen cable. Output of the Hall probe was recorded and displayed to assess flaw detection capabilities with several flaw configurations and various experimental parameters.

Unfortunately, many difficulties were encountered with this approach, primarily, associated with developing a suitable but realistic specimen, achieving a high flux density in the specimen, and the necessity to use filtering to remove anomalous signals caused by the specimen. (A review of these difficulties is presented in Section II, Parametric Investigation.) Because of these difficulties only minimal progress in the detection of interior defects had been achieved by October

1987. Specifically, detection of a 1.0 percent cross-sectional area flaw could not be achieved at a depth greater than approximately 1.0 in for a specimen consisting of a 6.0-in I.D. by 0.28-in wall steel pipe 20 ft long filled with 370 rods 0.25 inch in diameter by 20 ft long. The pipe was used to simulate the 0.2-in diameter spiral steel wrap used on some main cables, and also provided support for the wire bundles and the rudimentary scanning assembly. Potential effective solutions to extend the detection depth were so elusive, even after intensive efforts including computer studies of magnetic models, that the research team considered the possibility that a high flux density could not be obtained with the 200-lb electromagnet because of fundamental limitations. The source of these limitations was the high magnetic reluctance caused by magnetic saturation of the "line of contact" region from rod to rod. As magnetic flux was forced into the interior rods, it became increasingly difficult to force more flux deeper because the line of contact region became more saturated, and the surrounding steel pipe increasingly shunted flux as the magnet current was increased. The magnetic model investigations indicated only modest improvement even if a much larger electromagnet was used. In fact, progress was so marginal that termination of the program almost seemed to be in the best interests of both FHWA and the research team.

However, before reaching such a conclusion the steel pipe was replaced by a 6.0-in I.D. by 0.28-in wall aluminum pipe, to minimize anomalous signals caused by the steel pipe, and detection sensitivity was significantly improved. Since the parametric investigation had required considerably more funds and time than had been programmed, it was necessary to review the program status with FHWA personnel at the Turner Fairbank Research Center (February 2, 1988) and to suggest more limited equipment features as an option to complete the program within the contract funding. Such a decreased scope was approved and also the field demonstration and associated detailed equipment design was targeted for a demonstration on the cable-stayed bridge at Luling, Louisiana.

A photograph of the Prototype Magnetic Perturbation NDE Cable System (MPC) is shown in figure 8 with a laboratory specimen (extending from the near end) simulating a stay cable from the Luling Bridge. The scanning assembly is visible near the upper center; overall length is 16 ft and weight is approximately 2800 lb. Figure 9 is a photograph of the specimen before insertion into the black polyethylene pipe; nonmagnetic stainless steel tie bands to compact the bundle (271 rods 20 ft long by 0.25-in diameter) are located at intervals. PVC rings are also spaced at intervals to aid in positioning the bundle concentrically in the polyethylene pipe; the pipe was not filled with cement grout because removal, modification and reinsertion of the wire bundle was anticipated. The insert is a close-up photograph of the cable cross section, and red paint on the ends identified the "flawed" rods in the bundle. Variation in the regularity of the compaction is apparent, and radial movement of rods caused by the strong magnetic forces resulted in such high

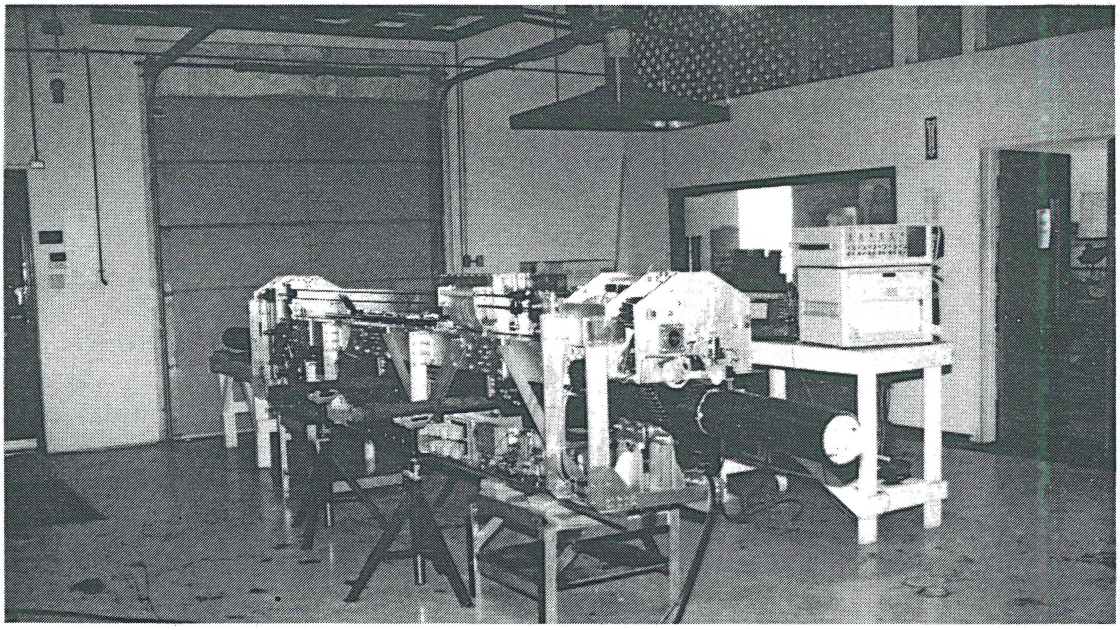

Figure 8. Prototype magnetic perturbation NDE cable system *(MPC).*

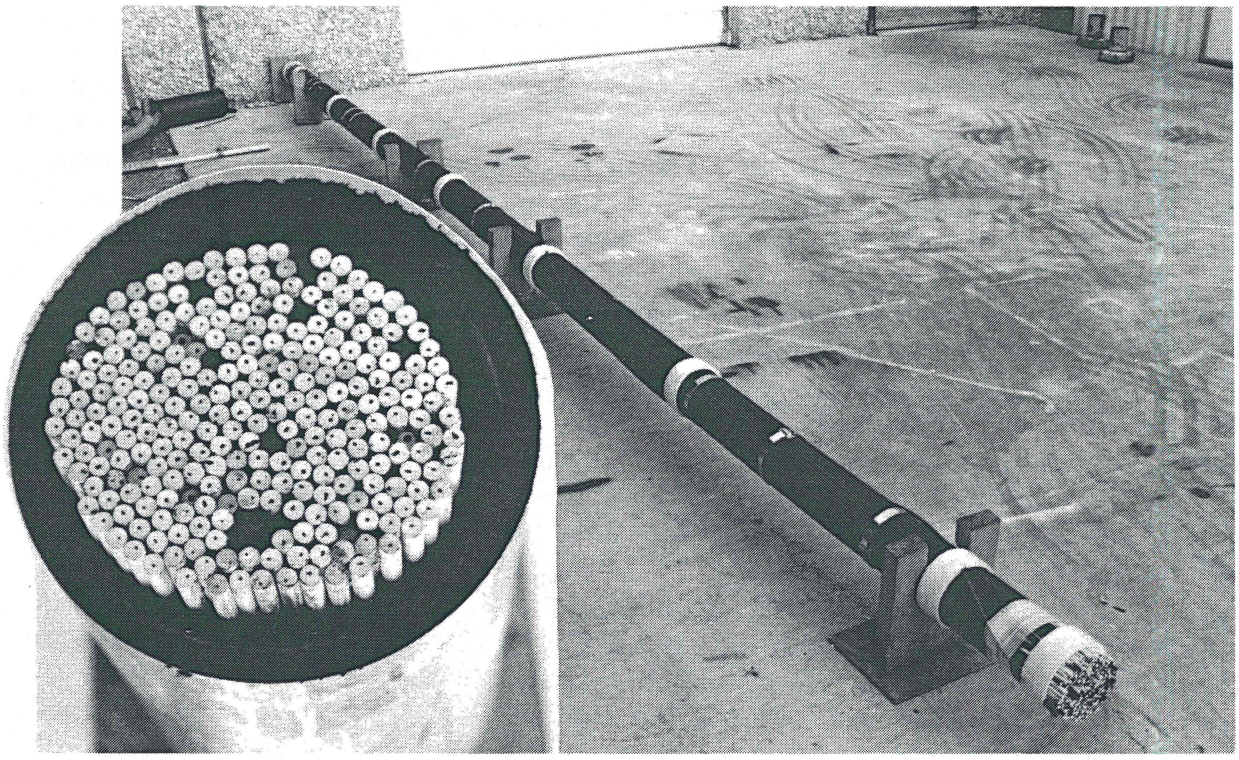

Figure 9. System flaw detection verification specimen *(271 rods 1/4-in diameter by 20 ft with 1/4-in diameter spiral cable wrap before insertion into black polyethylene tubing 6.30-in O.D. by 5.62-in I.D. simulating stay cable of Luling Bridge).*

magnetic background signals that it was necessary to add many additional PVC rings after preliminary runs. The system and specimen are more fully described in Sections III.A. and III.B.

Before presenting detailed information on estimated detection capabilities, it is informative to describe, briefly, the characteristics of magnetic perturbation signals and then to review selected experimental records obtained with the prototype MPC system. In the upper part of figure 10, a spherical volume (flaw or defect) with a permeability μ' is embedded in a ferromagnetic material (steel) with a permeability μ and is magnetized along the X direction by the magnetic field H. When a magnetic sensor is scanned over the region containing the flaw as shown at the bottom, the magnetic field component in the Y direction (H_y) is measured and a continuous plot produces the record or signature. Characteristic features that are very useful in relating NDE data to flaw size, depth, location, etc. are tabulated. This brief description will provide a foundation for understanding inspection records obtained with the MPC system during laboratory investigations and also during the field demonstration. A comprehensive review of the magnetic field perturbation method including: theory, principles and analyses, experimental results, estimates for cables, significant attributes, etc. is presented in appendix C.

Figure 11 presents records from 5 of the 6 Hall probe sensors spaced at 0.69-in intervals in an array covering approximately 4-in circumferential distance on the specimen. Information on sensor channel, sensitivity, scanned distance, etc. is provided on the records. Simulated flaws were produced in several 20-ft long rods by a 0.25-in long aluminum plug inserted between the ends of each 0.25-in diameter rod. Flaws are located at 10 in, 25 in and 40 in and at depths from the sensor of 1.1, 1.4, and 1.25 in, respectively. Channel 3 and channel 4 signatures are prominent from the flaw located at 10 in, but only nominal amplitudes are produced by the flaws at 25 in and relatively modest signatures are present on channel 1 through channel 5 for the flaw at 40 in. Since the channel 1 sensor is approximately 1.8 in from the center line of the flaw, located at 10 in, little or no signal is generated in this channel at this sensitivity. When channel 1 is subtracted from channel 3 the record at the bottom shows a prominent, easy to recognize signature at 10 in; also the flaw signature at 40 in is significantly improved. However, since there are three separate flaws at the 25-in location of the cable cross section, [approximately under sensor 1 (depth 1.4 in), sensor 4 (depth 1.7 in) and sensor 6 (depth 1.4 in, but sensor 6 output is not shown)], channels 1 through channel 5 produce approximately the same amplitude signal. Accordingly, the CH 3 - CH 1 record does not provide a major improvement. With the specimen rotated 80° to position only one of the flaws at 25 in approximately beneath the channel 5 sensor, the greatly improved signal shown in the insert is obtained. Also, note that the peak to peak separation in the scan direction is slightly greater for the flaws at 1.4-in depth compared with the 1.1 and 1.25-in deep flaws; this peak separation is an indication of depth from the sensor to the flaw centroid as previously explained.

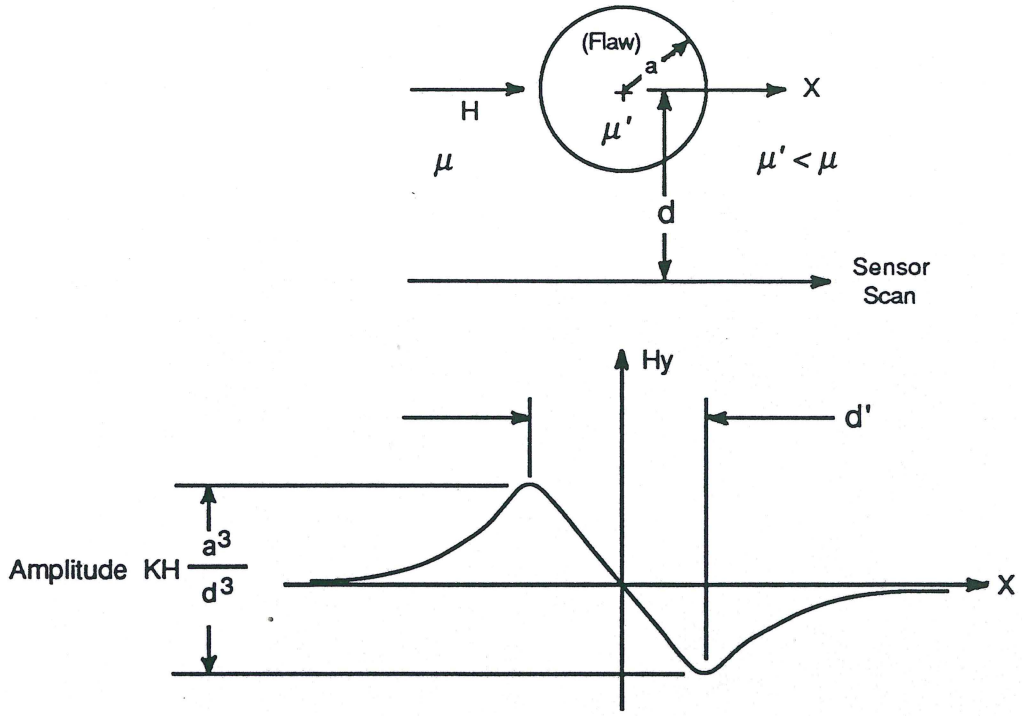

SIGNATURE FEATURES:

1. Bipolar and symmetric
2. Polarity as shown for fracture gap or corrosion pit; polarity reversed for soft spot in steel of "ferrule" splice
3. Peak separation d' equals depth to flaw d (independent of size)
4. Amplitude indicates flaw volume (dependent on depth)
5. Maximum amplitude obtained when scan path is directly over flaw
6. Amplitude decreases with flaw depth d (decrease: $1/d^3$)
7. Signal amplitude increases continuously as the magnetic field (H) is increased

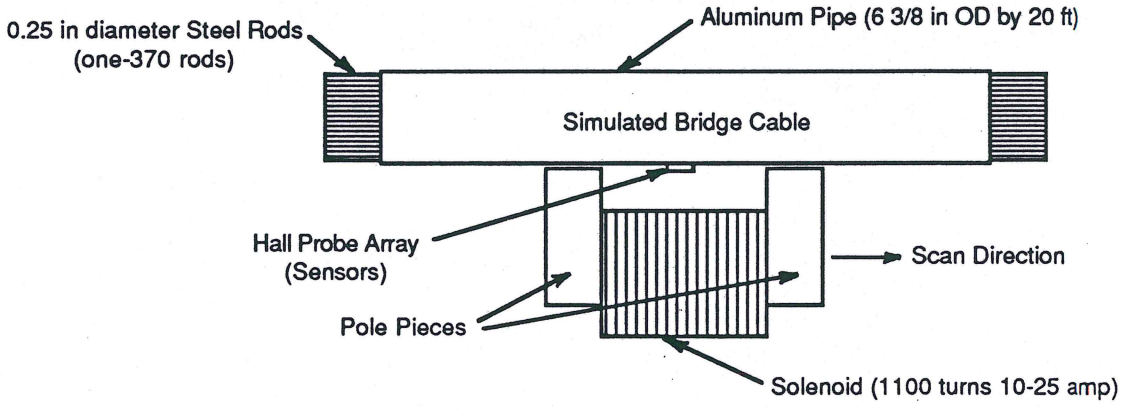

Figure 10. Magnetic perturbation signature features and magnetizing method.

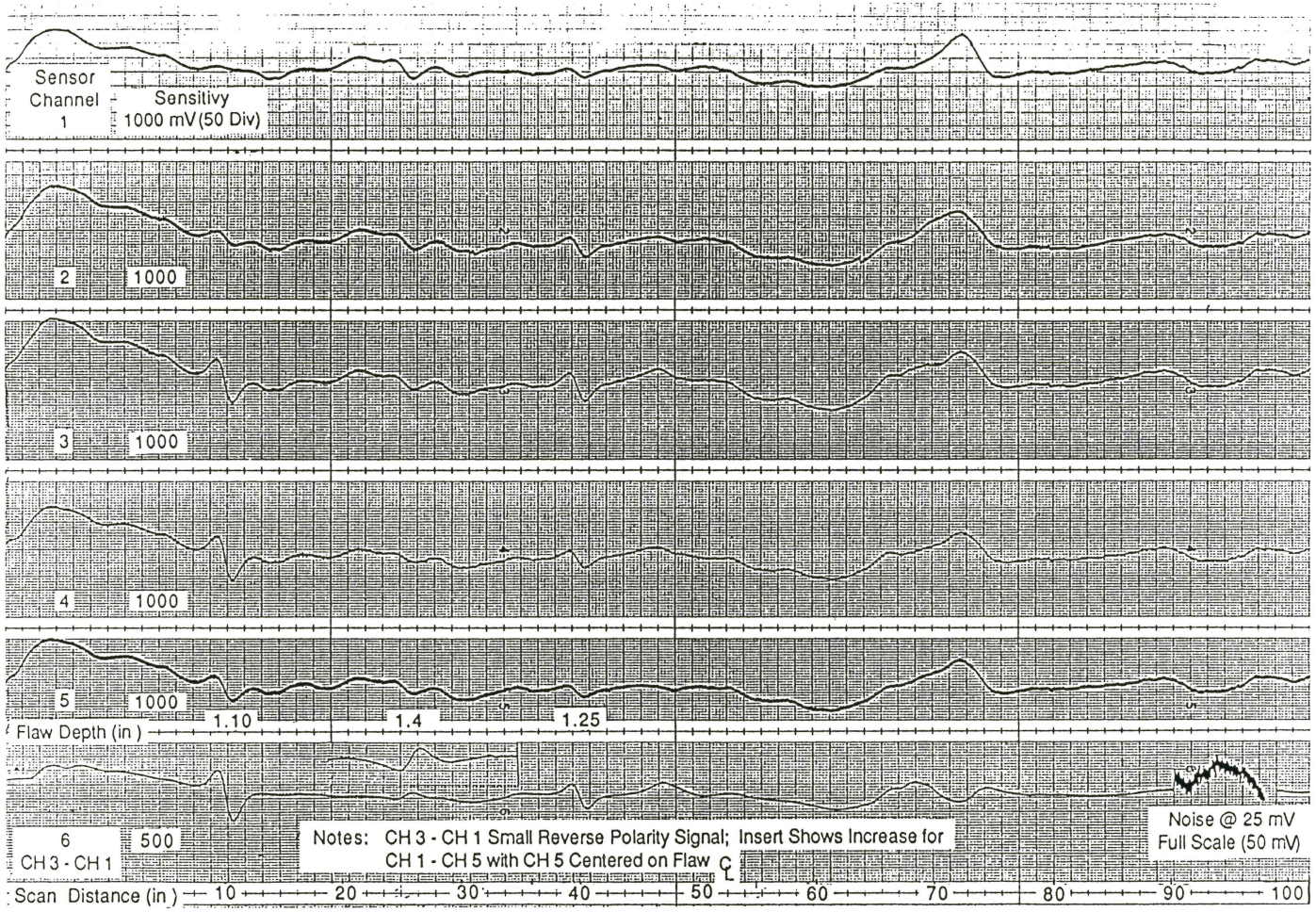

Figure 11. Signatures from flaw *(0.25-in gap in 0.25-in diameter rods)* at three depths *(Luling Bridge specimen)* obtained with prototype MPC.

On record 6 in figure 11, the peak to peak amplitude is 86 mV for the signature at 40 in and the "noise" (segment at 90 to 98 in) is only 3 mV or a signal/noise (S/N) ratio of approximately 30/1. Assuming a S/N=3/1, a flaw 1/10 the size of this 0.37 percent flaw (one fractured wire of the 271 total) or a 0.04 percent cross sectional area flaw could be reliably detected at a depth of 1.25 in! Alternatively, one 1/4-in diameter wire with fractured ends separated 1/4 in could be reliably detected at an estimated depth of 2.7 in with a S/N ratio of 3/1.

Many of the approximately sinusoidal undulations as well as the relatively large excursion at approximately 70 in are caused by movement of the rod bundle, since the electromagnet exerts a relatively high force on the individual rods as well as the wire bundle as a whole (approximately 300 lb at each magnet polepiece). Such anomalous movement would not have occurred if the rods had been under tension and encased with cement grout as would be anticipated for an actual cable.

Additional records indicating variability (caused by rod and specimen flexibility, construction and support constraints, etc.) and also detection of a somewhat larger defect at a greater depth, are shown in figure 12. The large flaw produced the prominent signals near the middle of all 8 records. The flaw was approximately centered beneath the channel 3 sensor, and this signal amplitude is about two times the amplitude of the channel 1 signal. The CH 4 - CH 1 records produce the signals near the middle of the bottom two records. Note the excellent signal-to-noise ratio and also that both signatures are nearly identical. The bottom record as well as the lower channel 3 record were obtained after rotating the specimen a complete 360°. After rotation, the channel 3 record contains several undulations and other features which were not present in the record immediately above. Note also that the characteristic signal shape is somewhat different and the negative peak (for the after-rotation record) is considerably changed. These features are attributed to the relatively loosely constrained bundle and movement of individual rods as well as the bundle by the rotation and also by the magnetic force of the scanner. Even with such specimen-associated difficulties, the CH 4 - CH 1 signatures at the bottom are nearly identical. A somewhat more prominent signature would have been produced if channel 1 had been subtracted from channel 3 rather than channel 4 because the channel 3 signature is larger. In practice the data processing system provides a variety of routines which would permit addition or subtraction of several channels and other combinations of data processing.

For the records in figure 13, the specimen was rotated to position the large flaw approximately beneath the channel 6 sensor (a record is not shown from channel 6 because channel 6 was used for a subtraction channel); this rotation resulted in the flaw being approximately 1.7 in from the channel 5 sensor and 1.9 in from the channel 4 sensor. None of the five records contains a signal that is easily recognized above the background features; however, a prominent, easy to recognize signal is obtained after subtracting channel 1 from channel 4 as shown by the bottom record.

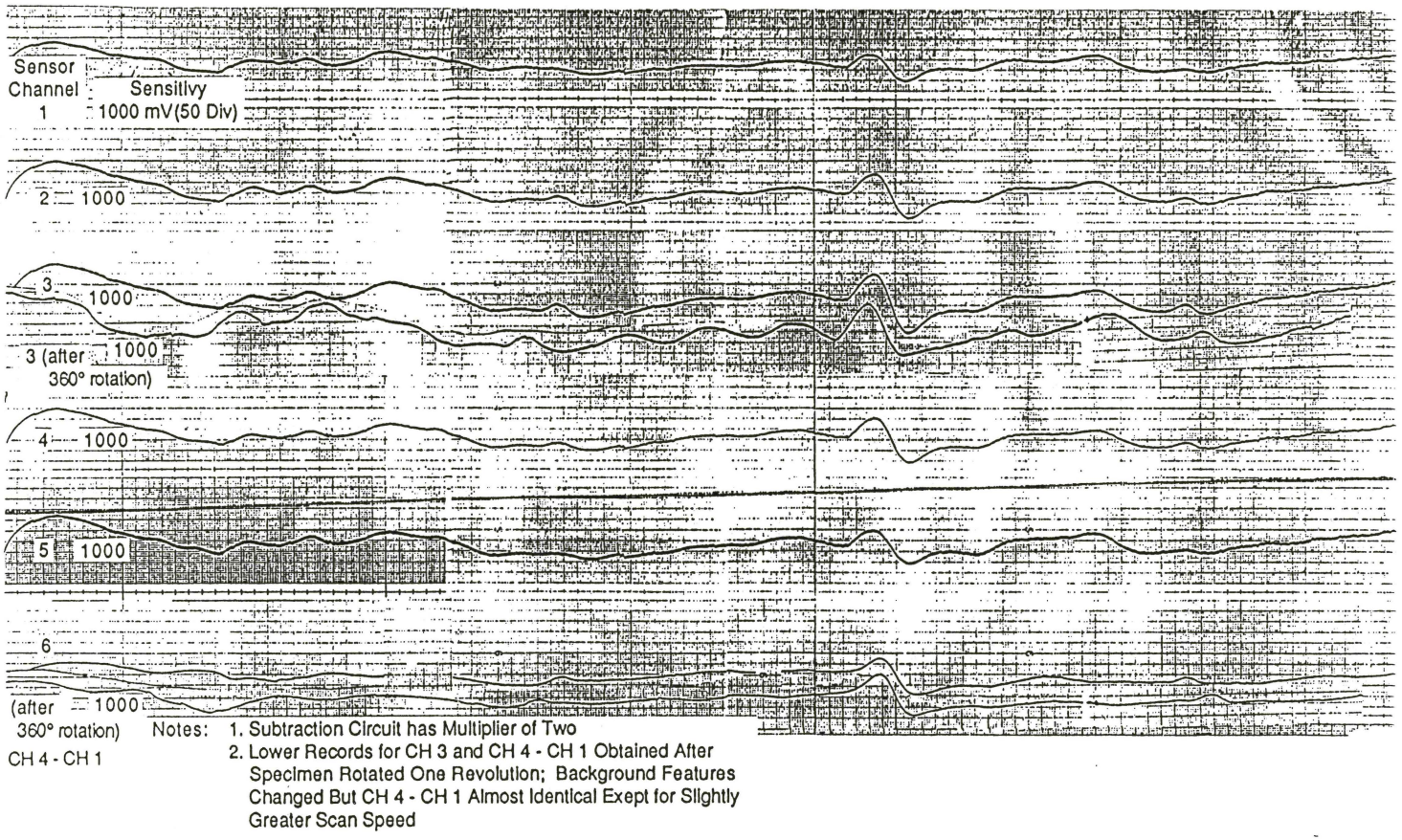

Figure 12. Signatures from flaw *(0.5-in gap in four 0.25-in diameter rods)* at depth of 1.69 in *(bottom record flaw S/N ratio > 24/1)*.

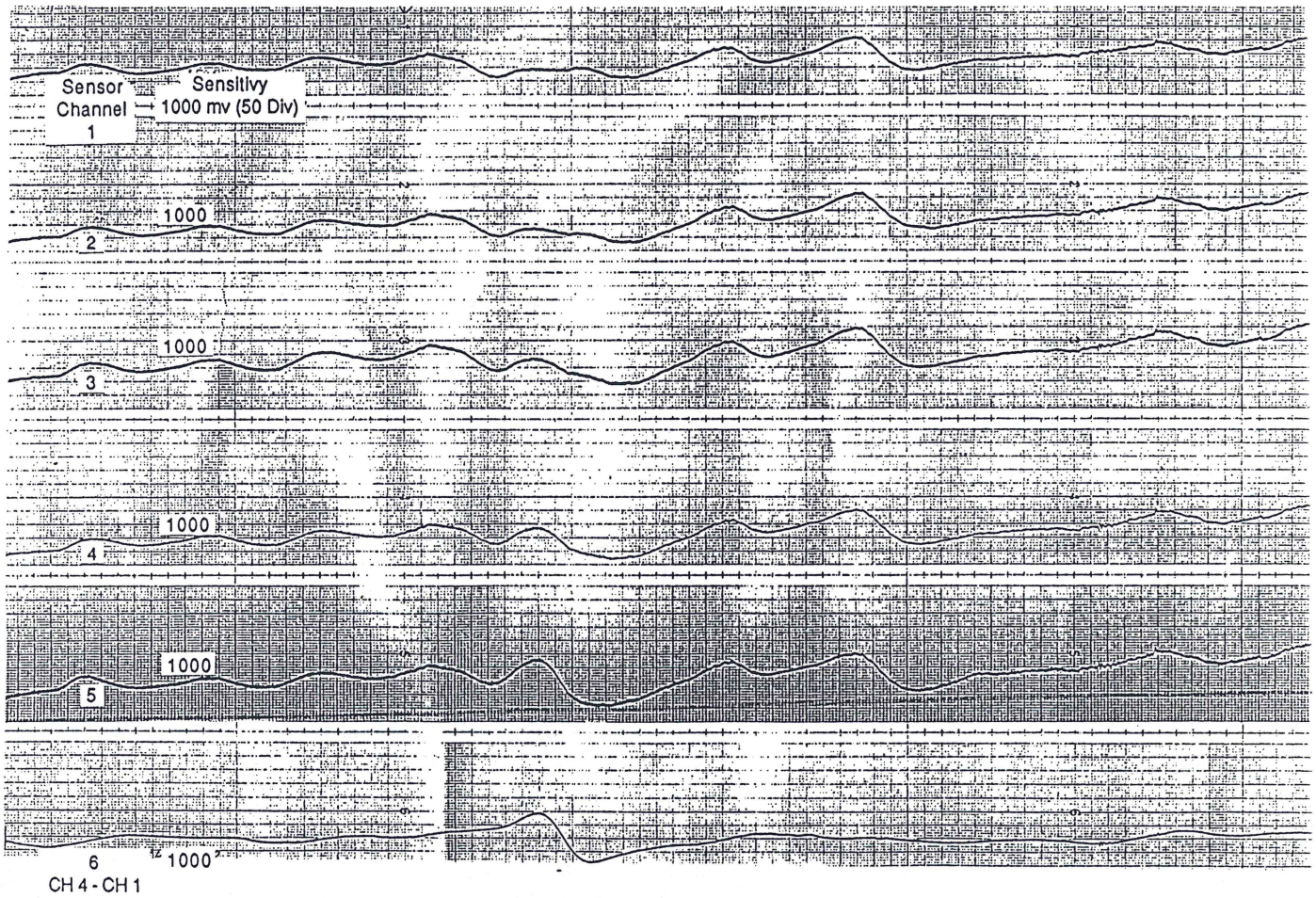

Figure 13. Signatures from flaw *(0.5-in gap in four 0.25-in diameter rods)* at depth of 1.90 in *(bottom record flaw S/N ratio > 24/1)*.

These and many other records were analyzed and estimates calculated to forecast the detection capability anticipated on the Luling Bridge stay cables and other cables. Results of these calculations are presented in table 1, along with previous estimates for comparison. Estimates have been made for several different diameter cables with a variety of protective coverings. Attention is called to the fourth column of data, since these estimates were originally presented in the proposal for this program and were based on data obtained with previous experiments but not on cable specimens. The third column of data are estimates after completion of most of the parametric investigations. These results were presented at the FHWA review (2 February 1988). The second column presents the estimates based on results from analyses of many records obtained with the prototype MPC system and exemplified by the records of figures 11, 12 and 13. It is emphasized that the estimates in the second column are not mere guesses but are based on engineering data; however, the investigation has not been comprehensive enough to permit development of specimens with sufficient rigidity and with enough discrete flaws at known locations and known sizes to completely verify these detection capabilities. While, it was anticipated for the Luling Bridge stay cables that these approximate detection sensitivities could be achieved provided such flaws existed in the cables that were scanned, magnetic background and system noise significantly limited flaw detection sensitivity. For larger diameter cables much larger and more powerful electromagnets would be required; also, for small diameter suspender ropes detection sensitivity would be significantly better than has been indicated for the 5-in diameter cables.

It is informative to consider the significance of these detection capabilities from the perspective of practicing professional bridge engineers. During the 1988 meeting of the Technical Advisory Committee for the Williamsburg Bridge, a brief review was presented of the research and the flaw detection capabilities anticipated for the cable NDE system being developed for the FHWA.[12] The consensus appeared to be that the flaw detection capabilities (one 1/4-in diameter wire with ends separated 1/4 in to a depth of approximately 1.0 in) would be of only marginal benefit since inspection of the total cable cross section was required. However, after further discussion, and in consideration of the very limited cable segments that could be inspected by the visual procedures, the engineer in charge of the extensive renovation program being conducted by Steinman Boynton Gronquist & Birdsall indicated - *that a system which could provide reliable detection of one fractured wire to a depth of one inch for extensive lengths of the cables would be very useful.* Wires in the cables are 0.196-in diameter, and the previous discussion of data on record 6 in figure 11 indicates that one fractured wire could be detected to a depth of approximately 2.7 in. In one scan a cable segment approximately 10 ft long by 4 in wide by 2.7 in deep could be inspected; this is equivalent to approximately 200 wires that could be examined in less than five minutes without removal of the spiral wire wrap. [A larger electromagnet would be required because of the greater cable diameter.]

Table 1. Estimated capabilities of magnetic method.

Cable Diameter (in)	Minimum Flaw Cross-sectional Area Detectable			Covering Thickness (in)	Wire Size Diameter (in)	Broken End Separation (in)	Depth (in) (d)
	Phase I Estimate (c)	Revised Estimate	Original Estimate*				
21/2		1%	1%	None	1/4	1/4	11/4
		0.02%		None	1/4		Exterior
5(a)		1.5%	3.5%	3/8 Plastic	1/4	1	21/2
		3%	7%	3/8 Plastic	1/4	1/2	21/2
	0.21%	-----	-----	3/8 Plastic	1/4	1/4	21/2
	0.1%	0.1%		3/8 Plastic	1/4	1/4	Exterior
61/4 (Luling Bridge)	0.37% 0.12%	-----	-----	(3/8 Plastic + 3/8 Cement Grout)	1/4 Pit (0.08 dia. x 0.08 deep)	1/4	31/8 Exterior
7(a)		3%-5%		1/4 Neoprene	0.12	0.2	31/2
(Portsmouth		0.05%		1/4 Neoprene	0.12	0.2	Exterior
Bridge)			0.03%	0.2 Wire Wrap	0.12	0.2	Exterior
15(b)		3%-6%	10%	3/8 Plastic	1/4	1	71/2
		0.1%		3/8 Plastic	1/4	1/4	Exterior
36(b)		3%-6%		0.2 Wire Wrap	0.196	1	8 in - 12 in
		0.1%		0.2 Wire Wrap	0.196	0.2	Exterior
			2.0%	0.2 Wire Wrap	0.196	4	18

(a) For the 5-in and 7-in diameter cable sizes estimates are based on experimental data obtained with the 200 lb electromagnet during parametric investigation.
(b) Much larger electromagnet required and confirmation of detection capability in the deep interior regions would require extensive experimental data beyond present parameter investigation.
(c) Based on experimental data obtained with prototype 10/25/88 and 10/26/88.
(d) Since system inspects 360° circumference, depth to cable center includes total cross section.
* From table 3-1, page 3-17 in Reference 11.

From this brief summary, it should be apparent that the prototype MPC system has exceeded, significantly, the proposed detection capabilities, and is in fact unique and greatly exceeds the capability of any other systems known to the principal investigators. This development incorporates the high sensitivity, excellent resolution, precise three dimensional location capability, long-term stability, and other features (appendix C) of the magnetic perturbation method with modern microprocessor control, digital communication, computer archival storage, and signal analyses routines, etc. into an integrated, advanced, state-of-the-art NDE system. Such a system is a key element that now makes it possible to apply modern structural lifetime assurance strategies to suspension bridge cables.

C. Summary of Phase II – Field Demonstration

As indicated earlier the bridge selected for the field demonstration of the MPC system was the Luling Bridge on I 310 across the Mississippi River at Luling, Louisiana, about 15 miles west of downtown New Orleans. The bridge was opened to traffic in October 1983, and the cable stayed main span of 1222 ft was a record for this type bridge in the U.S. Initially, the demonstration was scheduled to begin on 6 December and an alternate target date was 12 December 1988. It was not possible to make the 6 December date because of several desirable modifications; these included the addition of a stiff semicircular thin metal sheet approximately 10 ft long that was forced against the exterior of the polyethylene pipe and provided a uniformly smooth surface for the magnet support rollers during scanning. This "shield" was made of nonmagnetic stainless steel and provided a method to minimize the abrupt vertical motion of the magnet (and associated false signals) as the rollers traversed the polyethylene weld bead and other surface anomalies; in addition to provide reference signals for each scan small straight wire segments approximately 1/4-in long, aligned along the scan axis and centered on one of the sensor channels were imbedded on the top surface of the shield. These targets were located near the beginning of the scan, near the middle, and a third was located near the end of the scan; prominent reference signals were generated by these three targets on channel 3. As will be explained later, these reference signals proved to be very useful in the interpretation of the field inspection records.

In general the field demonstration was very successful; however, as is often the case with the first field use of a prototype system, a few difficulties were encountered. While it was not anticipated that there would be any broken wires in the bridge cables some unexpected and very interesting results were obtained and these will be described later.

The complete MPC system was transported by truck from Austin, Texas to the New Orleans area (12/11/88) and stored over night at the Louisiana Department of Transportation and Research (LADOTR) facility, and then moved to a maintenance facility near the bridge (12/12/88). A complete system check out, using a 6.3-in OD steel pipe fixture, and other preparations for the field demonstration were

completed on 12/12/88; demonstrations were initiated on 12/13/88 as shown in figure 14. Several views of data logging activities during the *first inspections ever performed on an actual cable* are presented in figure 15. Complete circumferential coverage requires five different inspection tracks (each with six data channels), at intervals of 72°. In figure 15 rotation to three tracks is shown, clockwise from upper left Track 3 or 0°, Track 2 or –72°, Track 1 or -144°. The power and instrumentation cable is attached to the lower end of the system, and the wire rope extending from the upper end of the system is attached to a "SKY-CLIMBER" at the top of the tower to provide auxiliary force that aids the self-contained drive system during movement along the cable. Also, this wire rope ensures that should a complete failure of the system occur the equipment will not slide down the stay cable. Two other views of the MPC system are shown in figure 16. In the upper photo, the system is approximately 70 ft along the cable and is in the 0° or track 3 position. One of the weld beads which protrude approximately 1/4 in above the surrounding surface can be seen on the top cable to the left of the system and several feet back down the cable. Also, by very close examination of the cable exterior bottom surface in a region several feet this side of the MPC system, an anomaly is observed in the otherwise cylindrical contour of the polyethylene pipe. Measurements of cable circumference by LADOTR indicated variations as much as 1 in from the nominal 19.8-in circumference at locations separated by only approximately 1 to 2 ft. Such increases were attributed to excess pressure during grouting, and also in fluid grout leakage past a "cured" interface.

A concrete truck is observed in the right lane and it was noted that each time a loaded concrete truck came onto the bridge a rather pronounced vibration occurred.

In the lower photo the system is approximately 130 ft up the cable and is in the 288° (or -72°) or track 2 position. At the left edge on top of the tower the man who operated the SKY-CLIMBER to assist in moving the MPC along the cable can be observed, almost. With the foregoing photos as a background a few inspection records will now be reviewed.

Approximately 70 scan sequences or 420 data tracks (each 100 in long) were recorded. Since these data sets were the first ever recorded from installed cables, it has been very difficult to develop analysis approaches which can provide an understanding of record features associated with possible cable details. From comparisons of many records along the cable length as well as around the cable circumference, several tentative correlations have evolved. Figure 17 will be useful in developing a basic understanding for the reader.

In figure 17 all six analog records have been reconstructed by the computer using the digital data recorded during actual scanning operations; such records can also be displayed on the operator's computer screen or an auxiliary TV screen

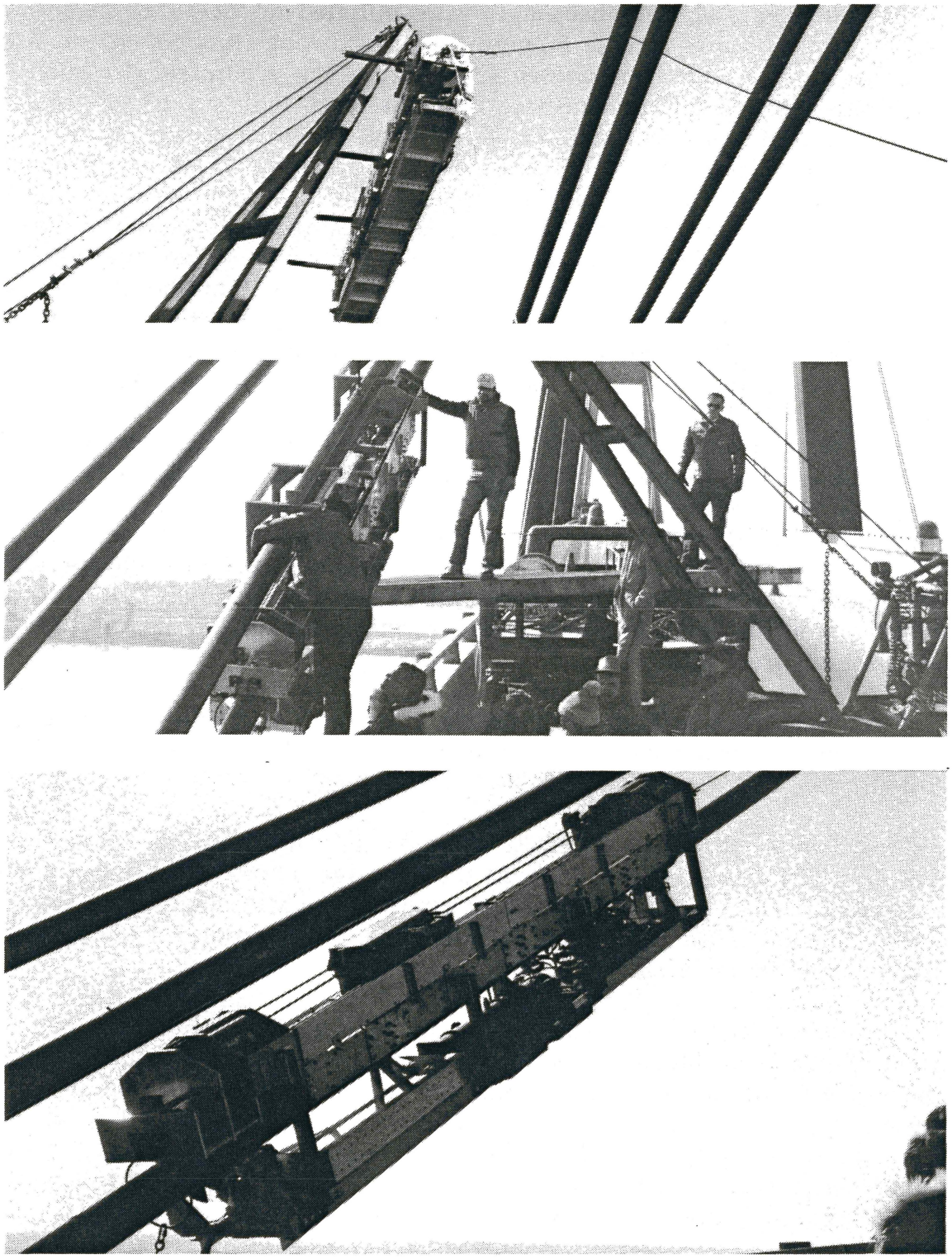

Figure 14. Views of MPC system inspection module attachment to Luling Bridge cable LN 3 on 12/13/88 for first field demonstrations ever conducted *(upper, support arms and clamp chains "open"; middle, "secured" and lifting fixture removal; lower, attachment "complete").*



Figure 15. Views of data logging activities on Luling Bridge *(Clockwise from upper left, inspection module in 0° position or Track 3 on 525 ft long stay cable LN 3; Track 2 or -72° position; Track 1 or -144° position; operators command, data acquisition-storage-processing-display computer).*

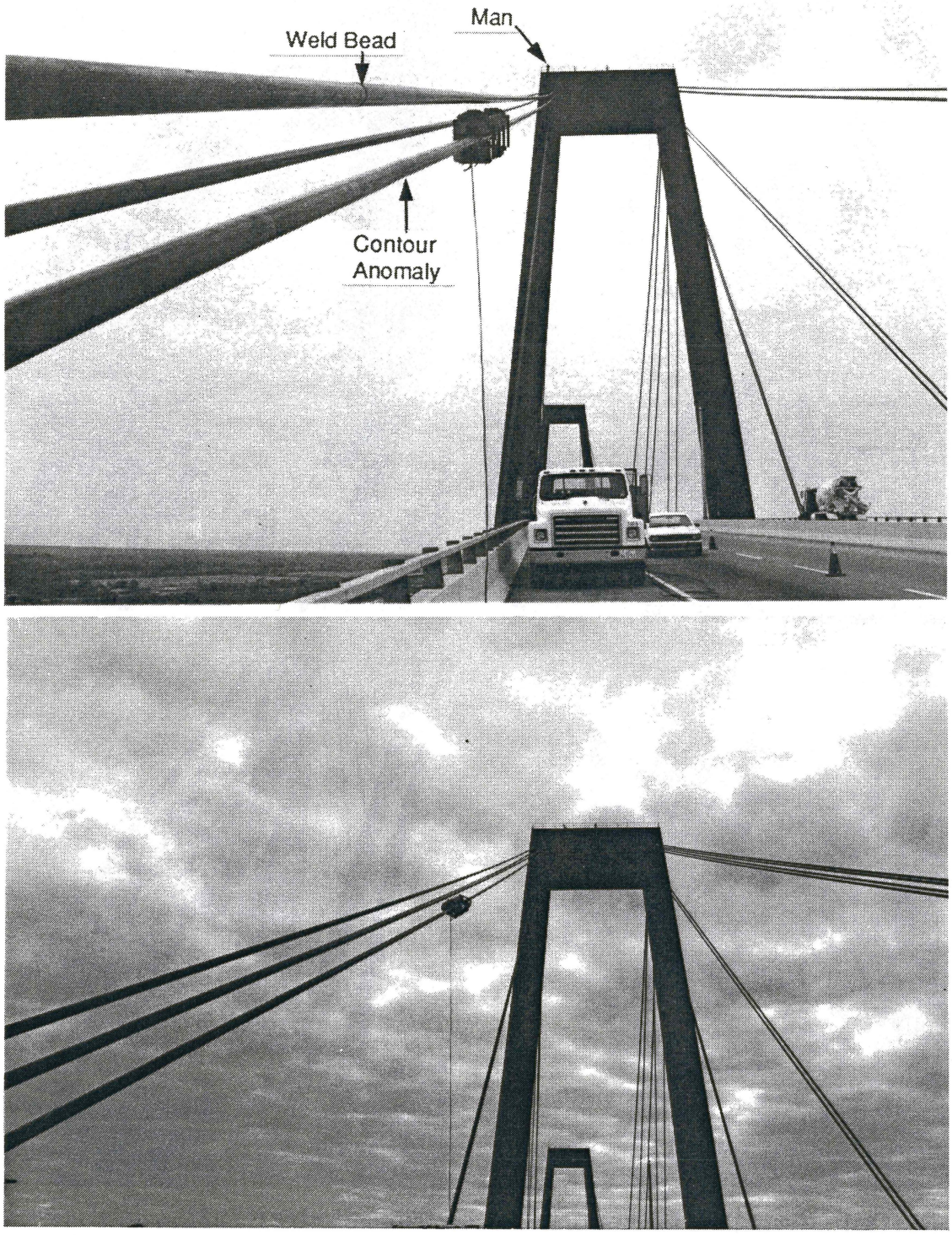

Figure 16. Data acquisition at approximately 70 ft, 0° position, Track 3 *(Upper)* and 130 ft, 288° position, Track 2 *(Lower)* cable LN 3, 12/14/88.

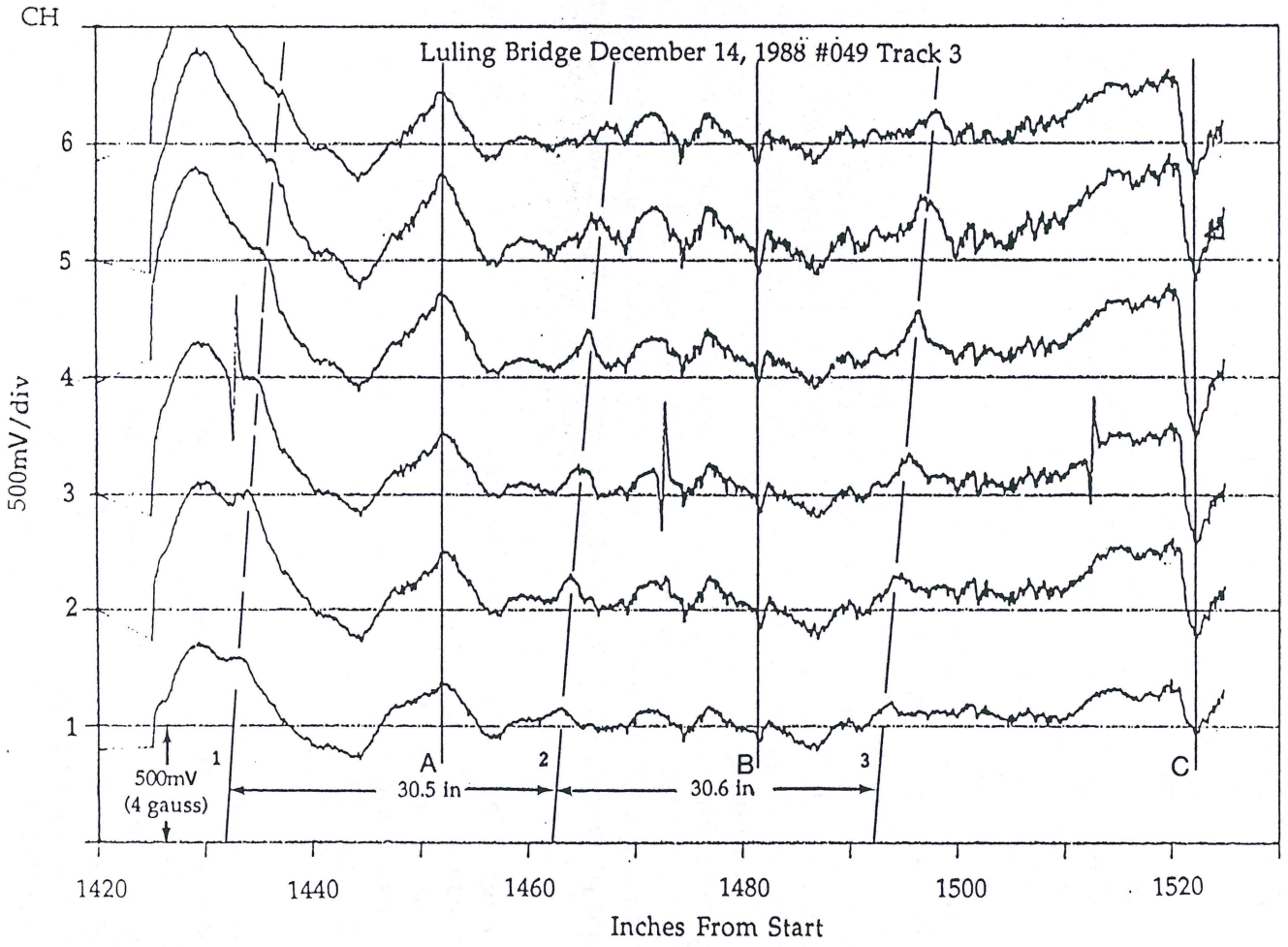

Figure 17. Typical analog records obtained during one scan of the Luling Bridge cable *(1/4-in diameter wire rope spiral wrap signals indicated by broken lines 1, 2, 3; other features occur simultaneously at solid lines A, B, C; note three reference signals on CH3).*

during the magent return sequence. All six records were obtained simultaneously along the cables and cover a segment approximately 4 in wide by 100 in long. These records are centered on top of the cable at the 0° reference or track 3 position; four additional similar sets of data acquired from tracks spaced at 72° intervals are required for complete coverage of the circumference. On channel 3, the downward going and then upward going signatures at approximately 1433, 1473, and 1512 inches are produced by the three target reference wires mentioned previously. Most of the features for example A, B, C and others are in direct alignment across the record; however, the somewhat nebulous features indicated by the broken lines 1, 2 and 3 are also aligned but at a slight angle across the record which corresponds to an angle across the cable. These "angled features" are observed on all track 3 records regardless of the location along the cable. These angled features become prominent in figure 18 after a digital point-by-point subtraction of channel 6 data from all five other channels was completed before reconstructing the analog records. This procedure eliminates features which occur simultaneously on all six records. (The subtraction routine is not perfect because of magnetic field variations across the record and also possibilities of minor differences in gain of signal channels.) Note the increased recording sensitivity of these records compared to those of figure 17. The distance along the cable at which these features reoccur is approximately 29 to 30 inches in these records. Only the upward going signal is angled across the records (cable); the downward going signal segment which is aligned across the records is not produced by the cable but is an artifact produced by subtracting the channel 6 data from all other channels. This downward going segment is inverted because channel 6 is subtracted and the position of each of these downward going signals would indicate the precise position of the original upward going signals on channel 6.

Since this angled feature is consistently observed throughout the cable length examined, it is reasonable to associate this feature with the 1/4-in diameter wire rope spiral wrap; however, the manufacturer's drawing indicated a pitch of 6 ft or 72 in for the spiral wrap while spacing of these features would indicate a pitch of approximately 30 in. Spacing of these signals along the cable ranges from approximately 25.0 in to 35.0 in.

Another observation which appears to be relatively consistent on records is that the reference signal increase is usually associated with a decrease in the "spiral wire rope signal". The records in figure 19 are useful in describing this observation. The 30 records in the left column were obtained at the same position along the cable and represent data from the complete circumference or for all five tracks spaced at 72° intervals. Such an array of data appears cluttered but this arrangement will be useful in the discussion that follows. There are several areas of "noise" on these records particularly from track 1 and track 4 in the region from 50 in to 100 in and for track 5 throughout the record, and this relatively high frequency noise is attributed to the instrumentation and will be explained later. In the left column of

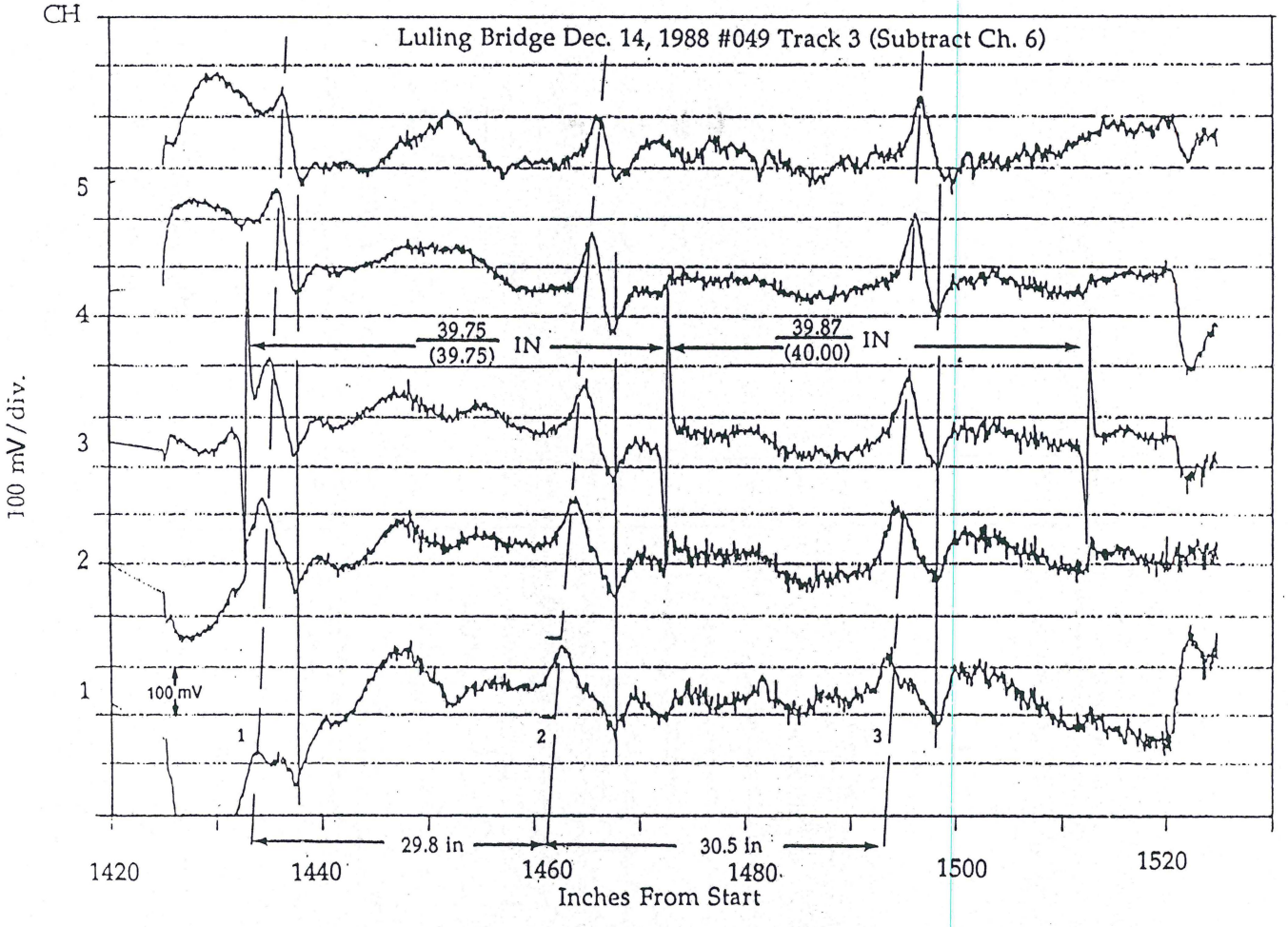

Figure 18. Typical analog records computer "reconstructed" after digital subtraction of CH 6 data from CH 1 thru CH 5. Note prominence of spiral wrap signals *(broken lines 1, 2, 3)*, artifacts caused by subtraction *(Solid vertical lines)*, and CH 3 reference signal separation *(Upper value from magnetic record and lower value tape measurement)*.

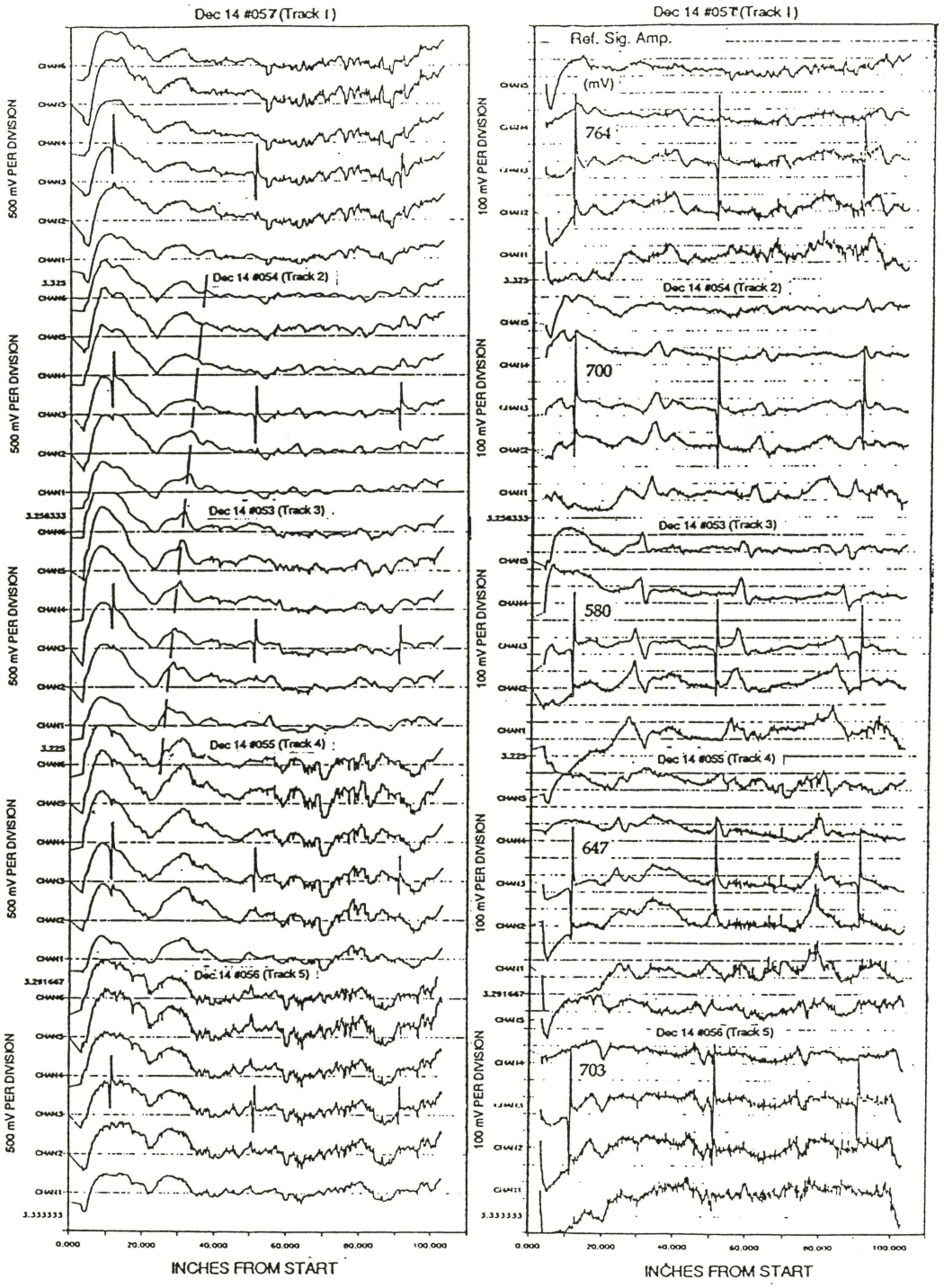

Figure 19: Array of records around circumference illustrating possible variation of grout coverage.

records there is an angled feature, although difficult to observe but indicated by a broken line, that extends from approximately 27 in on channel 1 of track 3 to approximately 33 in on channel 3 of track 2. The right column of records, obtained after subtracting channel 6 from each record, show prominent angled features for the track 3 records. These features extend almost completely around the cable circumference but with decreased prominence for the track 1 and track 5 positions which are located, symmetrically, on the bottom region of the cable with a separation of 72°. The reference signal amplitude from the first target ranges from 580 mV on track 3 to 764 mV on track 1 and 703 mV on track 5. These observed inverse changes of the reference signal in relation to the wire rope signal can be explained as follows. The prominence of the angled feature will increase with increases of flux density in the cable and the cable flux density will increase as the distance between the magnet pole pieces and cable decrease or in other words, as the reluctance of this air gap decreases. If this pole face to cable air gap increases the flux density in the cable decreases and, correspondingly, the angled feature amplitude decreases. However, the reverse is true for the reference targets which are imbedded in the stainless steel shield that rests on the polyethylene pipe. These reference targets are in the direct leakage path between the two pole pieces, and as the flux which enters the cable decreases (because the pole face to cable gap distance increases) more flux leaks directly from one pole to the other. This increase of direct flux leakage causes the signal from the reference target to increase. Therefore, these data indicate that the "magnet to steel bundle gap" is greater on the bottom (tracks 1 and 5) than the top of the cable, and probably indicate that there is more grout coverage in the bottom regions than there is on the top of the cable in the track 3 region.

Still a further perplexing observation on many of the records is presented in the records of figure 20. The photograph at the top shows the MPC system at a location approximately 130 ft up the cable which was the highest point examined during the demonstration. Numbers have been added at the approximate location for the array of six records below the photograph. The records extend from 920 inches in the left column to 1520 inches in the right column; no record is included for the 1220 in interval since, inadvertently, records were not reconstructed with these scales, but record features were similar to the 1120-in interval. The records at 1420 in show two major undulations in addition to the usually observed excursion near the beginning of most records. The wire rope signal is very prominent and these angled wire rope features appear to be somewhat synchronized with the three vertical excursions; for the 1120-in records and the left part of the 1320-in records a similar observation can be made. In regions where these undulations are observed the wire rope signal is near the "node" and has never been near the "crest". A possible explanation for these features is that grout coverage is so incomplete in these regions that the attractive force of the magnet poles (approximately 300 lb at each pole) could be moving several wires between the anchorages (nodes) provided by the wire rope spiral wrap.

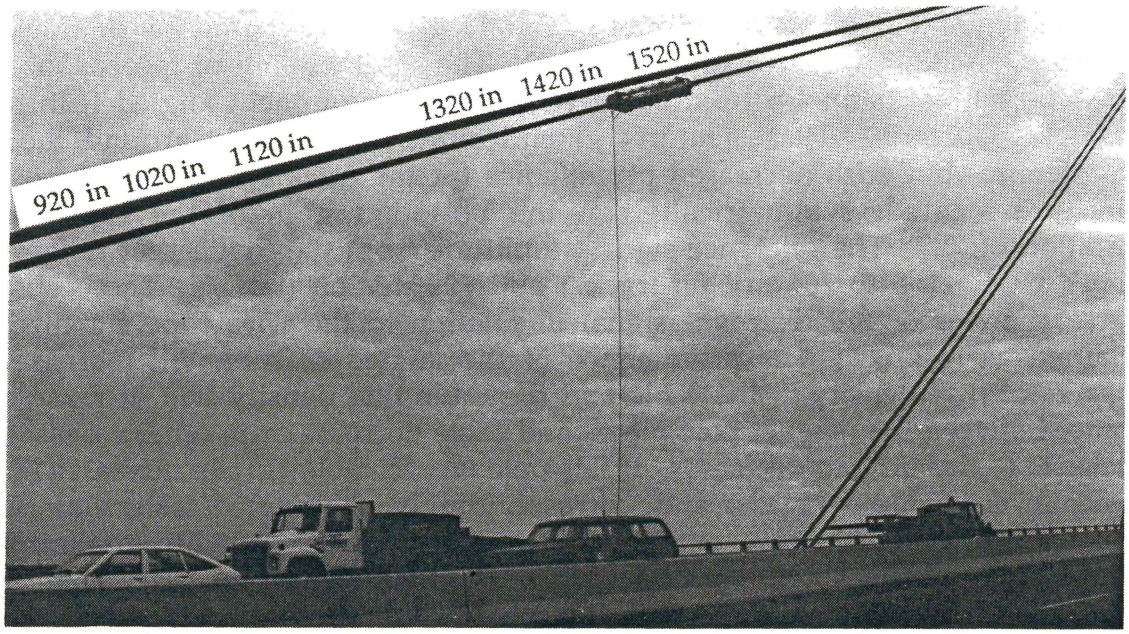

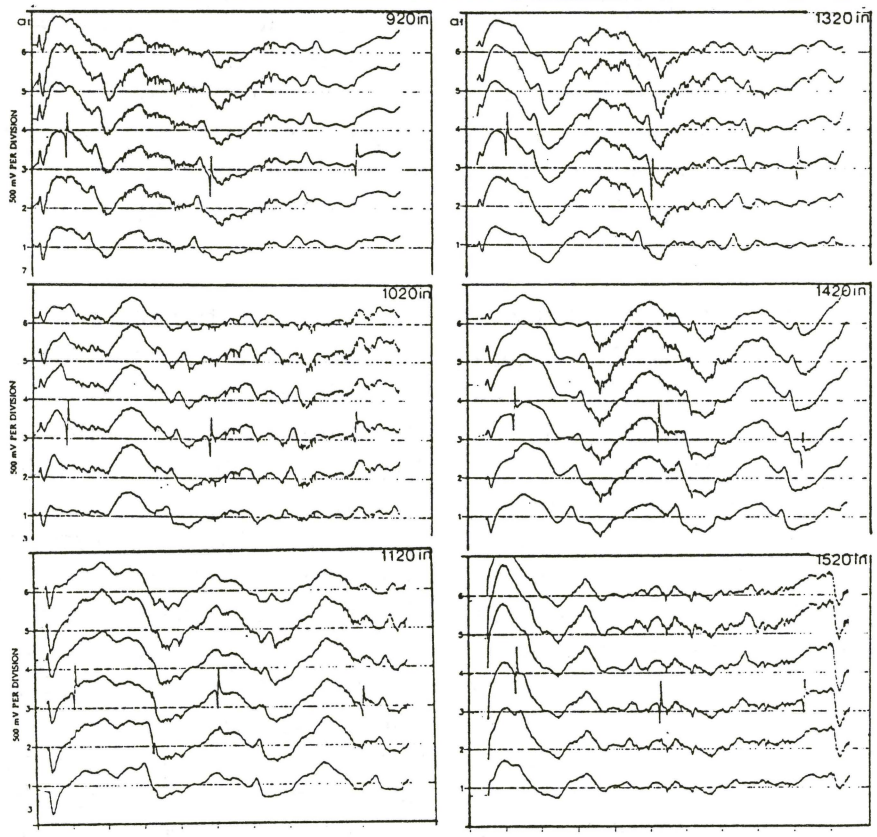

Figure 20. Sequence of records selected to illustrate the possibility of grout coverage variation on 0 or top region of cable *(Note:major background excursions and also prominence of spiral wrap signals for records @ 1420 in; background excursions, all records track 3; data sequence @ 1220 in not included).*

II. PARAMETRIC INVESTIGATION

A comprehensive set of experiments was outlined to provide data for determining the relationship between the various parameters that govern magnetic perturbation flaw detection (see figure 10 and appendix C) and also to provide information for the prototype equipment design. Because of unanticipated difficulties caused by: local magnetic anomalies in the steel pipe; run out of support rollers and associated background noise which obscured low amplitude signals from flaws, low flux density and associated low amplitude signals even from large flaws located at depths greater than approximately 1 in, etc.; it was not possible to obtain useful data from most of the scheduled and completed experiments. Eventually, after several corrective actions (which included use of an aluminum pipe to replace the steel pipe, increasing the current in the electromagnet by a factor of two, scan assembly modifications, filtering corrections, etc.) enough valid data were obtained to justify continuation of the prototype design and fabrication.

The following paragraphs summarize the parametric investigations.

A. Specimens

As experience has shown, a crucially important factor contributing to the success of NDE investigations is the availability of test specimens that are realistically representative of the inspection applications under consideration. For this program, choice of specimen is even more important because of the very limited resources which could be allocated for parametric investigations in the laboratory. The fact that most suspension bridges have structural cable and rope details that are unique to each bridge also greatly compounds the difficulty of selecting specimens as well as flaw configurations. From preliminary analyses it was determined that one of the most difficult problems would be obtaining adequate magnetization to permit reliable detection of relatively small flaws in the interior regions of main cables. To minimize this "already difficult problem," an intermediate diameter cable, approximately 15 inches in diameter, was selected and for the several reasons previously mentioned, the diameter was subsequently reduced to approximately 6.0 in. It would have been desirable to include a spiral wire wrap on the exterior of the parallel wire cable specimen (as shown in figure 7); however, it was anticipated that several different flaw configurations would be required as the program progressed. With a spiral wrap construction, removal and reinsertion of a variety of flaw configurations at different depths and at different longitudinal locations would be extremely difficult, and furthermore an auxiliary method of supporting the cable specimen would be required. The use of a steel pipe was selected as a reasonable compromise between realistically representing a cable segment and the utility required for the experimental investigation and additionally would be approximately within the cost allocations for this specimen effort.

In practice several flaw configurations were inserted as the straight lengths of wire (rods) were positioned in the pipe. A flaw was "constructed" by separating the rod ends using an aluminum plug, and then the flaw region was wrapped with vinyl tape to maintain the plug and rod ends in a fixed position. For larger flaws two or more individual rods were separated by plugs, then several additional rods were assembled around the flaw region, and the entire bundle was maintained as a unit by wrapping with vinyl tape. In those cases where the experiment required a flaw located in the interior regions of the cable several rods were assembled around the flawed rod in a symmetrical bundle, and the entire bundle secured with vinyl tape; when a large near surface flaw was required the rods in an approximate 180° sector were omitted from the bundle assembly. To facilitate build up of the cable, a longitudinal cut was made through both walls to separate the pipe into two halves. Rods could then be placed in the pipe and maintained in an orderly array without becoming skewed or crossed.

Figure 21, is a photograph of the steel pipe supported by rollers mounted on platforms, and a supply of steel rods is shown on the floor. In figure 22 the steel pipe-parallel wire (rod) specimen for one of the experimental arrangements is shown in an early state of assembly. Other views of selected steps in the steel pipe-parallel rod cable construction are shown by the photographs of figure 23.

This type construction proved to be a judicious choice since many difficulties were encountered in detecting flaws and it was necessary to disassemble and reassemble the specimen many times during the investigation. Although prominent signatures were produced by flaws at the interior surface of the steel pipe, even very large flaws could not be detected above the magnetic background produced by the steel pipe when the flaw was located at depths beyond approximately 1.0 to 1.5 in.

To eliminate the background signals caused by the steel pipe, an aluminum pipe was substituted for the steel pipe. Several views of this aluminum pipe-parallel wire specimen are shown in figure 24. In the upper view note the significant sag of the pipe produced by the weight of the 370 rods and the weight of the scanner and magnet assembly. Nonmagnetic stainless steel bands were used to force the upper and lower halves of the pipe together and these were located beyond the extremities of the scan.

Experiments were also conducted with the aluminum pipe-suspender rope specimen shown in figure 25. A few rods were nested alongside the suspender rope to minimize the air gap caused by the 0.28-in thick wall of the aluminum pipe supporting the suspender rope, and these rods made it possible to achieve a somewhat higher flux density in the suspender rope. The socket extends beyond the aluminum pipe and was supported by a hoist. This particular cable was one of

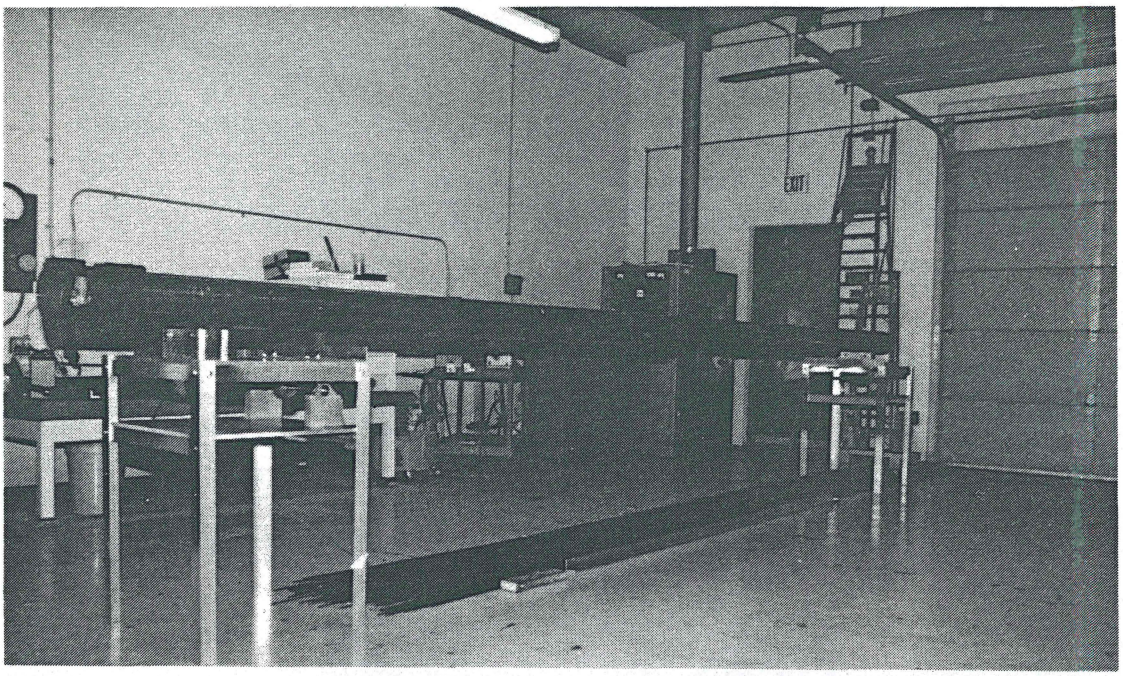

Figure 21. Steel pipe 20 ft by 6.0 in I.D. by 0.28 in wall; 20 ft by 0.25 ft by 0.25 in diameter cold drawn ASTM 1018 steel rods.

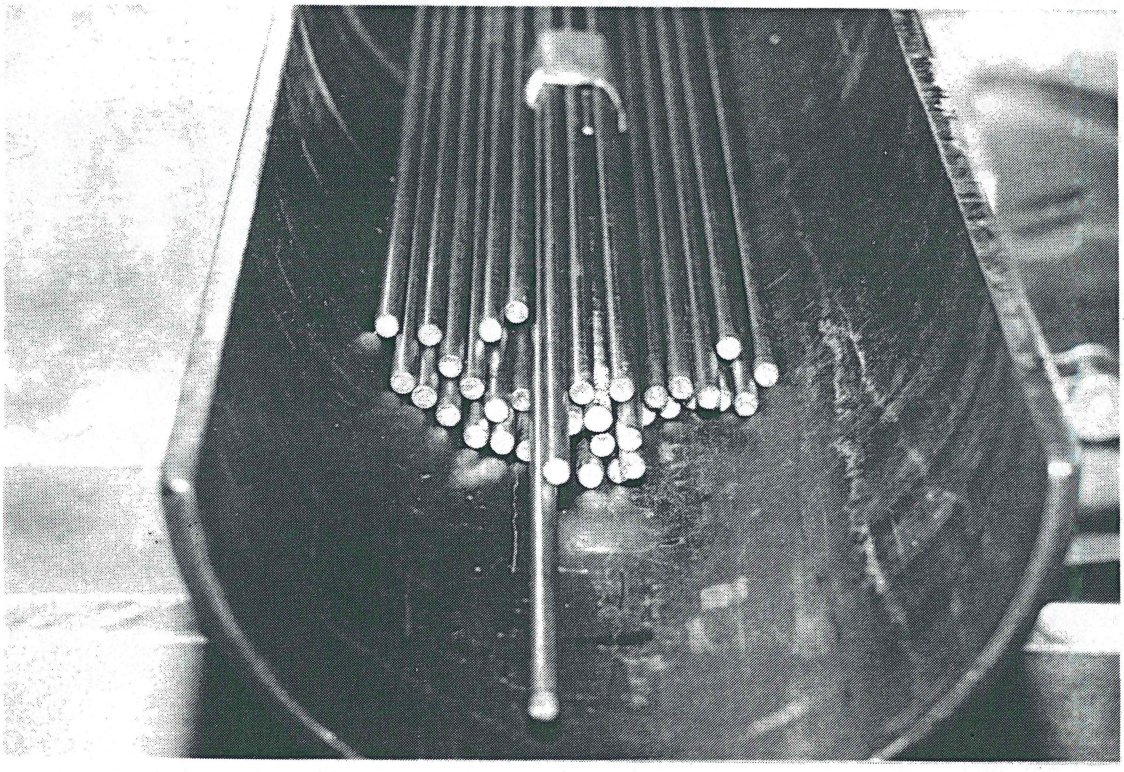

Figure 22. Steel pipe-parallel wire *(rod)* specimen for parametric investigation.

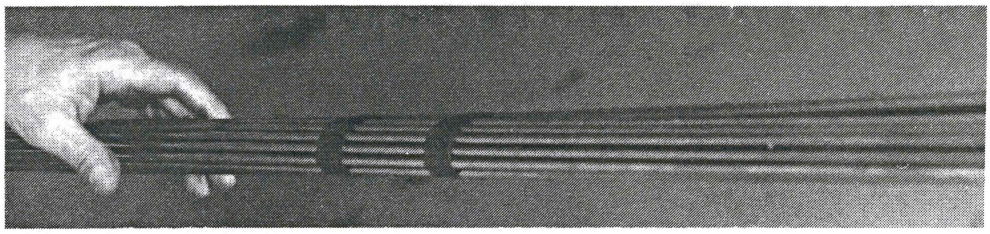

Typical flaw "bundle" with ends separated on interior rods to simulate flaws.

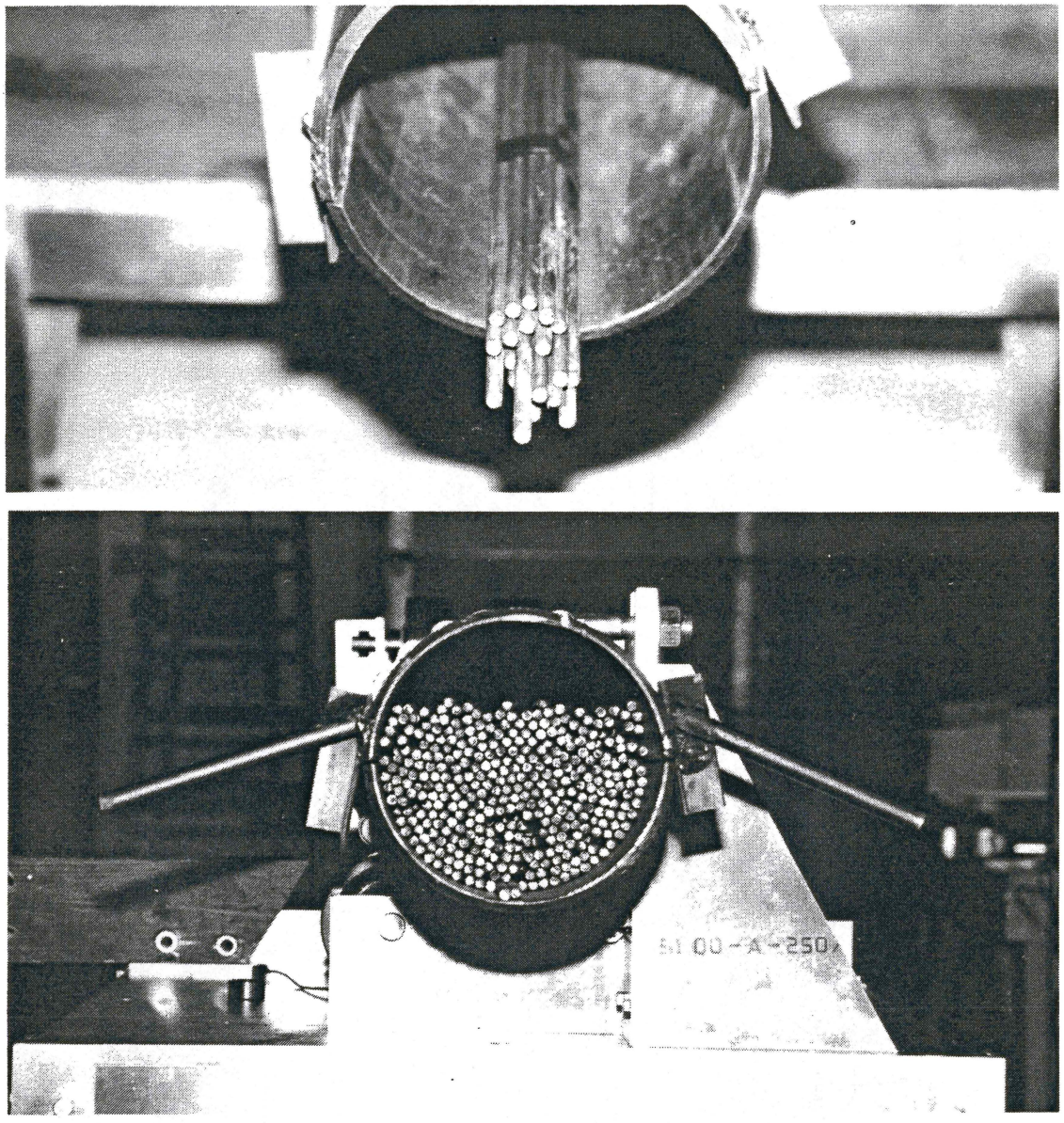

Figure 23. Views of steel pipe-parallel wire specimen with flaw bundle only *(Upper)* and with 370 rods *(Lower)*.

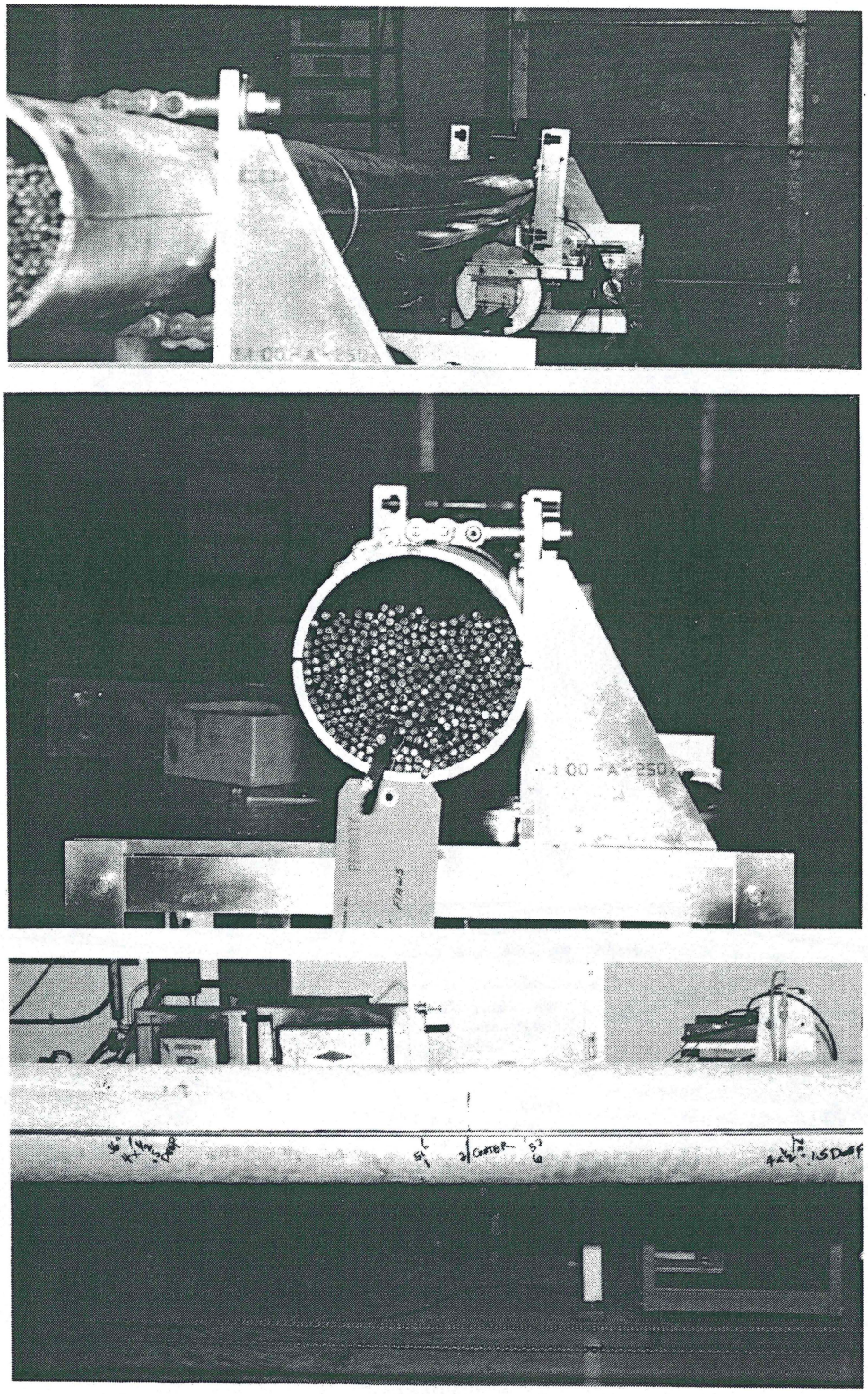

Figure 24. Views of aluminum pipe *(20ft by 6.0 in I.D. by 0.28 in wall)* parallel wire *(rod)* specimen.

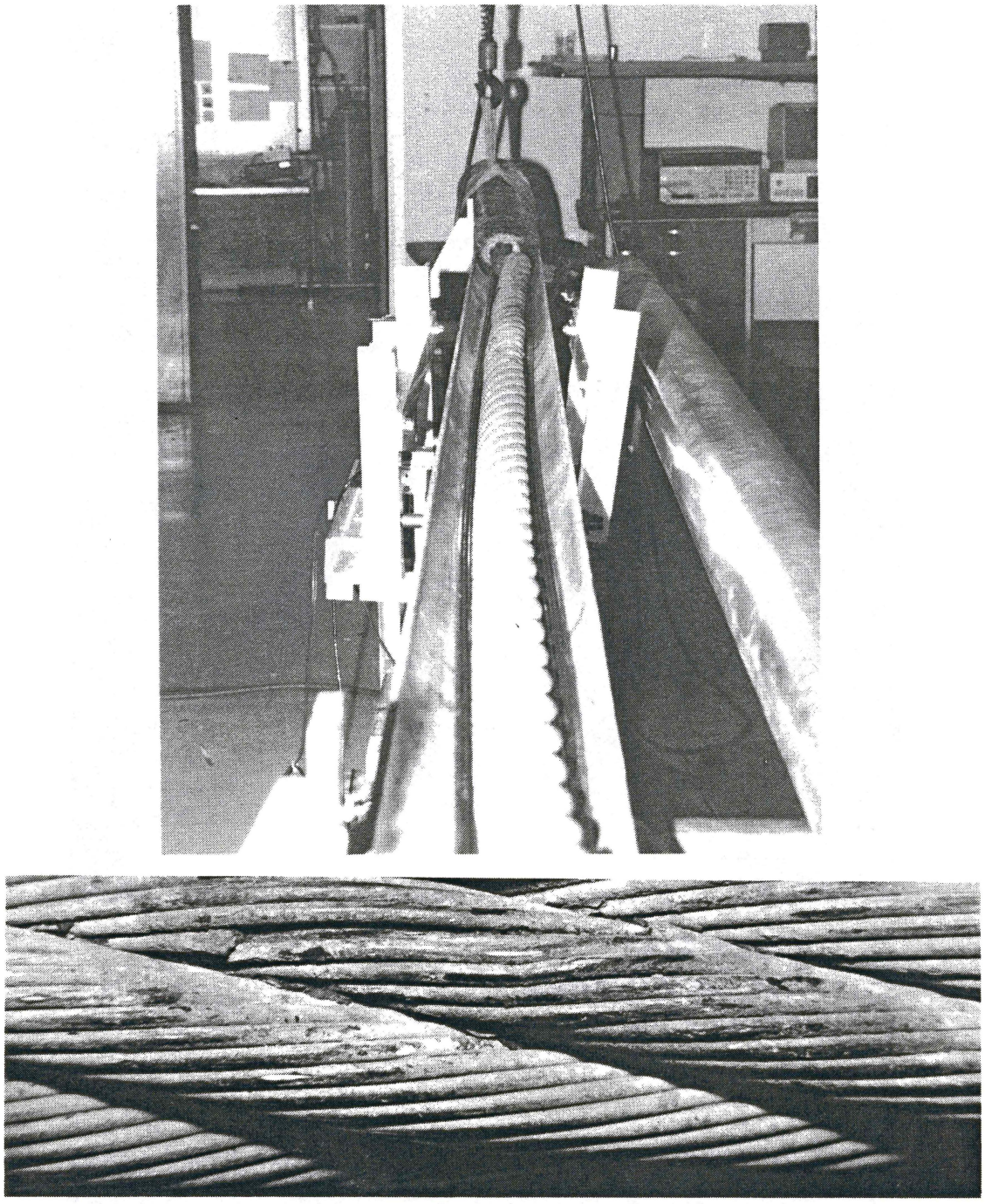

Figure 25. Aluminum pipe-suspender rope specimen *(Upper, 2 11/16-in diameter suspender rope with socket removed from the Golden Gate Bridge; lower, broken wire 0.14-in diameter with missing segment 2 3/4-in long detected during magnetic experiments).*

several obtained from the Golden Gate Bridge Highway and Transportation District and was residue from a recabling effort and contained a single broken wire as shown in the lower photograph.

A variety of flaw configurations located at selected depths in the cable specimen were used in the parametric investigation. The flaw schedule of table 2 assigns a number to each flaw configuration and also provides other information describing the flaw. The flaw number will be useful in a review of the experimental results. Also, the cross-sectional sketches in figure 26 indicate the location and number of flawed rods for several of the specimens used in the investigation. The numbers identify the flaws as described in table 2.

B. Rudimentary Scanning Assembly

After selecting a cable diameter it was possible to initiate design and subsequent purchase of the electromagnet; also design of the assembly to support the electromagnet and permit a scan motion along the length could be initiated. Several views of the scanner assembly are shown in figures 27 and 28. The lower photograph in figure 28 is a view of the scanner system control, data processing, and data display station. The scanner was moved at selected speeds by a stepper motor in response to selections made by the operator using the keyboard. Direct current for the electromagnet was provided by a power supply which was manually adjusted for the desired current.

C. Data System

The data system is illustrated schematically in figure 29. The primary sensor was a Hall effect probe attached to the magnet assembly and positioned near the surface of the cable and centered between the pole pieces of the electromagnet. The probe was connected to a F. W. Bell, Model 620, Gaussmeter. The probe and gaussmeter electronics were calibrated using a null chamber and calibration magnet.

The output of the gaussmeter, a DC signal between -10V and +10V, was connected to the input of a Data Precision D6000 Wave Form Analyzer. The D6000 was used as an A/D converter and data buffer. Data acquisition was synchronized to sensor position, along the cable, by triggering the sampling process using external clock pulses provided to the D6000 by a rotary pulse generator and pulse divider. The pulse generator was coupled directly to the shaft of the stepper motor used to drive the magnet assembly along the cable.

At the end of each scan the data for the complete scan were transferred to a HP Vectra computer for display, analyses, and storage. The data were stored on hard disk, displayed on the computer screen, and plotted on a HP 7475 plotter. Data regarding test date, test circumstances, etc. were included on the plot and were included in the header of each stored file.

Table 2. Flaw schedule.

FLAW (number)	LOCATION (inches)	CROSS-SECTIONAL AREA (%)	DEPTH TO CENTROID FROM PIPE I.D. (inches)	DEPTH TO CENTROID FROM MAGNET (inches)	DESCRIPTION	TYPE
1	28	0.01	-0.025	0.35	Flat Bottom Holes Drilled In Pipe: 0.063 in Diameter, 0.050 in Deep	Inside
2	32	0.01	-0.255	0.12	Flat Bottom Holes Drilled In Pipe: 0.063 in Diameter, 0.050 in Deep	Outside
3	36	0.41	0.48	0.85	Gap In 2 Rods; 0.78 in Deep	1/2 in
4	52	0.09	0.08	0.45	0.10-in Saw Cut Gaps In 1/2-in Diameter 7 Wire Reinforcement Strand	1 Wire
5	55	0.18	0.08	0.45	0.10-in Saw Cut Gaps In 1/2-in Diameter 7 Wire Reinforcement Strand	2 Wires
6	58	0.55	0.25	0.62	0.10-in Saw Cut Gaps In 1/2-in Diameter 7 Wire Reinforcement Strand	6 Wires
7	72	1.45	1.65	2.02	Gap In 7 Rods	1/2 in
8	79	0.01	-0.025	0.12	Same As Flaw 2	Outside
9	82	0.01	-0.255	0.35	Same As Flaw 1	Inside
10	36	0.83	0.50	0.87	Gap In 4 Rods	1/2 in
11	72	0.83	1.44	1.81	Gap In 4 Rods	1/2 in

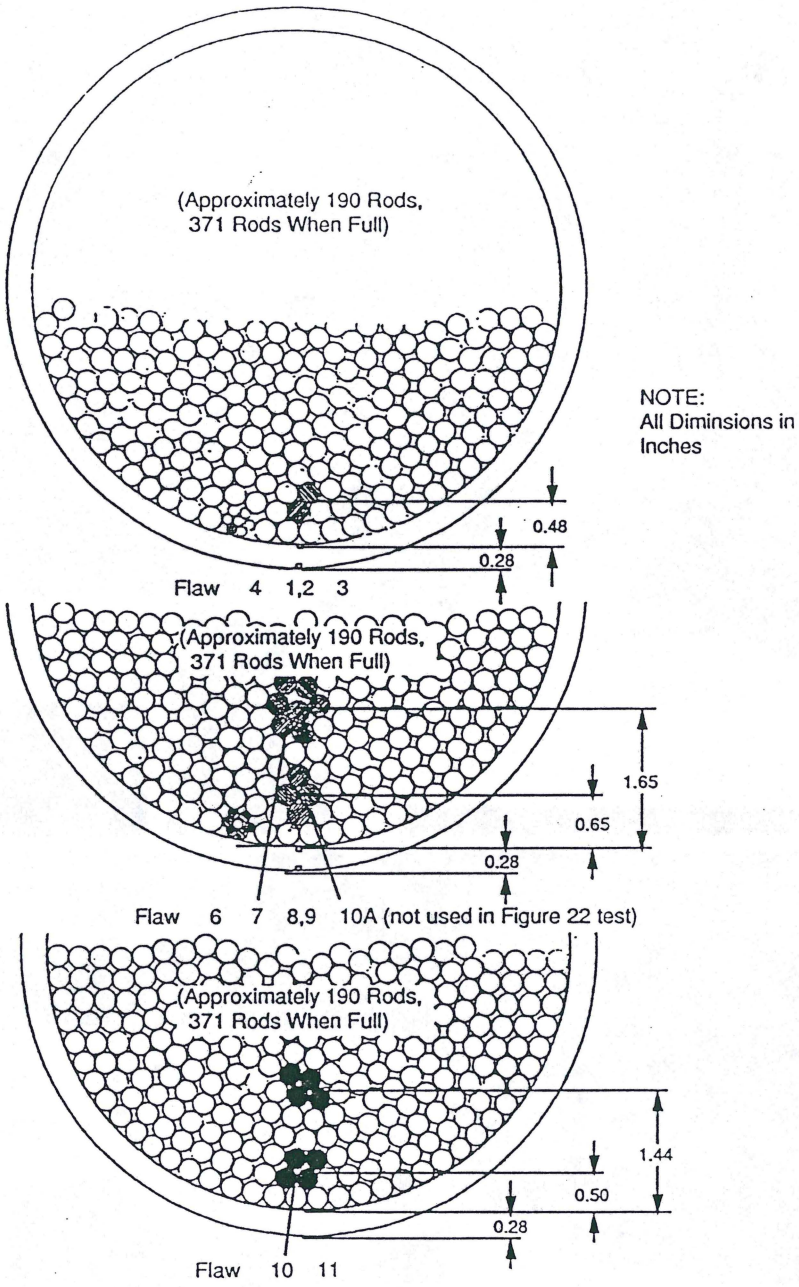

Figure 26. Flaw configurations used in steel pipe *(upper two sketches and Figure 31 records)* and aluminum pipe *(lower sketch and Figure 32 records).*

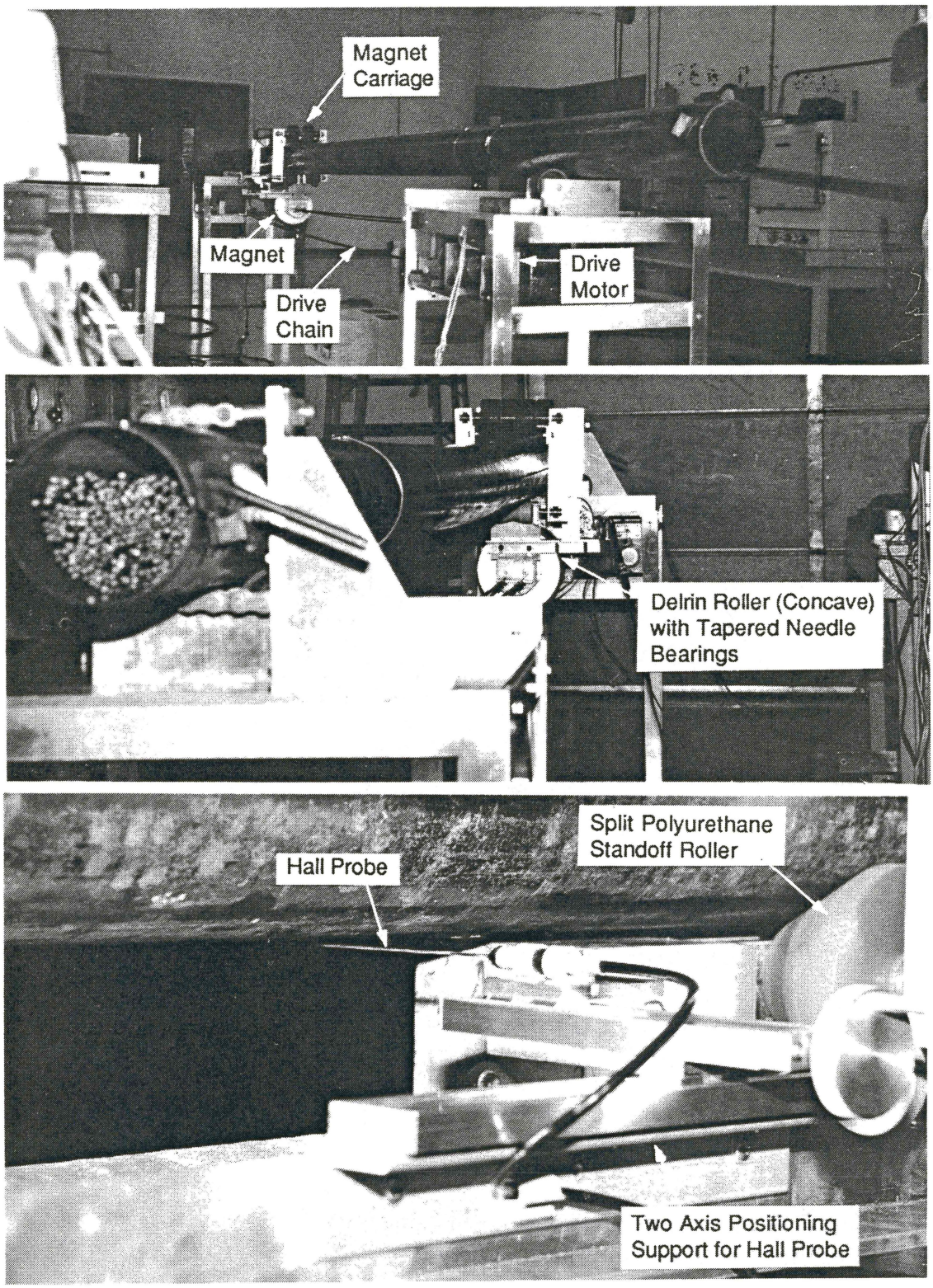

Figure 27. Several views of laboratory scanning equipment.

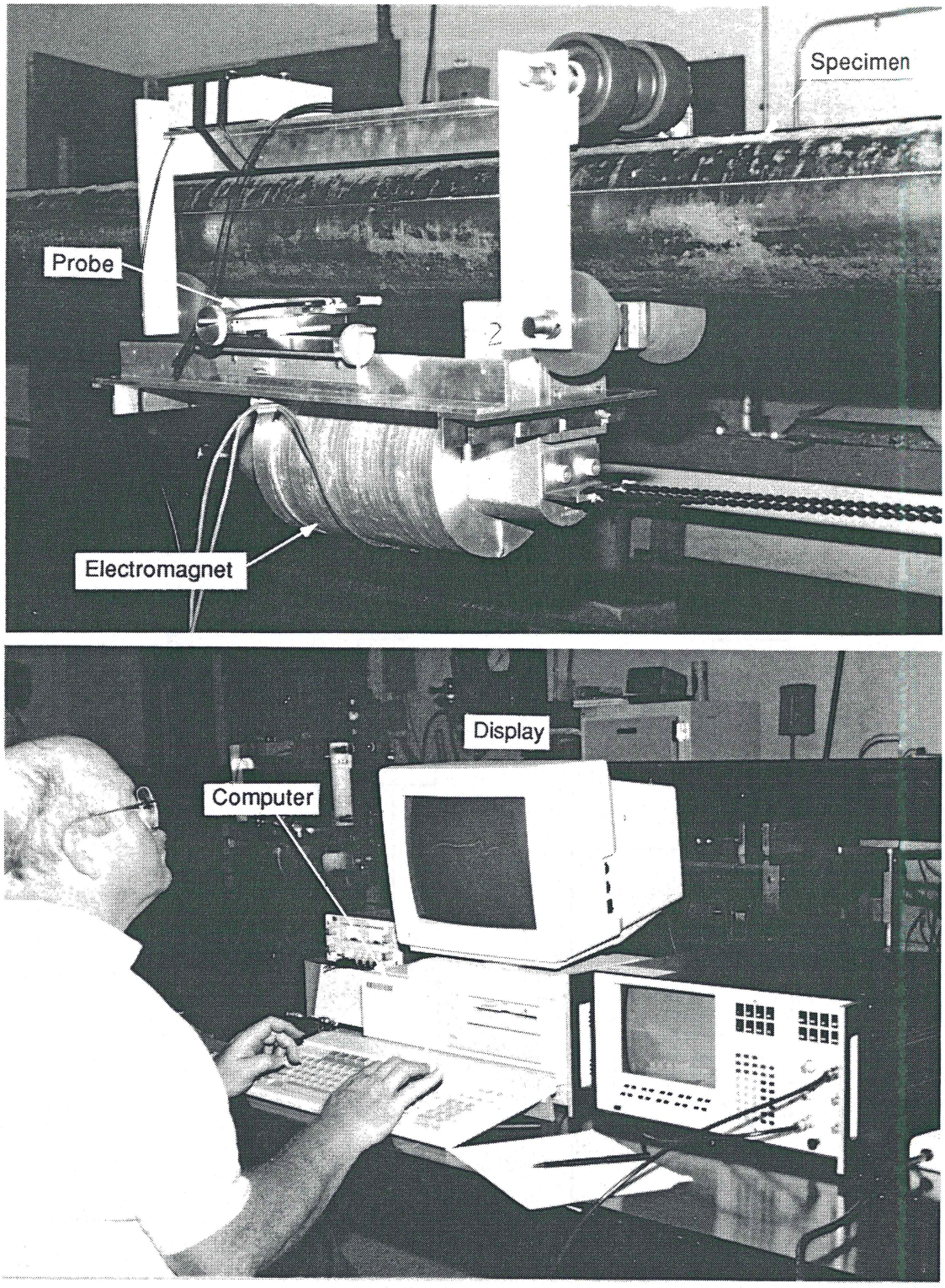

Figure 28. Photographs of the laboratory scanner and computer controls.

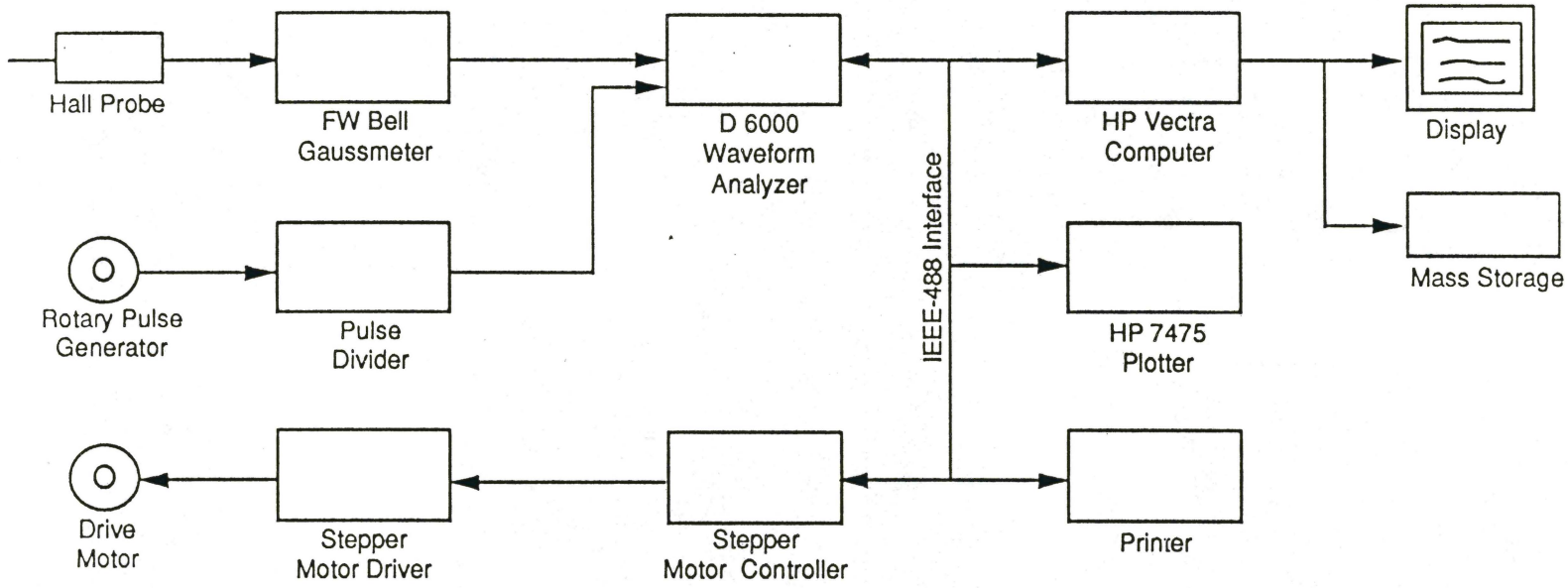

Figure 29. Data collection system.

All communication between the Vectra computer and external devices was via an IEEE 488 interface. In addition to data acquisition tasks, the interface was used to control the stepper motor used to drive the magnet assembly along the cable. The operating program was written in BASIC and, through prompted operator interaction, controlled all aspects of the scanning, data acquisition, and data display and storage.

D. Experimental Results

As indicated at the beginning of this section, significant difficulties were encountered during the parametric investigation and several records will be reviewed which illustrate the detection capability as well as some of the sources of difficulty. Figure 30 presents four records to illustrate flaw signatures and the influence of the flux density on the characteristic shapes of the signatures. All records were obtained with a magnet current of 10 amperes and the flux density was varied by varying the number of rods inserted into the pipe. For the upper record a single 0.25-in diameter rod with a 0.25-in long gap was inserted into the 6.0-in I.D. steel pipe. Distance from the magnet pole pieces and the probe is slightly more than 0.4 in. With this arrangement a prominent signature is produced with characteristics similar to those predicted by theory, namely, bipolar with negative and positive peaks equal; however the peak separation is approximately 1.0 in rather than being approximately 0.4 in. After 20 additional rods were inserted into the pipe and nested around the flawed rod the second record was obtained. Peak to peak amplitude has increased slightly even though the cross sectional area of the steel has increased from 5.57 in^2 to 6.55 in^2; furthermore, the signal characteristic is more nearly identical with that predicted by theory and the peaks are now separated by only approximately 0.5 in. The flaw size is only approximately 0.7 percent of the total steel cross section. The more extended horizontal interval of the upper signature compared to the second signature can probably be attributed to the magnetic poles induced by the gap in the rod being somewhat more distributed with the single rod, than when magnetic material completely surrounds the flawed rod as in the case of the second record.

The two lower records in figure 30 were obtained with the same flaw configurations at 36 in and 72 in. In the third record both flaws produced relatively prominent signatures although amplitude of the flaw at 36 in is almost the same amplitude as the undulations between 40 to 60 in and also 80 to 105 in. For this experiment only 170 rods were inserted into the pipe.

The lower record in figure 30 was obtained after adding an additional 200 rods for a total of 370 rods. Because of the much lower flux density in the specimen, only the flaw at 72 in (0.78 in deep) can be resolved from the other undulations on the record. Overall amplitude of this signature has decreased to 9.3 gauss compared with the 19.0 gauss signature of the preceding record. Also for the lower record a

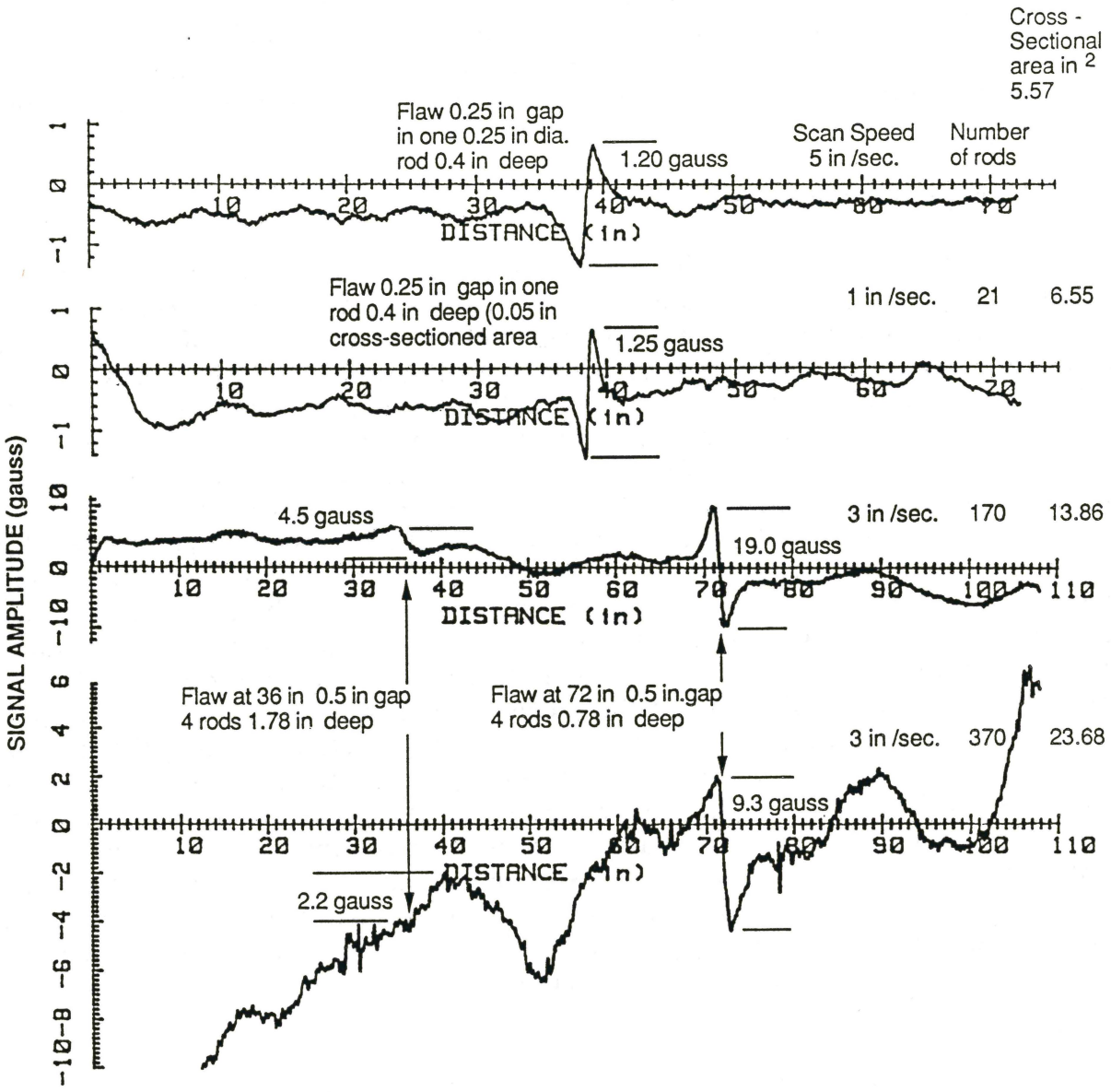

Figure 30. Records selected to illustrate flaw signatures and influence of flux density *(Steel pipe-parallel wire specimen; 10 amp. mag current; cross-sectional area of pipe 5.52 in^2; 2.2 gauss signature expected at 36 in position).*

large gradient is present and extends from -10 gauss at 0 in to approximately 6.0 gauss at 105 in; in addition the undulations between 40 and 60 in and 80 to 105 in are more prominent than in the prior record. It is emphasized that at the 36-in location the flaw produces no observable signal, although if the fractional reduction observed for the flaw signatures at 72 in is applied to the 4.5-gauss signature a 2.2-gauss signature should be present at the 36-in location. When the flux density in the pipe is very high, as is the case for the upper two records, not only is the background noise produced by the pipe in the regions 40 to 60 in and 80 to 105 in considerably reduced from approximately 6.0 gauss to less than 0.4 gauss, but also the gradient is reduced from approximately 16.0 gauss to less than 1.0 gauss. Even though the specimen is 20 ft long, when the flux density is somewhat below saturation, the magnetic poles at each end of the specimen generate the gradient observed in the bottom record. As the length of the specimen is increased this gradient effect will also decrease.

The gradient can be minimized by using a low frequency (high pass) filter to remove the relatively slowly varying components of the record, and some low frequency filtering was used in the records for figure 30 as well as a high frequency filter to remove a 5.0 kHz signal from the Hall Probe electronics. When nonperiodic wave shapes are encountered, as is the case for the characteristic flaw signatures, it is difficult to avoid distortion of the characteristic shapes because both very low frequency and very high frequency components are included in the characteristic signature.

The records of figure 31 were selected to illustrate the complex effects of flux density and filtering on flaw signature characteristics. Note in the upper record that none of the nine flaws produce signatures which can be recognized with high confidence, while all nine flaw signatures are prominent and can be readily recognized in the bottom trace. Although there is some filter induced distortion in the signatures of the bottom record the shapes are similar to those predicted by theory. These effects are caused by the significantly increased flux density in the specimen with only 34 rods compared to the upper record in which the specimen contained 370 rods. The gradient for the upper record extends from approximately -10 gauss at 0 to somewhat more than +10 gauss at 105 in even though some low frequency filtering was included to minimize the gradient. By contrast, in the bottom record the gradient extends from only +4.0 gauss at 0 to -4.0 gauss at 105 in.

The middle record provides a further illustration of the complications of signal shapes and the severe distortion caused by filtering. For this record an auxiliary electromagnet was attached to the top of the scan assembly (approximately 180° from the main magnet) and current for this magnet was adjusted to 6 amperes while the main magnet current was 10 amperes as was the case for the upper record. This additional increased magnetization dramatically influences the signatures detected from the various flaws. For example those flaws that are near the inside

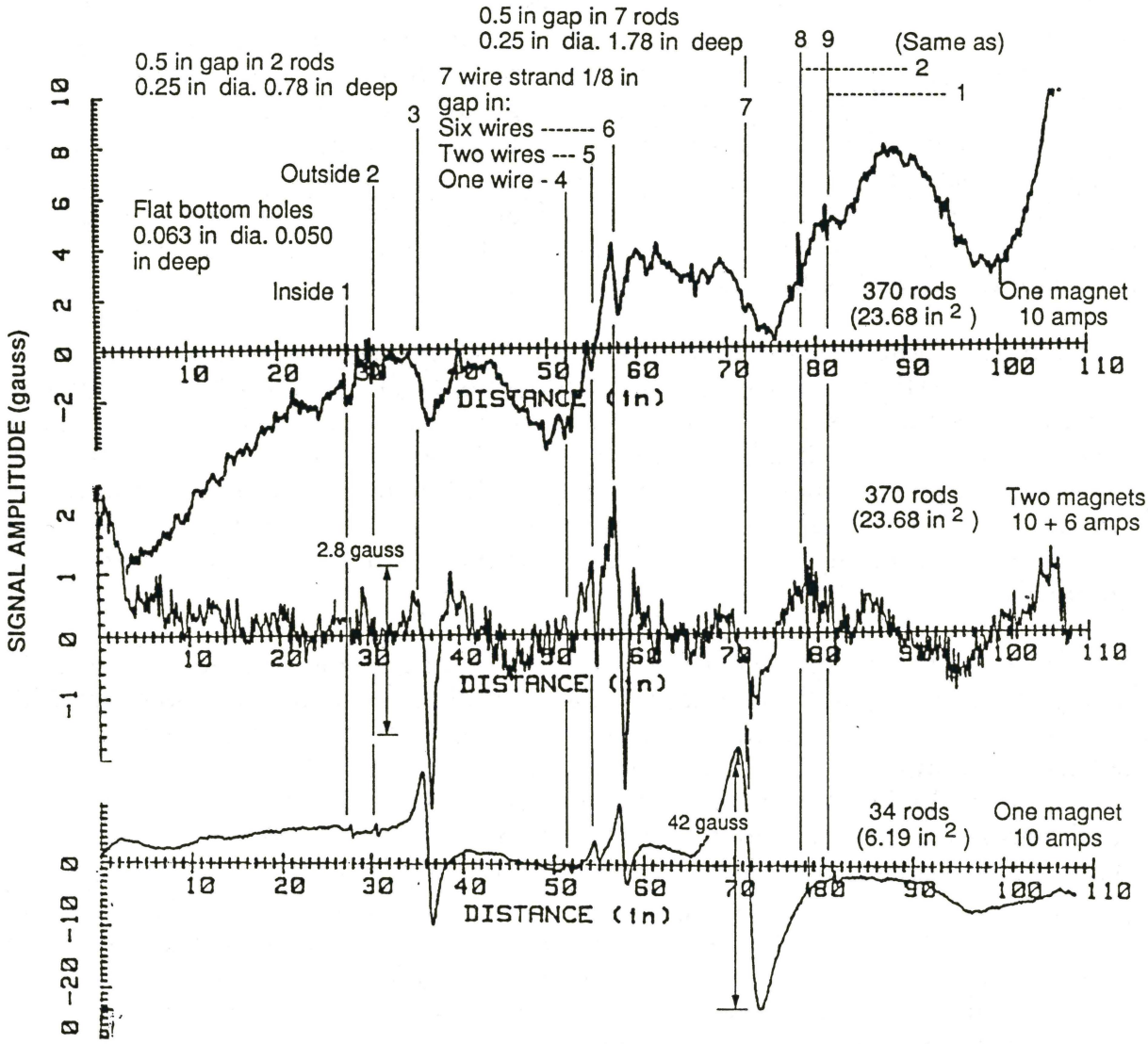

Figure 31. Complex effects of flux density and filtering on flaw signature characteristics *(Steel pipe-parallel wire specimen + one 7 wire by 1/2-in diameter strand).*

surface or outside surface of the steel pipe (Flaws 1, 2, 4, 5, 6, 8, & 9) retain the bipolar characteristic similar to those shown in the bottom record. However, the two deeper flaws (3 at 0.78 in and 7 at 1.78 in deep) are changed from a bipolar characteristic signal to a unidirectional downward going signal. This shape is characteristic of the differentiation of the bipolar signals shown in the bottom record and is caused primarily by the low frequency filtering. Note that the effect is more pronounced on the deeper flaw at 1.78 in than it is for the flaw at 0.78 in and this is because the deeper flaw contains more low frequency components. Note that the vertical scales are different for each of the three records.

To minimize the difficulties caused by magnetic anomalies at low flux densities in the steel pipe wall and also to more nearly simulate conditions that would be encountered in cable stays where the steel is encased in a plastic tube, an aluminum pipe specimen was substituted for the steel pipe. Many experiments were conducted with this specimen and the detection sensitivity was improved significantly. Figure 32 presents a record selected to illustrate detection capability in this aluminum pipe-parallel wire specimen. Both flaw 10 and flaw 11 produce recognizable signatures; however, the low frequency filter has distorted the flaw signature at the 72-in location into the quasi-unipolar downward going signal. There is also distortion in the flaw 10 signature and this is partially indicated by the positive going segment on the trailing or right side of the signal. This characteristic is also observed in the flaw 11 signature. The upward going unipolar signal at approximately 55 in is caused by three adjacent flaws (4, 5, 6) in the 7-wire strand; however, these flaws were not located directly beneath the probe.

The significantly improved detection capability that was obtained using a differential Hall Probe but without the low frequency filter is shown in figure 33. In this aluminum pipe-parallel wire specimen 370 rods were inserted into the pipe and 0.25-in long gaps were in each 0.25-in diameter steel rod located at 20, 32, 51, and 69 in, respectively, and at various depths as shown on the record. Data from this record indicate good agreement between the peak separations and depths, the peak amplitudes and the decrease with depth; however, the experimentally determined exponent is 2.22 rather than the theoretical value of 3 (see section V). This lower value would increase the maximum depth at which a specified flaw size could be detected.

One final set of data, recorded from a suspender rope will now be reviewed. Only limited data from a single specimen were obtained because of schedule and funding constraints, and selected records are presented in figure 34. The approximately sinusodial segment (4 cycles) between 60 and 70 in was produced by the "lay" of the twisted wire ropes, and before filtering these signals obscured the the flaw signal at 54 in. Comparisons of the upper and lower records indicate that the increased magnetizing current (20 amps) has increased the signal from the flaw at 54

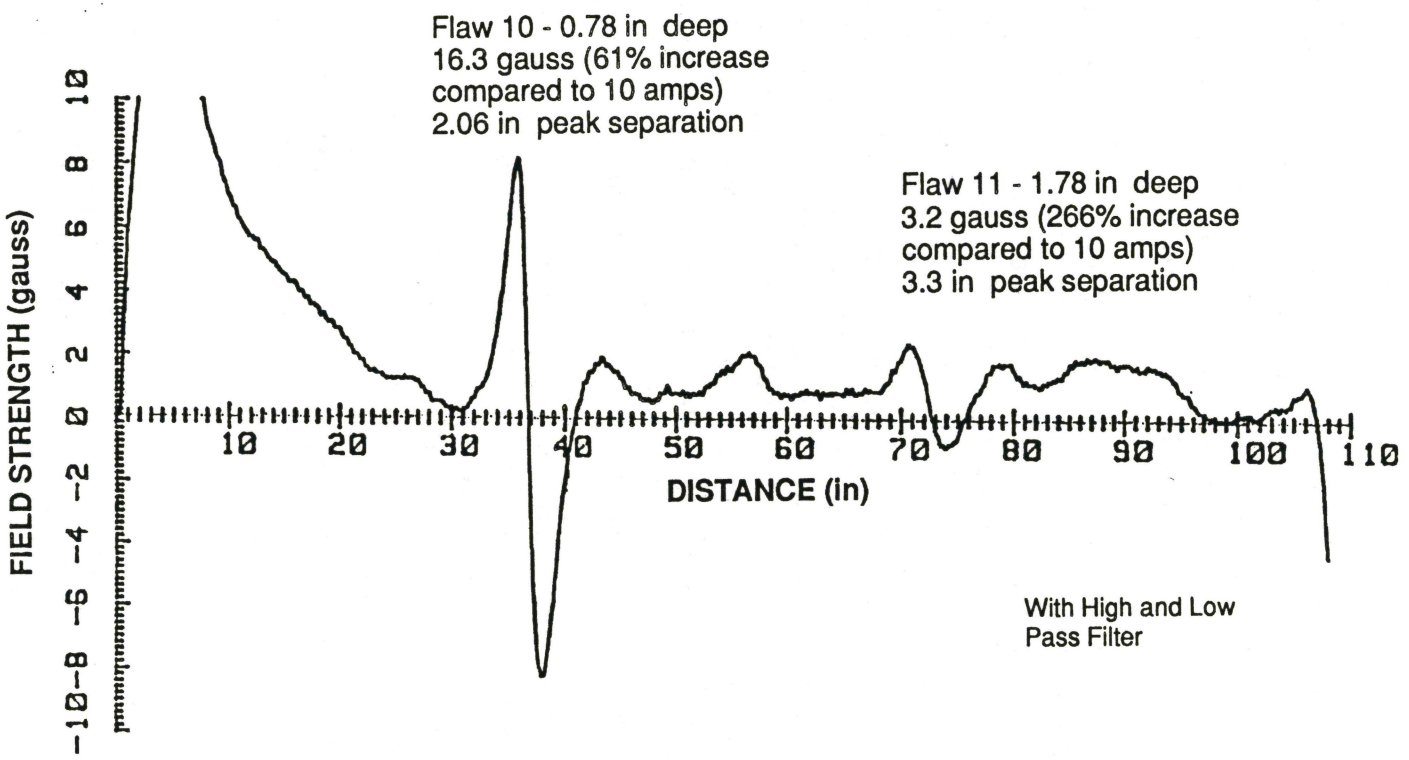

Figure 32. Decreased magnetic background and improved flaw detection with aluminum pipe-parallel wire specimen and increased magnetizing current of 20 amps *(Flaws 0.5 in gaps in four 0.25 in diameter rods, 370 rods total).*

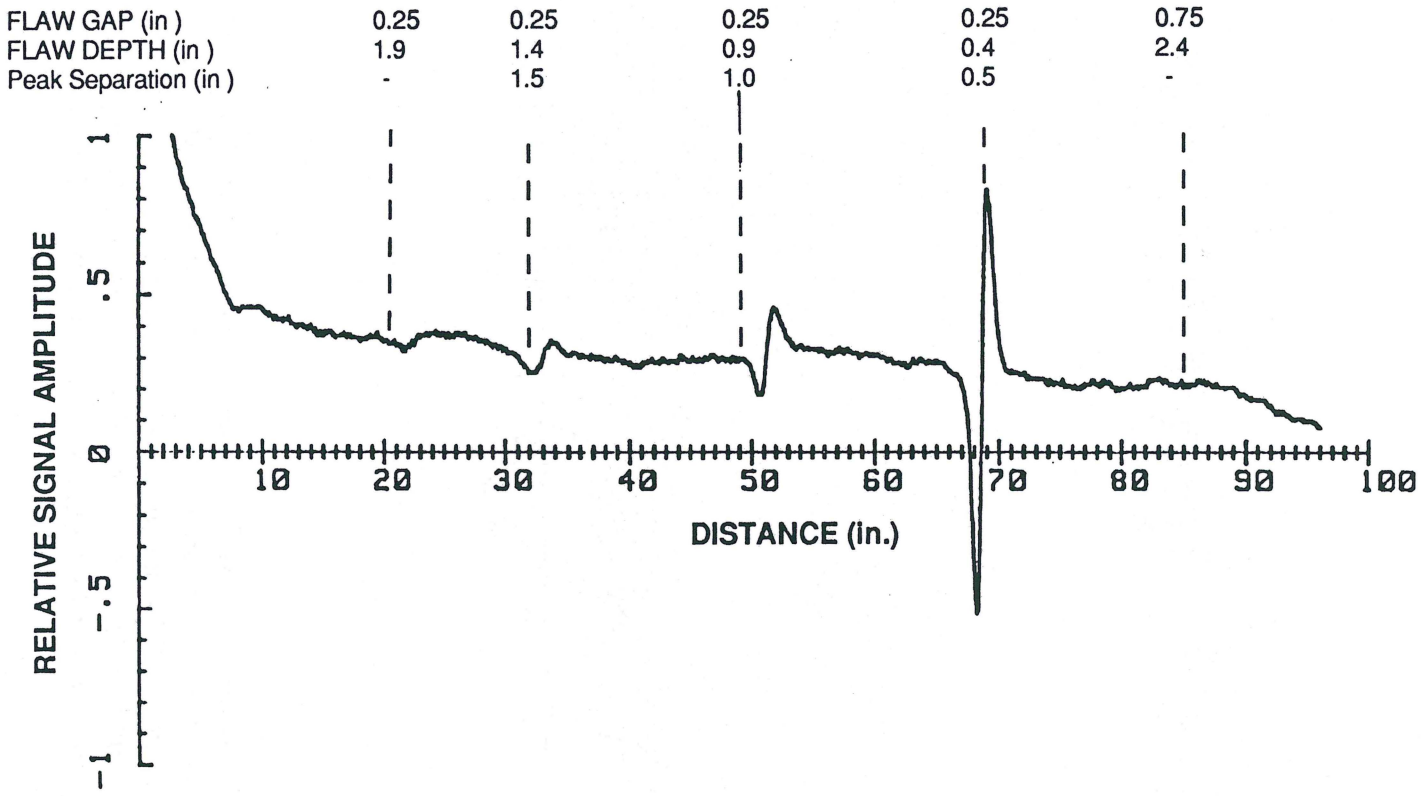

Figure 33. Improved flaw detection with differential Hall probes and no filtering
(Front to back Hall element spacing - 1.0 in, 20 amp magnetizing current).

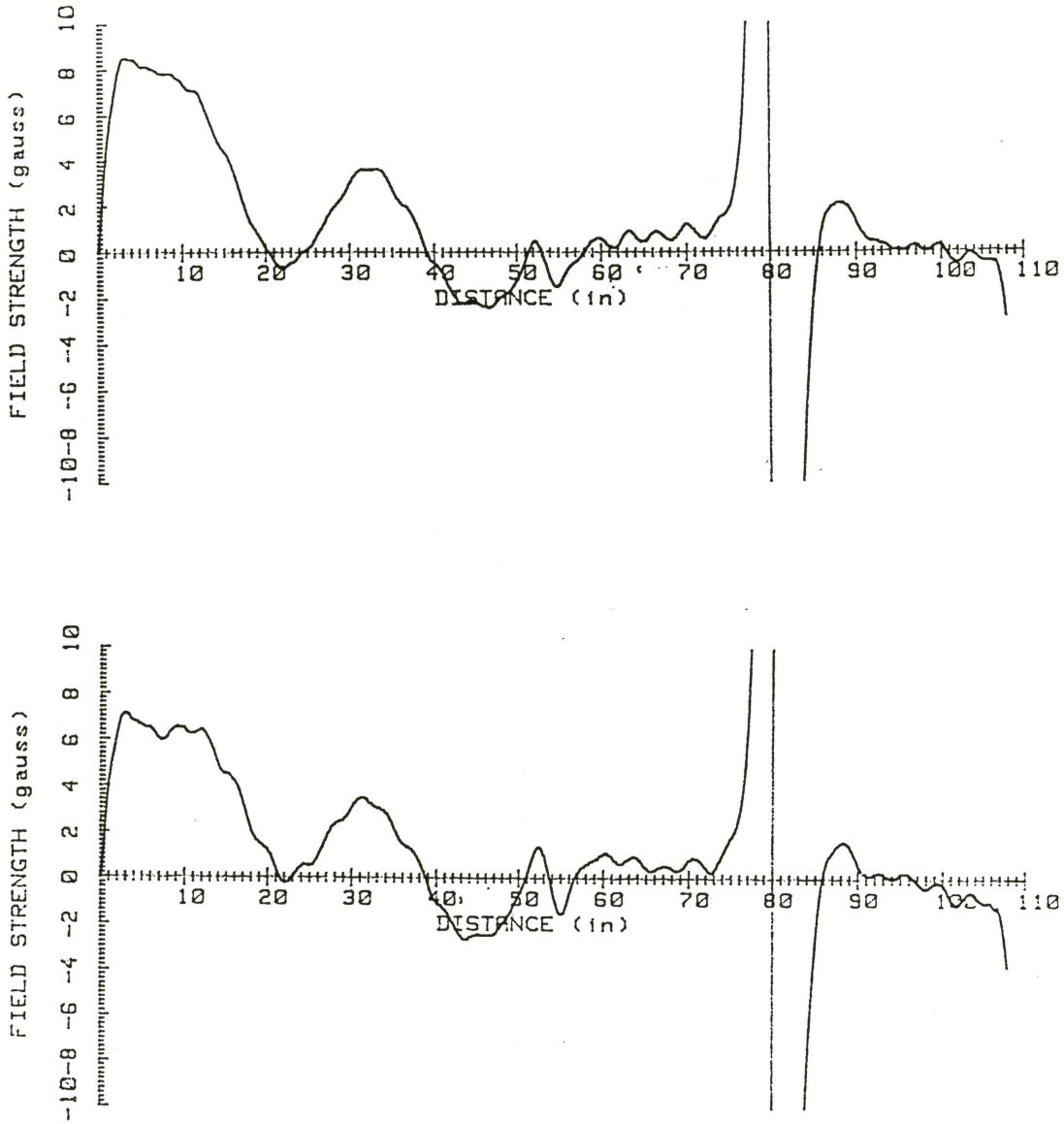

Figure 34. Records obtained during detection experiments on Golden Gate suspender rope specimen shown in Figure 25 (*Flaw signal @ 54 in from 2 3/4 in long missing segment of 0.14-in diameter broken wire; flaw signal @ 80 in from 0.5-in gap in 4 rods 1/4-in diameter at depth of 0.65 in; 14 rods + suspender rope in aluminum pipe; magnetizing current 14 amps, upper, 20 amps, lower; filter used to minimize signals from wire rope lay).*

in by approximately 45 percent, but the prominent excursions at 10 in and 30 in and also the sinusodial signal have all decreased. Use of the digital subtraction routine (not available until later) would have greatly enhanced the signal caused by this flaw in the suspender cable removed from the Golden Gate Bridge.

III. PROTOTYPE MAGNETIC PERTURBATION NDE CABLE SYSTEM (MPC)

A. Equipment Description and Operation

1. Overall System

The MPC is an integrated electromechanical system consisting of (1), a magnetic sensor assembly attached to a moving electromagnet; (2), electrical and hydraulic motors and actuators; (3), an electronic control and data acquisition system directed by a remotely located host computer; and (4), a self-propelled frame housing the entire system. The system is designed to be placed directly onto bridge cables and is capable of moving itself along the cable acquiring magnetic perturbation data relating to the presence of corrosion damage and broken strands. The paragraphs which follow provide brief descriptions of the mechanical and electrical elements of the system. Table 3 lists the physical dimensions and weights of the major system components.

2. Mechanical System

The primary elements of the mechanical system are illustrated in figure 35. A photograph of this system was presented previously in figure 8. The magnet assembly, including the magnetic sensor assembly and the electromagnet, is supported by two parallel rails 12 ft long. These rails also support the equipment tray on the opposite side of the cable. The longitudinal drive assemblies and the circumferential drive assemblies and cable clamps are attached to the opposite ends of the two rails. The system is statically balanced around the centerline of the cable.

In normal scanning operation the clamp chains in the circumferential drive sections are tightened by hydraulically actuated tensioners so the entire system is held firmly against circumferential rollers within the circumferential drive assemblies. These chains are powered by electric motors located in the longitudinal drive sections. Application of power to these motors rotates the entire system about the centerline of the bridge cable to position the system to a scan path in a new circumferential position. When thus positioned, the magnet can be lowered to the cable by actuating two small lift motors (not shown) on the magnet assembly. Scanning is accomplished by applying hydraulic power to the scan drive motor. The magnet assembly is pulled along the rails by a roller chain as shown in the illustration.

When scanning of a section is completed, the entire system is advanced along the cable using the features of the longitudinal drive sections. The longitudinal drive motors and drive rollers are pressed against the cable by hydraulic cylinders to overcome the tension in the clamp chains and to clamp the cable between the drive rollers and the pin rollers. The pressure in the chain tensioner cylinder is then

Table 3. Equipment physical parameters.

Subsystem	Approximate Size (in)			Approximate Weight (lb)
	L	W	H	
Inspection Module	190	25	34	2800
Host Computer	15	9	9	11
Power and Communication Cable	250 ft	--	--	85

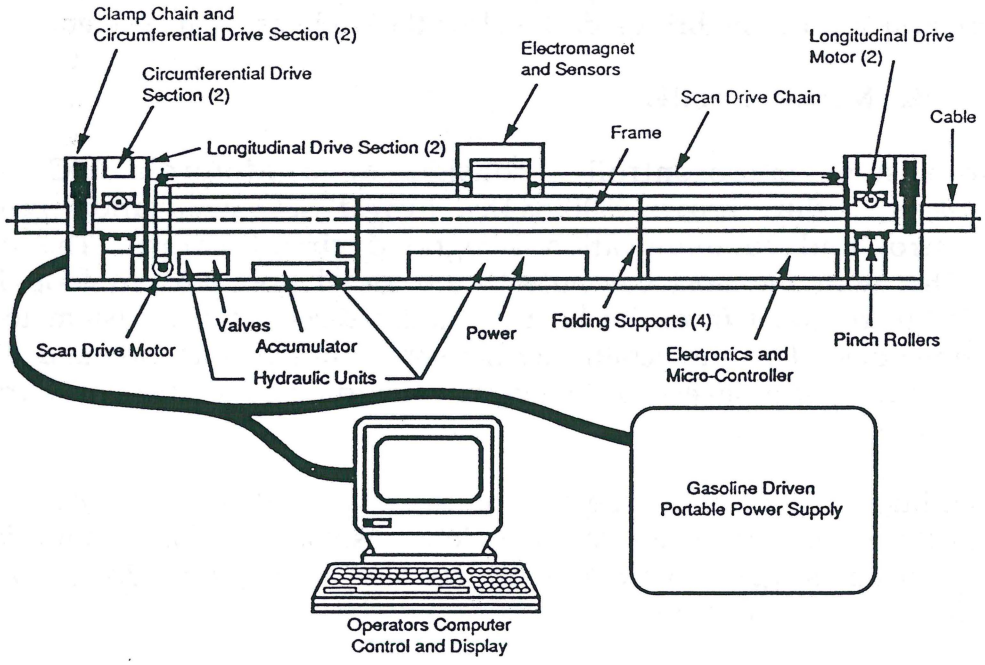

Figure 35. Schematic illustration of mechanical system.

removed allowing the clamp chains to hang free. The longitudinal drive motors are then actuated to move the assembly along the cable. The procedure is reversed to clamp the system to the cable in a new position. The system longitudinal advance sequence takes place with the system azimuthal orientation with the electromagnet on top (12:00 position) of the cable as shown in figure 35.

The equipment tray supports the pin rollers, the power and control elements of the hydraulic system, and the electronics and electrical control systems. Lead weights are added to the equipment tray to balance the system about the centerline of the cable.

3. Electrical and Electronic Subsystem

a. Host Computer

As shown in figure 36, overall control and data logging is performed by the host computer, a DATA PortaComp LCD 286. The computer is programmed to present the operator with the full current status of the system, prompt him to make the appropriate entries and commands, and to store all inspection data on an integral hard disk. Ultimate archival of inspection records will be on floppy disks. The computer is located along with other peripheral equipment in an instrumentation van on the bridge deck below the cable being inspected.

b. Microcontroller

The system microcontroller consists of a Motorola MC 68705U3S microprocessor, a Burr Brown SDM854XG hybrid data acquisition system, and several control and communication integrated circuit chips. The controller communicates with the host computer via a serial port current loop interface. Commands are received from the host computer directing the system to perform specified functions. The microcontroller interprets these commands and directs the required output voltage levels to the system according to a program stored in the controller PROM.

In addition to controlling the system, the microcontroller accepts inputs from pressure switches, limit switches, and position sensors. This information is used in formatting certain system commands and is also transmitted down to the host computer for the operator display.

Another vital function performed by the microcontroller is the acquisition of inspection data. Analog voltages representing the magnetic fields sensed by the six channel probe are converted to digital format and transmitted to the host computer for storage and display. The microcontroller also maintains an accurate accounting

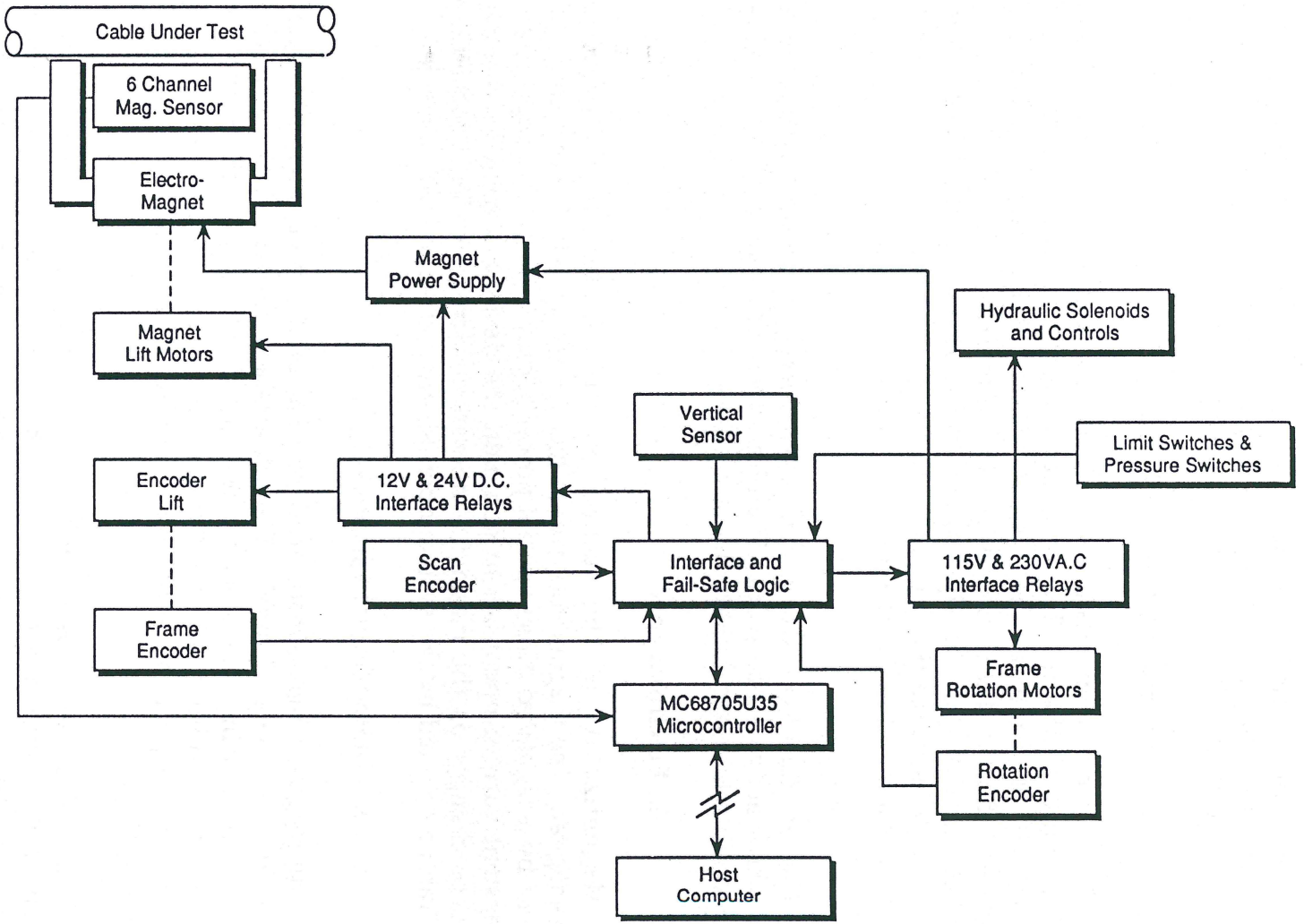

Figure 36. Electronic and electrical block diagram.

of the sensor longitudinal and rotational position. This information is transmitted to the host computer with each data sample. The sampling interval, typically 0.1 in, is selectable from the host computer by the operator.

c. Interface and Fail Safe Logic

These circuit elements are contained in a printed circuit card file located on the electronics platform. The microcontroller outputs and inputs pass through these circuits in route to the system sensors and actuators. The logic blocks commands which could cause danger to the system by combining these signals in integrated circuit logic with signals from pressure and limit switches. For example, a command to advance the frame would be blocked if the rotation chains were not loose, or a command to lift the magnet with the magnetizing current "on" would be ignored.

The interface logic also provides the necessary power to drive the solid state relays which activate the hydraulic and electric actuators and motors as well as the power to the rotary and longitudinal encoders.

d. Electromagnet

Magnetization of the section of cable under test is provided by an electromagnet. The magnet coil, which has approximately 2 ohms cold resistance, is powered by a regulated direct current power supply. The power supply is configured for constant current operation to maintain the desired current level when the coil resistance changes as the magnet temperature increases. Two presettable current levels can be selected by the system operator from the computer console.

e. Analog Signal Channels

The magnetic field sensor array consists of 12 Hall effect sensors connected in pairs to form six data channels. The sensors are positioned circumferentially in a probe shoe or housing on 0.35-in centers. Spacing between sensors is 0.1 in forming an active sensor width of 4.15 in. On a 6.3-in diameter cable, five longitudinal scans will suffice to inspect the entire outer surface of the cable with approximately 5 percent overlap.

The Hall sensors operate with a 5 kHz excitation current. Low frequency magnetic field components normal to the sensors produce proportional 5 kHz voltages at the sensor output terminals. These signals are amplified and demodulated to yield baseband analog voltages proportional to flux leakage amplitude and polarity. After additional amplification these six channels of data are directed to the analog to digital converter. The converter scans these inputs at each data position interval, transmitting the digitized data to the host computer in essentially real time.

4. Attachment and Removal

Placement or attachment of the system onto a cable to be inspected requires the use of a removable lifting harness and frame and a crane capable of lifting the system to the required height and horizontal distance. If the frame of the system cannot be reached from the bridge deck when it is positioned on the cable, then it will be necessary to employ a "cherry-picker" to position a person where the system chains and clamps can be manually attached.

A typical attachment scenario would proceed as follows: The system is transported to the bridge using a flat bed trailer or truck. The hoisting fixtures and harness are attached as shown in figure 37 and the crane hook attached to the lifting harness. The lifting frame is next adjusted so the angle of the frame when suspended matches the angle of the cable. The side frames and clamping chains on the system are opened and the system is hoisted and swung into position on the cable. Note that the "C" hooks on the frame allow the system to be placed on the lower cable of a vertically spaced pair. It is necessary to manually slide the system sideways into final position on the cable. When the system is in position on the cable and is resting lightly on the circumferential rollers, three functions must be performed. First, the side frames must be lowered and secured; second, the clamping chains must be wrapped over the cable and the joining links attached; and third, the movable lower pin rollers must be raised to the proper position and secured. These functions will be performed from a scaffold or a cherry-picker as required. At this time the system power can be applied and under manual control, the pin rollers energized. The system can now be placed under computer control and the scanning procedures started after the lifting frame has been removed and the safety/assist cable has been attached.

Removing the system from a cable is essentially the same as above in reverse. The lifting frame is brought into place and attached to the system. With the crane supporting the weight of the system, the system power is removed, the clamping chains and side frames opened, and the lower pin rollers lowered. The system can then be returned to the trailer or placed on the next cable to be inspected.

B. Performance Verification

1. Specimen

The specimen for verifying flaw detection performance was previously presented in figure 9. Since the scan assembly rode on top of the polyethylene tube for these experiments, the flawed rod (painted red) in the exterior layer and located at the top was used as the 0° reference location. In design of the specimen only a limited number of flaws were included to minimize possible interactions, and only one gap was included in each rod to ensure that the flux in each rod was continuous

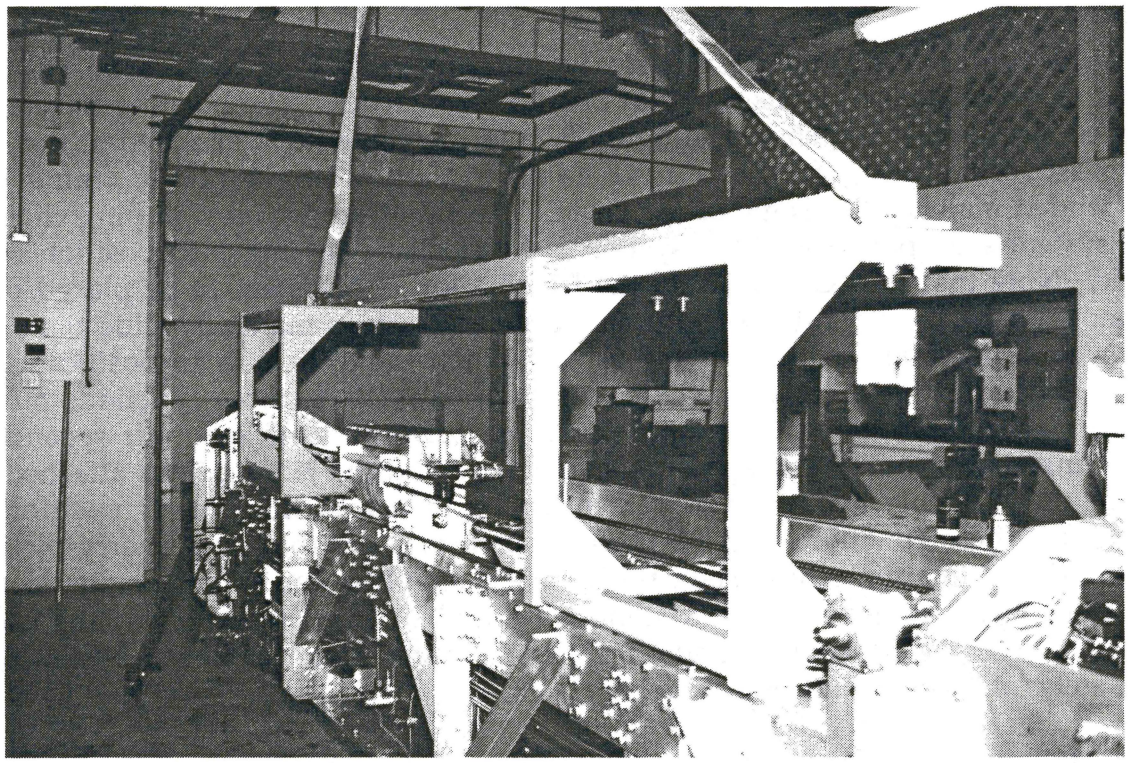

Figure 37. System lifting harness.

except at the gap. Seven separate flaws were produced by using 0.25-in diameter by 0.25-in long aluminum plugs held in place between two rod ends by a wrapping of vinyl tape. Also one large flaw was produced by inserting four aluminum spacers 0.5 in long and wrapping the four rod bundles with vinyl tape. This large flaw is at the 180° location in figure 9. The flaw slightly to the right of the 0° position and the two flaws at approximately +50° and -35° were intended to be symmetrically spaced and at the same depth. Analyses of the relative signal amplitudes from these three flaws would indicate the extent of magnetic flux decrease at the extremities of the six element Hall probe. Unfortunately, in actual construction apparently this configuration was not precisely achieved. The exact final configuration is imprecise since individual rods may shift slightly during construction, and also the relative position of rods at the reference end may be slightly different than at the flaw locations. This imprecise configuration possibility must be considered during data analyses.

2. Calibration and Reference Data

Many attempts were made to obtain precise calibration and reference data from all flaws in the laboratory specimen cable; however, in general only qualitative data were obtained and these were not considered sufficiently accurate to develop the relationship between flaw signal amplitude, location, depth, and size. Examples of most of these data have already been presented, and because the schedule for the field demonstration did not allow enough time to conduct calibration experiments with the final equipment configuration it was decided to postpone such calibration efforts until return from the field demonstration.

On 12/20/89, after the field demonstration, the polyethylene pipe was removed from the cable bundle in an attempt to provide additional constraints for the individual 20 ft rods and also to more rigidly constrain the cable bundle in the polyethylene pipe. Several additional stainless steel tie bands were installed, and several of the PVC spacers were taped more securely to the cable bundle. It was anticipated that these modifications would result in a cable specimen that was less flexible and, accordingly, would minimize the prominent background excursions observed during prior experiments. In figure 38 four data sets are presented which were obtained after the modifications. Unfortunately, as can be observed in the left column of records, very prominent background undulations are still present. In fact, by comparison with the records of figures 11 through 13 the background variations are considerably more severe than was the case when the specimen was initially assembled and the initial data sets obtained. For the upper record flaws were located at approximately 16, 31, and 46 in, and for the lower left record a large flaw was located at 66 in.

The flaw signal in the upper record at 16 in is in an area of severe gradient and is practically obscured; the flaw signal at 31 in is prominent enough to identify

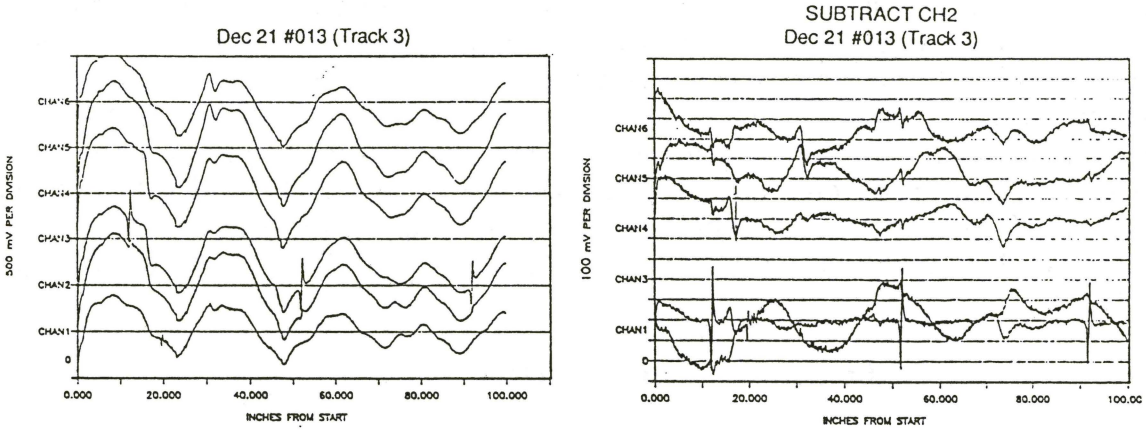

Flaw @ 16 in approximately centered under CH4, depth 1.25 in *(outermost layer);* flaws @ 31 in approximately centered under CH1 and CH6, depth 1.50 in *(layer 2),* also CH4, depth 1.80 in *(layer 4)* ; flaw @ 46 inches approximately centered under CH4, depth 1,50 in *(layer 2)* ; all flaws 0.25 in gap in 0.25 in diameter rod.

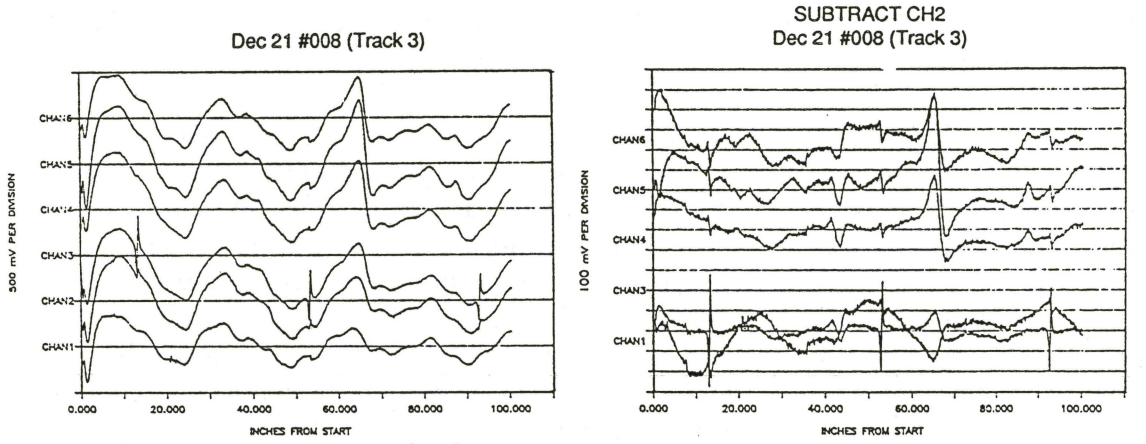

Flaw @ 66 inches approximately centered under CH5; depth 2.0 in *(layers 3,4,5)* 0.5 in gap in four 0.25 in diameter rods.

Figure 38. Records from laboratory specimen cable obtained with MPC system after field demonstration *(records in right column obtained after digital subtraction of CH2).*

on channels 4, 5, and 6, but the gradient also obscures the flaw at 46 in. For the lower record the large flaw (four 0.25 in diameter rods each with a gap of 0.5 in) can be readily identified but it is also in an area of rapidly changing gradient which distorts the signatures from this large flaw. The three wire reference targets at approximately 12, 52, and 92 in are readily observed; note that the polarity of these reference signals are opposite to the polarity of the flaw signals, and this feature can be helpful in identifying features on field records that are possibly associated with flaws in cables. The vertical scale on these sets of records is the same as used in presenting most of the field inspection records and, accordingly, facilitates comparisons.

Records in the right column were obtained after digital subtraction of channel 2 from all five other channels. During data retrieval and analysis, occasionally, incorrect information has been entered on records and the three reference signals have been extremely helpful in clarifying such cases. For example, the small amplitude upward and then downward going signals on channels 1, 4, 5, and 6 are part of the subtraction process and were caused by the small amplitude signal obtained on channel 2 from the reference flaws. As will be seen later, when channel 3 is subtracted from all channels prominent reference signals are obtained on all channels. In the upper right set of records well-defined flaw signals are observed on channel 4 at approximately 16 in, and this symmetrical bipolar signal is opposite in polarity to the reference signals. Peak-to-peak amplitude of this signal is reduced somewhat because a small amplitude flaw signal was obtained on channel 2 and during the subtraction process this was subtracted from the overall signal amplitude on channel 4; a similar statement applies for channel 3 and only a small amplitude signal is observed from the flaw. Recognizable signals are also generated on channel 5 and channel 6 at 31 in but no recognizable signals are generated by the flaw at 46 in. Opposite polarity somewhat nebulous signals are observed on channel 3 and channel 6 at the 46-in flaw location. By referring to figure 11, the amplitude of the flaw at 40 in is approximately the same on channel 2 and channel 3 and this digital subtraction of the channel 2 flaw signal is the reason for disappearance of the flaw signal at 46 in on channel 3 in figure 38.

For the lower right set of records the large 4 rod flaw causes a large amplitude signal at 66 in. Only a small amplitude signal is observed on channel 3 because the channel 2 and channel 3 signatures are approximately the same amplitude for this deep flaw.

Since both the time and funds planned for specimens had already been greatly exceeded, and since the contract completion date was imminent it was necessary to abandon further efforts to obtain precise quantitative data.

3. Data Analyses and Flaw Detection Forecasts

Measurement of the flux density at the electromagnet 'poleface' indicated approximately 5,000 gauss with a coil current of 25 amperes. Since cross-sectional area of the poleface is 16.0 in^2 and the cross section of the 271 steel rods in the specimen is 13.3 in^2, maximum flux density in the specimen is 6,000 gauss neglecting leakage. However, the large air gap (0.9 in) between the specimen and the poleface would cause significant leakage and the maximum flux density would be lower, probably 4,000 to 5,000 gauss. Flux density measurements at different locations in rods with small gaps of only approximately 0.04 in would have provided more precise values, but this would have required significant funds and was not done. Actual values of flux densities would be very useful in analyses and forecasts, but relative values from different flaws must be used in the following data analyses.

The records of figures 11, 12 and 13 and the data of table 1 previously discussed have summarized much of the flaw detection verification information. A discussion of a few other aspects of performance will follow.

Referring to figure 11, the single flaw at 10 in produces a maximum amplitude on channel 4; and since the channel 3 amplitude is greater than channel 5 (channel 3 and 5 sensors are each spaced approximately 0.69 in from the channel 4 sensor) the flaw centerline is located between sensor 3 and 4; also the centerline is closer to sensor 4 than sensor 3. Actually, by changing the azimuthal location until the signal amplitude is maximum, the centerline can be determined precisely, probably within less than 0.1 in for exterior rods.

Similar analyses at the 40-in position indicated that the flaw centerline is nearly centered under sensor 3 and only slightly displaced toward sensor 4. Note that the signature at 40 in is symmetrical while the signature at 10 in is distorted and has a smaller positive peak than the negative peak. This distortion is probably caused by the gradient and the filtering. The flaw at the 10-in position is in the exterior layer of rods, see figure 9 (approximately 1.14 in from the sensor), while the flaw at 40 in is in the second layer or approximately 1.25 in from the sensor. If the amplitude of the signal at 10 in was not distorted the exponent n could be experimentally determined (see equation 3 in section V). For the table 1 estimates, n=3 was used.

Data from the deeper (approximately 0.8 in beneath the surface of the steel and 1.7 in from sensor 4) and larger flaw, 4 rods with 0.5-in gaps, at the approximate center of the records in figure 12 will now be discussed. Since the amplitudes of channel 2 and channel 4 as well as channel 1 and channel 5 are approximately equal and channel 3 is maximum the flaw centerline is under sensor 3. By comparing the channel 5 and channel 3 signals (ratio = 1.8/1) of figure 12 with the channel 1 and

channel 3 signals (ratio = 2.9/1) of figure 11, it is apparent that the deeper flaw could be detected over a wider range of azumithal location than the near surface flaw at 10 in.

The preceding are just a few selected examples of the many analyses that have been performed to verify flaw detection, flaw location, and estimated flaw size detection capabilities of the prototype MPC. Additional parametric investigations using specimens configured to minimize anamolous movements and associated signals and also use of increased flux density will be required to refine the parametric relationships. This is particularly true for the signal amplitude decrease with increasing flaw depth relationship, and also for the influence of scanning speed on flux penetration into the interior regions and the associated flaw response. Higher scan speeds are desirable to minimize inspection time, and a few experiments at 2 in/sec were performed, but results were inconclusive.

IV. FIELD DEMONSTRATION, CABLE-STAYED BRIDGE ACROSS THE MISSISSIPPI RIVER

A. Preparation and Team Training

Only very limited simulation of an actual inclined cable was possible and, accordingly, operational training of the team and operational check-out of the MPC prototype was very limited. Preliminary "climbing trials" disclosed that the drive rollers slipped when the cable specimen was inclined only a few degrees. For these operational trials a cement filled steel pipe was inserted into a polyethylene pipe and the annulus between the steel pipe and the polyethylene pipe was filled with cement grout. A pivot support was arranged at one end of the pipe and the other end could be elevated using a forklift. Travel of the MPC system along this simulated cable was limited to less than 5 ft. These operational trials also disclosed that friction between the steel clamp chains and the polyethylene pipe was inadequate to prevent slipping at times. To improve performance thin layers of rubber were bonded to the drive rollers and also to the clamp chains. While these modifications appeared to solve the clamp chain problem and also improved the traction force on the drive rollers, it became obvious that an auxiliary force would be required to move the MPC system up the steeply inclined cables. The only solution that appeared reasonable was to arrange for a cable attached to the machine and extending to the tower with a winch or other pulling device located on the tower. Eventually, it was decided that a "SKY CLIMBER" on the tower could be used to provide tension on the auxiliary cable.

Although rotational operational sequences could be conducted on the cable simulation fixture, it was not possible to conduct flaw detection experiments. With the flawed specimen it was necessary to support the MPC system on stands resting on the floor, and then operational sequences at different angular locations were simulated by rotating the cable with the machine stationary.

B. Site Demonstration

1. Equipment Setup, Check-out and Installation

Operational and inspection demonstrations of the MPC Prototype System were conducted on two different cables of the cable-stayed bridge across the Mississippi River at Luling, Louisiana during the period 12 December 1988 through 15 December 1988. The two cables were identified as LN1 and LN3 and, respectively, were the upper and lower inboard cables of the four cables terminated near pier 4 on the North side of the bridge. These cables are approximately 525 ft long and are inclined at an angle of approximately 24°. The polyethylene pipes enclosing the 271 rod bundle of 0.25-in diameter rods have a nominal O.D. of 6.3 in.

In general, the field demonstration was very successful as was indicated before, and a brief chronology of activities follows. The first day, 12/12/88, was used for a thorough equipment check-out on a fixture, and this was conducted in the LADOTR maintenance facility near the bridge. Also the SKY CLIMBER was hoisted up the tower and installed, and the wire rope for providing the auxiliary force was threaded through an existing pulley on the tower. On the morning of 12/13/88 the team arrived at the maintenance facility at approximately 7:15 am ready to move the equipment to the bridge for installation on a cable. However, several unexpected delays were encountered and actual operations did not begin until approximately 9:00 am. Attachment and removal of the MPC system on cables was accomplished with a truck mounted "A-frame" and winch cable. The initial installation required nearly 1 1/2 hours, although the elapsed time after adjusting the "A-frame" height and truck position was only 3/4 hours. Subsequently, installation and removal sequences each required approximately 1/2 hours. After the system was lifted and pulled into place, frame supports were secured, then the chains on either end of the system were secured, and power was applied to the system. The chain clamp actuation was completed on command from the operator's station and at 10:20 am the lifting frame was removed. A magnet scan sequence was initiated at 10:26 am; the system was rotated to the vertical position or track 3 location on top of the cable and the *first data set obtained at 10:27.5 am.* All six records were displayed on the operator's screen, and the channel 3 reference signals spaced at approximately 40 in were very prominent.

2. Data Acquistion and Field Analyses

It had been anticipated that all records would be relatively straight without significant background variation which had been so troublesome with the laboratory specimen. However, significant background was observed and this was completely unexpected, since the rods should have been straight and parallel from the cable tension and the cement grout should have eliminated movement. In addition, it appeared that the electronic system noise level was relatively high. Use of the subtraction routine minimized the noise and background variations significantly, and in addition to the reference signals, periodic anamolous signals were observed at approximately the same intervals on all channels. Subsequently, the source of these signals was assumed to be the spiral wire rope. Attempts to rotate the system to the various inspection tracks were only partially successful, and the system components were examined for possible binding and/or other sources of malfunction, but none could be identified.

It had been planned to acquire data on each of the five tracks spaced at 72° interval around the cable and then advance the system forward to a new inspection location and repeat the sequence. Because of the rotational difficulties it was decided to acquire data from those tracks which could be accessed and then move to the next inspection position along the cable. Accordingly, most data sets are incomplete and usually only two to three of the five scan tracks could be accessed. Even with these

limitations, more data were acquired than it has been possible to analyze within the scope of the efforts provided for analysis and even supplemented by many additional man hours.

Data sets were acquired eventually from scan tracks 1, 2 and 3 but positions 4 and 5 could not be accessed at the initial installed location on cable LN3. The system was advanced approximately 10 in and additional attempts to access all tracks were conducted. At this location which was approximately 2 ft 10 1/8 in from the weld bead reference, scan tracks 1, 2, 3, and 4 were accessed, but track 5 could not be accessed. The system was moved approximately 100 in and again tracks 1, 2, and 3 could be accessed, but tracks 4 and 5 could not. The system was moved back down the cable approximately to the initial starting point at 2 ft 10 in and tracks 3, 4 and even 5 were accessed.

Since it appeared that the winch cable was winding rather tightly around the cable stay as the machine rotated (±144°), it was decided to move the location of the winch cable clevis to a point several inches further out from the axis of rotation to minimize this "wind-up". Unfortunately, this action did not correct the difficulty.

A polyethylene weld bead was visible on cable LN3 approximately 40 ft up the cable. It was decided to move the machine to this location to determine if the weld bead would cause any operational difficulties. The machine traversed the weld bead without any difficulty and a complete set of data were obtained from track 3. Later analyses of records indicated a significant background variation on all six channels in this location, but because of the major undulations observed later at many other locations it has not been possible to determine whether or not the weld bead produced an anomalous signal. If the shield had not been used and the magnet could have been made to traverse the weld bead the very large change in spacing between the electromagnet and the cable would have produced an extremely high amplitude (off-scale) signal; since no such signal was observed it appears that the shield is providing the necessary "smoothing" for which it was designed.

After removal of the MPC from the cable and return to the maintenance facility the system was installed on the check-out fixture, and a diligent effort was made to determine the source of the rotational malfunction. Although several corrective actions were taken and the system check-out fixture was elevated to the approximate angle of cable LN3, the system could not be made to malfunction as had been observed on the cable. However, the check-out fixture consists of a steel pipe and, accordingly, did not simulate conditions encountered on the cable. Nevertheless, several sprockets were aligned, set screws in sprockets that had apparently moved and allowed the sprockets to become misaligned were tightened, and it was judged that no other corrective steps could be taken.

The demonstration was continued on 12/14/88 and the machine was installed again on cable LN3 at approximately 8:30 am. Rotational difficulties were

encountered, immediately, and a variety of actions were taken in an effort to eliminate the malfunctions. The malfunction was primarily an inability to access track 1 and track 5 in the bottom regions of the cable, and usually track 2, 3, and 4 could be accessed without any difficulty. Accordingly, it was decided to limit the data acquisition to these three tracks (2, 3, and 4) and to acquire data at 100-in intervals up the cable, and such a sequence was followed. However, at approximately 2:15 pm the system had been positioned at approximately 1520 in up the cable and data had been acquired from track 2 and track 3 when a major malfunction occurred. The system was immobile and failed to respond to any commands from the operator. This alarming situation existed for approximately 15 to 20 minutes and then it was determined that a circuit breaker on the generator had been tripped. An enclosure to muffle noise from the generator apparently restricted air flow causing the generator to overheat and trip the circuit breaker. The enclosure was moved to provide more cooling flow and the circuit breaker reset. System operation was again normal, and although it had been intended to acquire data further up the cable, because of concerns about the consequences of possible malfunctions at these "nearly inaccessible heights" it was judged prudent to return the machine to the "near deck" region and perform additional calibration experiments at that location. Interestingly, after returning to the approximate location at which the demonstration was initiated it was possible to access all five angular positions although track 1 and 5 could not be accessed during the prior data acquisition attempts.

3. Comprehensive Analyses

As indicated previously, many more features were observed in the data sets than had been anticipated prior to acquiring data from installed cables. The variety of features was so great and with the lack of consistency along the cable as well as around the cable, the data appeared overwhelmingly complex, initially. Gradually, plausible explanations were developed to associate many of the features in the data sets with possible cable details as has been presented previously. Additional results of analyses will be reviewed in this section.

For a system to be of use in long-term structural integrity monitoring of the cables, the system must provide data with good resolution, high sensitivity, and excellent repeatability. Figure 39 presents two different data sets obtained at the same region on cable LN3. One data set was acquired on 12/13/88 from track 2 and the second was acquired on 12/14/88 from track 2 at approximately the same longitudinal position along the cable. The numbers 114.3 and 122.0 indicate that the two data sets were not obtained from exactly the same longitudinal location. A further factor which complicates precise comparisons of these two data sets is the fact that a precision measurement from a fixed reference location on the cable, such as the weld bead, to a reference location on the MPC was not determined on both days. Fortunately, the spiral wire wrap signals are caused by a source that is fixed at

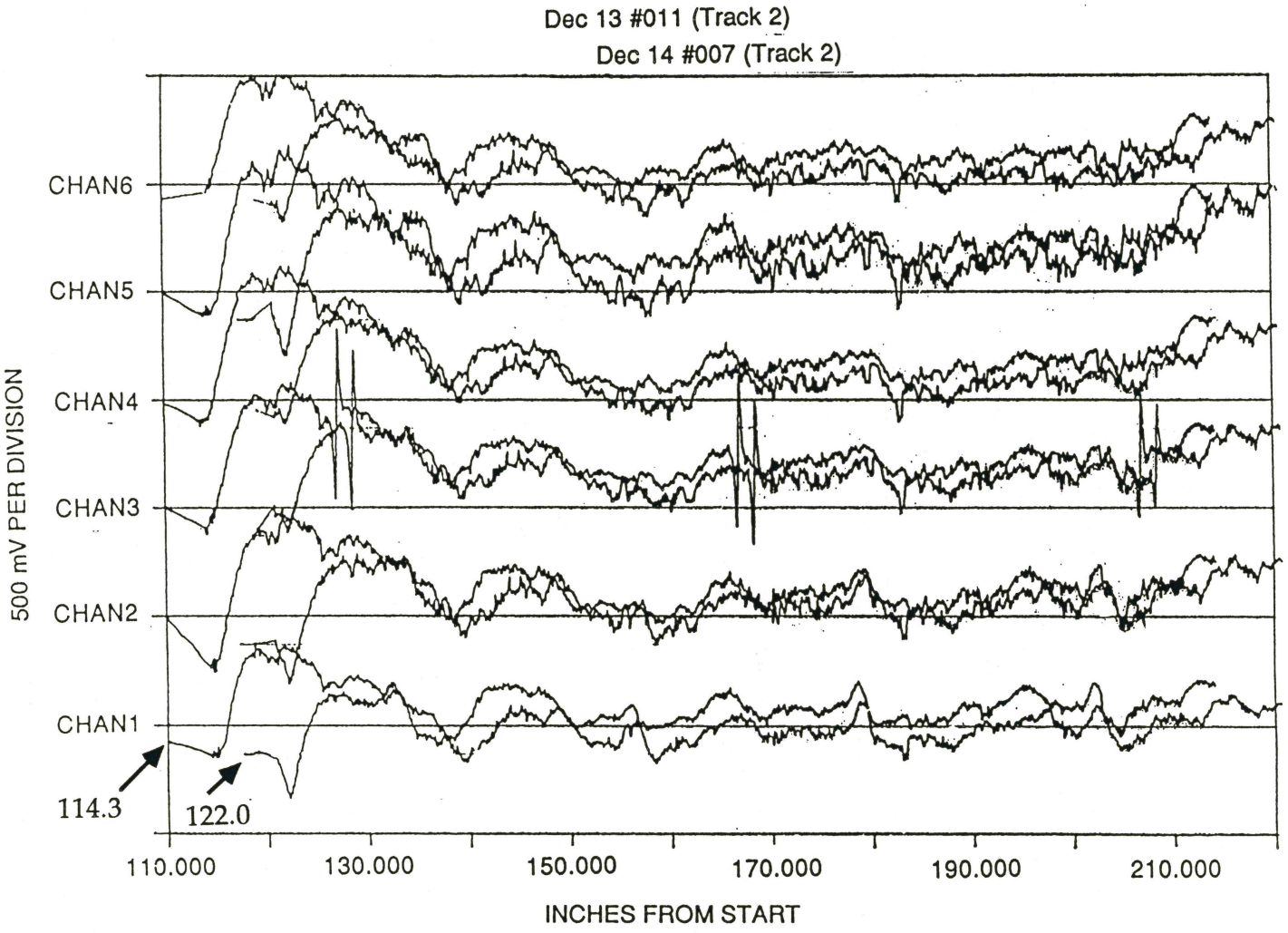

Figure 39. Comparison of data sets obtained on two different days from the same region.

the same precise longitudinal location and therefore, automatically, provide alignment features on both data sets. Accordingly, in figure 39 alignment of the two data sets was achieved by matching the longitudinal locations of the spiral wire wrap signals on channel 1 of both records. With this alignment, it is observed that many of the features in the records correspond; however, because of the significant electronic noise background only a qualitative comparison is possible. In addition, the relatively prominent excursions during the initial 10 to 15 in and also the upward excursions approximately 10 in further along the cable are unexplained. The high frequency noise was intermittent and after return of the equipment an investigation disclosed that an insulating bushing for the scanning assembly had slipped and intermittent contact was causing noise.

A more representative example of the achievable reproducibility and resolution is provided by figure 40. Figure 40 consists of two separate data sets with transparent overlays "in register" and it is seen that there is excellent reproducibility of nearly all features. Figure 41 presents the same two data sets but with a slight offset (approximately 0.07 in) to permit a more precise comparison. There is excellent repeatability and most features repeat to within approximately 5.0 percent; electronic noise accounts for approximately 3 percent to 4 percent of the possible variations, and if this noise could be lowered it is reasonable to expect that amplitude repeatability of a few percent could be consistently achieved. It is emphasized that within the scope of the effort which has been completed, more precise, quantitative, repeatability data have not been confirmed.

A direct comparison of features observed on data sets from the stay cable LN3 and the laboratory specimen cable is presented in figure 42. Several features in these data sets will be discussed. The reference signals in both data sets are approximately the same amplitude, and this is an indication that magnetization of the cable in the field demonstration and the laboratory experiments was approximately the same for the track 3 position (on top of the cable). In the upper record the spiral wrap signals can be recognized on all six channels and they repeat approximately three times in the 100-in scan. By contrast in the lower record no wire wrap signal is apparent. However, pitch of the spiral wire rope wrap in the laboratory specimen was approximately 72 in, and the angle at which the sensors crossed the spiral rope wrap was too large to generate a significant signal. In the lower record flaw signals were produced at approximately 16, 31, and 46 in; the flaw signal at 31 in is obvious and in some respects is similar to the spiral wire wrap signal of the upper data set. However, the flaw signals are aligned across the records while the spiral wrap signal is aligned at a slight angle across the record. Also the spiral wire wrap signal is essentially an upward going pulse while the flaw signals are bipolar. Also, note that the flaw signals have a polarity opposite to the reference signals on channel 3.

The initial upward going excursions on the field data are significantly less than is the case for the laboratory specimen. The source of the starting excursion has

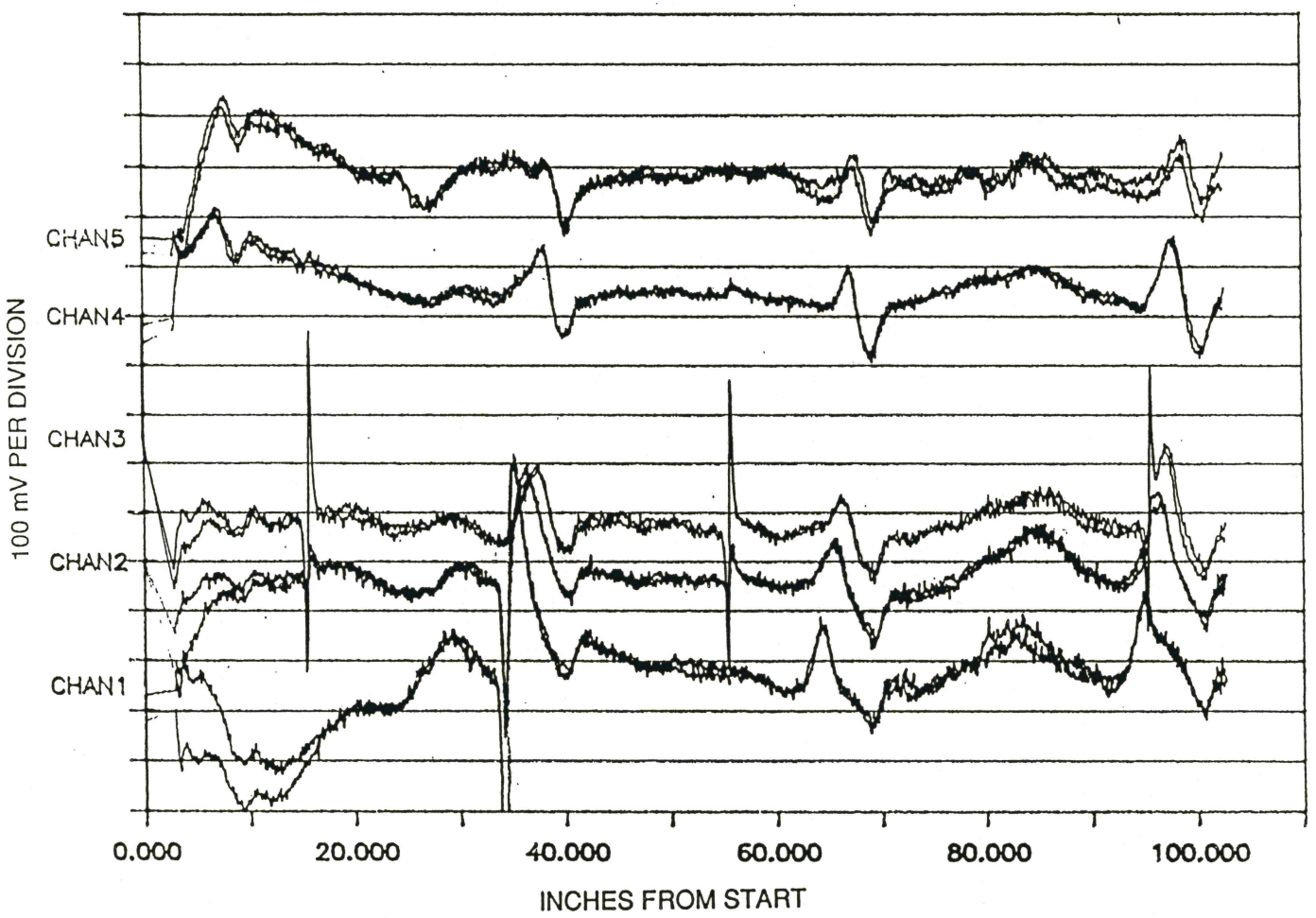

Figure 40. Overlay of two data sets indicating excellent repeatibility and potential for long term monitoring *(First set obtained, system rotated to obtain Track 3 data, then back to Track 2. Signal @ 34 in caused by 1/8-in diameter wire taped transverse to cable. Data from cable LN 1 Track 2 after subtracting CH 6).*

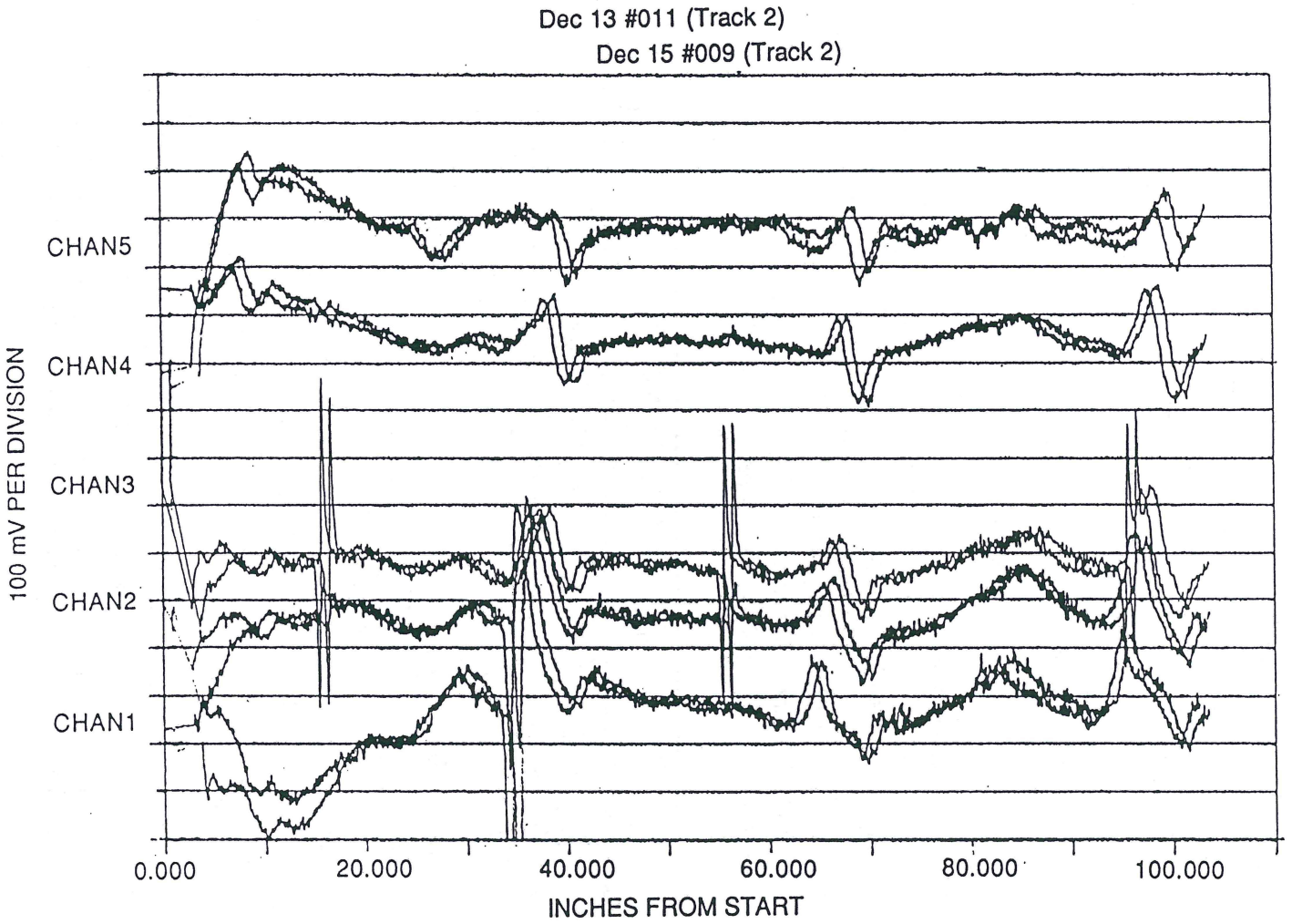

Figure 41. Overlay with horizontal offset of two data sets indicating excellent repeatability and potential for long term monitoring *(First set obtained, system rotated to obtain Track 3 data, then back to Track 2. Signal @ 34 in caused by 1/8-in diameter wire taped transverse to cable. Data from cable LN 1 Track 2 after subtracting CH 6).*

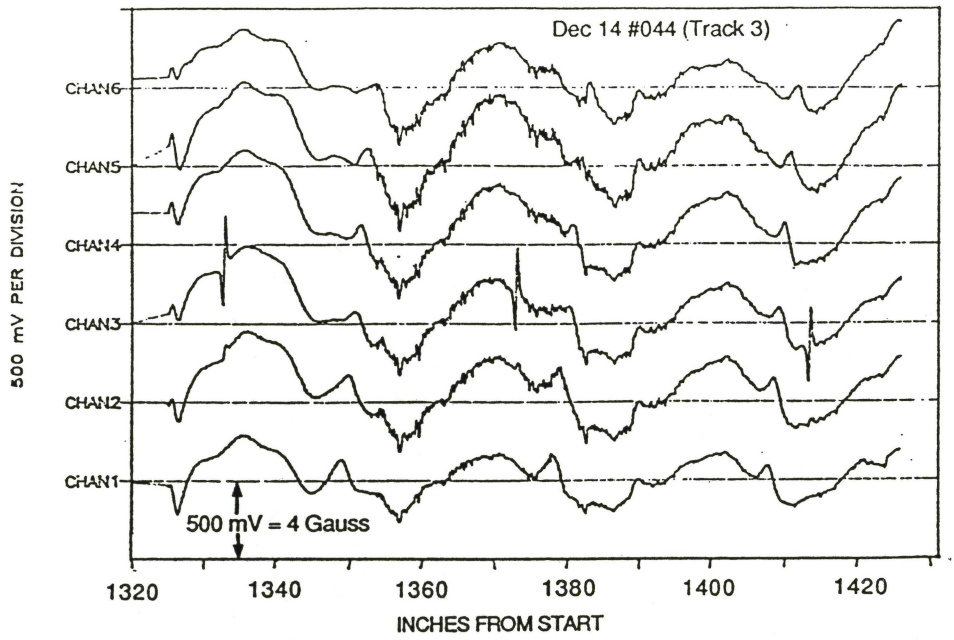

Luling Bridge stay cable LN3

(525 ft long cable comprised of 271 wires 1/4-in diameter inside 6.3-in OD polyethylene pipe and cement grouted

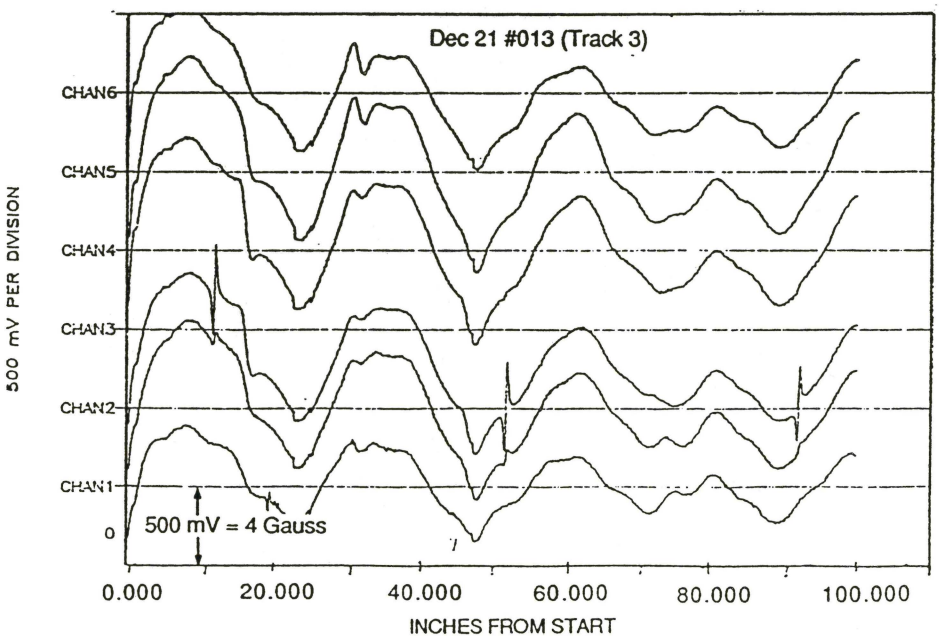

Laboratory specimen cable with flaws @ 16 in *(Depth 1.25)*, 31 in and 46 in *(Depth 1.50)*

(Flux density @25 amp. measured at pole to specimen gap 4500-5800 gauss).

Figure 42. Comparison of anamolous background signals *(undulations)* in Luling Bridge stay cable and laboratory specimen cable.

not been determined; however, in many cases for the field data, the excursion was only nominal and further comparative analysis may provide information concerning the source of this troublesome initial excursion. Intermittent high frequency noise is observed on the upper records and close examination indicates that many common features exist in this noise; these common features would be essentially removed or reduced using the digital subtraction routine. However, if overall gain of the channels are not identical residual signals would exist after subtraction. Even with identical gain in all channels, complete cancellation possibly would not be achieved because the flux density varies at the different sensors; furthermore, the output noise amplitude depends on "where and how" (electromagnetic, electronic, mechanical motion or vibration, etc.) the noise is introduced into the signal channels. Nevertheless, the digital subtraction routine has facilitated analyses.

As described earlier several attempts to minimize the undulations or major background excursions were unsuccessful and these excursions were eventually attributed to movements of the wire bundle and also individual wire segments between tie straps. During one experiment after the field demonstration, movement of the wire bundle of approximately 3/16 in was measured as the magnet was scanned along the cable. This was accomplished by inserting a small steel probe through a hole on the bottom side of the polyethylene pipe and contacting the steel bundle. As the magnet transversed this location both the steel bundle and the steel probe were pulled upward, and after the magnet had passed the location the steel probe was no longer attracted to the bundle and dropped to the floor. Since the experimental measurement indicated movement of the bundle in response to the magnetic attraction it is logical to assume that individual rods would also be slightly lifted from the bundle and could provide a source of the prominent undulations.

Many records from the Luling Bridge were reviewed in further efforts to explain the source of the undulations on track 3, and the results are presented in table 4. In these data prominent background undulations were observed on six of the 14 data sets from track 3; no prominent undulations were observed on any of the other 11 data sets from tracks other than track 3. Unfortunately, none of the data sets from track 1, 2, 4, and 5 were obtained at the same cable locations (longitudinal) as the track 3 records with the prominent undulations; the field logs indicate data sets from track 2 and 4 at locations where undulations were observed on track 3 records, but inadvertently, these data were not retrieved and reconstructed during analyses.

4. Summary of Results

From analysis of the many field data sets and by comparison with data recorded from the laboratory specimen a number of observations and possible explanations have been developed.

Table 4. Survey of Luling Bridge stay cable LN3 records for background undulations.

date	track #	record #	longitudnal location (in.)	comments	reference #1	signal #2	amplitude (mv) #3
12/13	1	006	10-110	no			
12/13	4	009	10-110	possibly slight @ 50"			
12/13	4	014	10-110	repeat slight @ 50"			
12/13	1	010	110-210	no			
12/13	2	011	110-210	no			
12/13	5	015	10-110	possibly very slight @ 70", 95"			
12/13	3	016	10-110	no			
12/14	2	003	10-110	no			
12/14	4	006	20-120	no			
12/14	2	007	120-220	no			
12/14	3	008	120-220	no	646	446	412
12/14	4	009	120-220	no			
12/14	5	010	120-220	no			
12/14	3	013	220-320	slight @ 273"	724	445	379
12/14	3	017	320-420	prominent @ 420" but more local not characteristic	658	479	513
12/14	3	021	420-520	possibly slight @ 470" has rope signal near crest	646	579	412
12/14	3	022	520-620	prominent @ 550" spacing 34.5" slight @ 583" spacing 35.0"	624	463	379
12/14	3	027	720-820	prominent @ 770", 798" spacing 29.5"	601	468	434
12/14	3	028	820-920	possibly slight @ 850"	546	479	395
12/14	3	032	920-1020	no spacing 32.5"	579	479	357
12/14	3	035	1020-1120	prominent @ 1070", 1100"	546	490	345
12/14	3		1120-1220	no records			
12/14	3	041	1220-1320	prominent @ 1258" spacing 30.0" + 28"	546	501	423
12/14	3	044	1320-1420	prominent @ 1370", 1400" spacing 29.5" + 29.5"	546	479	445
12/14	3	049	1420-1520	no spacing 28.5" + 30.5"	590	523	423
12/14	2	054	0-100	no	702	713	601

a. When system positioning is precise, repeatability of data are excellent and are considered adequate for long-term monitoring; however, an improved method of longitudinal position determination will be required.

b. Prominent signals, with precise spacing agreeing with the measured distance are provided by the three reference wires imbedded in the shield on the track 3 data channel. These wires facilitate confirmation of scale sensitivities during data reconstruction, provide a potential method for measuring the separation between the sensors and the steel bundle and the associated flux density in the steel cable (calibration of this measurement possibility is required), provide a method for precisely positioning the MPC system for marking the precise location on a cable of an interesting feature perhaps for later independent examination via excavation, etc., and provide the operator with an indication of system functioning during data acquisition.

c. Nominal amplitude unipolar (upward going) features are observed at intervals of approximately 25 to 35 in on track 3 (top of cable). These features (signals) are slightly angled across the cable and advance counter clockwise along the cable. Sometimes these signals are obscured by the system noise and the undulations on track 3; however, use of the subtraction routine makes all these signals prominent. The angled signals are continuous across all five tracks but amplitude decreases on tracks other than track 3. Such observations are consistent with these signals being produced by the spiral wire rope wrap with a pitch ranging from approximately 25 to 35 in; this possibility is almost conclusive even though the engineering drawing provided by the fabricator specified a pitch of 6 ft for the 1/4-in diameter wire rope spiral wrap.

d. Repetitive unidirectional signals are also observed on other tracks (other than track 3) and these signals are almost completely obscured by the background electronic noise and undulations particularly on tracks 1 and 5 near the bottom of the cable. As the spiral wrap signals decrease the reference signals increase in an apparent corresponding manner. This inverse relationship is consistent from record to record. A plausible explanation is that the distance from the polyethylene pipe O.D. to the steel bundle is greater on the bottom than on the top of the cable and also possibly from side to side of the cable. It is expected that the cement grout coverage probably varies correspondingly.

e. Prominent cyclic signal excursions (undulations) sometimes occur on the top regions of the cable (track 3). Often the spiral wrap signal is more prominent in these regions of undulations than in regions free of undulations. Also there appears to be a correspondence between the undulation nodes and the spiral wrap signals; examination of many data sets did not disclose a spiral wrap signal on the crest of any undulations. Furthermore, no cyclic excursions (undulations) were observed on any tracks other than track 3 although the number of such data sets was relatively small. The magnitude of these undulations is

approximately 1/2 the amplitude of somewhat similar background excursions observed from the laboratory specimen which was ungrouted. A plausible explanation for these observations is that the cement grout is either very thin or nonexistent in these regions and that the attractive force of the magnet moves individual wires or group of wires closer to the magnet poles and the sensors thereby providing the signal.

f. Based on the characteristic features obtained from flaw signals in the laboratory specimen when flaws were located in the outermost layer and the second layer, and since no such signals were observed on the field data it is concluded that no broken wires existed in these regions (1st and 2nd layers) of the cable examined. This statement applies with very high confidence to the track 3 region but decreases on other tracks. Sensitivity was not adequate to examine the entire cable cross-section with the required sensitivity to detect broken wires in the interior regions.

g. Although no broken wires were anticipated for stay cable LN3 it is important to establish the flaw detection capability of the MPC system during the field demonstration. This can be established by observing in figure 42 (lower records) that the calibration flaw at 31 in produces a 195 mV signal on channel 6, and the 50 mV signal on channel 4 is "recognizable" because of the distinctive signature characteristics. This calibration flaw was in the 2nd layer of rods in the bundle at a depth of approximately 1.4 in from the sensor. A similar sized flaw in the 4th layer, located beneath channel 6, would produce a 50 mV signal, and therefore should be recognizable provided a similar flux density was achieved in cable LN3. The reference signals on channel 3 are approximately the same amplitude for the calibration records and for most track 3 positions (top of cable) on stay cable LN3; accordingly, the flux density for track 3 is approximately the same for both cases and the calibration data can be used to estimate with high confidence the maximum depth at which a fractured wire could be detected. For the track 3 position this maximum depth is the 3rd layer and possibly the 4th layer of rods in the bundle. Use of the subtraction routine and also the correlation process could possibly extend the depth. No signals indicative of a fractured wire were observed on any of the data obtained during the field demonstration.

C. Assessment of Field Performance

Overall performance of the prototype MPC system during the field demonstrations was satisfactory although several areas of improvement and several malfunctions were encountered. Since this was the first field experience with the system and since facilities and time for prefield training of the team were very limited, operations were relatively inefficient. The inability to rotate to all five scan tracks and repeated attempts as well as many hours spent trying to determine the source of this malfunction also contributed to the inefficiency.

Although a large team was involved with this first field demonstration it is reasonable to expect that a three man team could perform the field inspection activities after several modifications had been completed on the prototype MPC system. One or more personnel would also be required for traffic control.

The quality of data was not as good as had been anticipated, and a significant factor was the intermittent noise apparently caused by a misaligned plastic bushing that provided insulation for the scanning electromagnet system.

Despite the foregoing, it is important to emphasize that much information, heretofore unavailable, was provided on the constructional and erection details of the stay cables which could be of significance in determining the susceptibility of various regions of the cable for exposure to the outside environment. These data may be important in plans for maintenance activities and possible future renovation of cable structures.

V. COMPREHENSIVE ASSESSMENT OF MAGNETIC METHODS AND MPC PROTOTYPE SYSTEM

Results from this program and previous results obtained from other programs have provided comprehensive data justifying selection of the Magnetic Perturbation Method for the cable inspection and monitoring system. Although it was anticipated that the program would provide enough quantitative data to provide high confidence in forecasts of flaw detection and monitoring capability based on parametric relationships, for the variety of reasons previously discussed this was not accomplished. However, subsequent to the field demonstration a few experiments were conducted to provide additional data indicative of the capability of the magnetic perturbation method as embodied in the MPC system.

One of the primary factors limiting the small flaw detection capability, particularly in the interior regions of cables, is the relatively low flux density which was obtainable with the magnet design used in the MPC prototype system. Previous results indicating the significant influence of flux density on flaw detection capability were reviewed in figures 31 and 33. Since it was not possible to increase the magnetizing force available with the MPC system, an alternative was to minimize the difficulty of magnetizing the laboratory cable specimen by significantly decreasing the separation between the pole pieces and the cable bundle. This was accomplished by removing the polyethylene pipe, the 1/4-in diameter spiral wrap cable, and the PVC spacers. Several additional stainless steel bands were added to assist in compacting the specimen, and the specimen was then supported in a semicircular segment of the aluminum pipe used during previous experiments. The bundle was held in the aluminum pipe by tie bands near each end. This assembly was then installed in the MPC system. Measured flux density in the pole to specimen gap was 8500 to 9500 gauss compared to approximately 4500 to 5000 gauss in the original laboratory specimen with the polyethylene pipe. Although only one experiment was conducted a marked improvement in flaw detection was obtained, and results are presented in figure 43 along with comparative results from the original laboratory specimen. Note that the vertical sensitivity is the same for both data sets; in the lower record the amplitude of the reference signals on CH 3 are only approximately 60 percent of the amplitude in the upper records where the flux density is considerably less. All flaws are prominent in the lower records; in the upper records, while the flaws at 16 in and 31 in are easily observed the flaw at 46 in is obscured by the gradient. The upward going excursion near the beginning of the lower record is significantly greater than in the upper records, and in several regions the background undulations are similar in amplitude but the undulations are more extended, spatially, in the upper record.

After subtracting channel 3 the improved records presented in figure 44 were obtained. Much of the background has been eliminated and noise is now approximately 20 mV. The signal to noise ratio of signals from all three flaws is

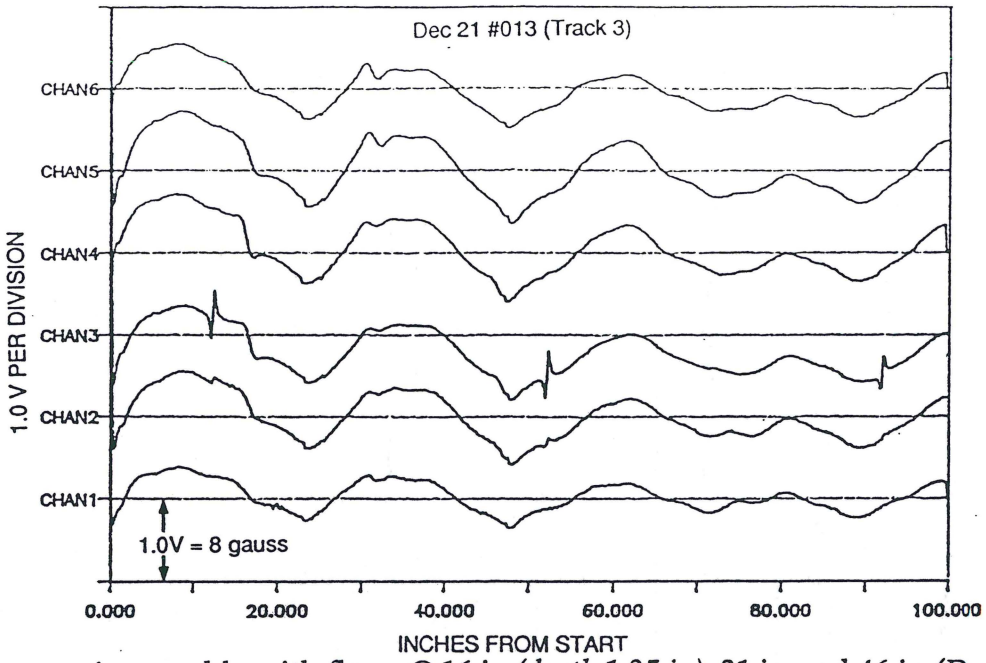

Laboratory specimen cable with flaws @ 16 in *(depth 1.25 in)*, 31 in and 46 in *(Depth 1.50 in) (Flux density @ 25 amp. measured at pole to specimen gap 4500-5800 gauss).*

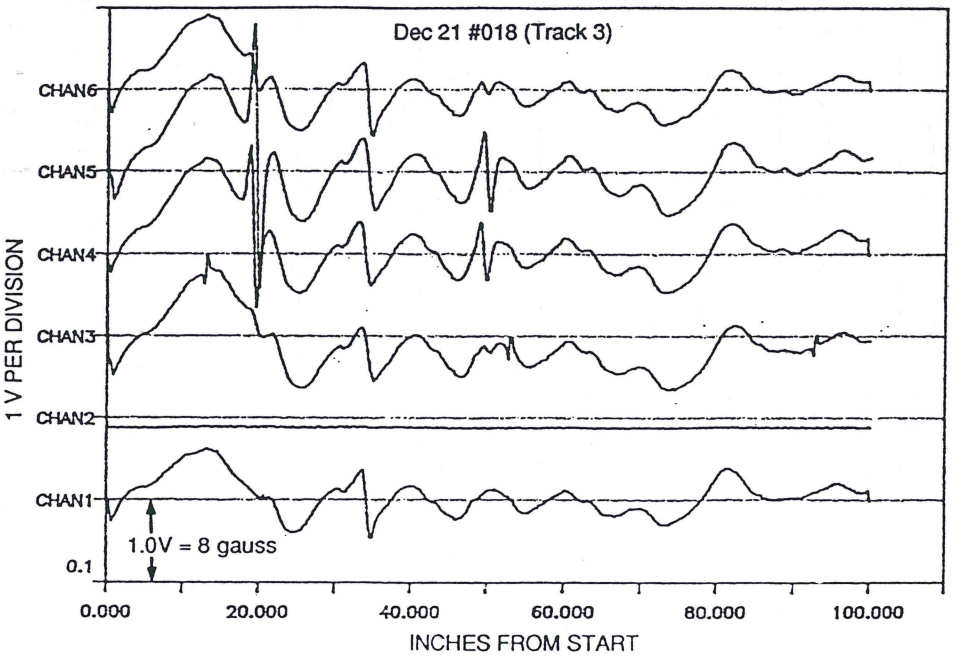

Modified laboratory specimen cable *(271 rod bundle w/o spiral wrap, PVC spacers, or polyethylene pipe, supported by lower half of aluminum pipe similar to Figure 22 flux density @ 25 amp. 8500-9500 gauss; lower record CH2 inoperative).*

Figure 43. Major improvement in flaw signal amplitude at higher flux density.

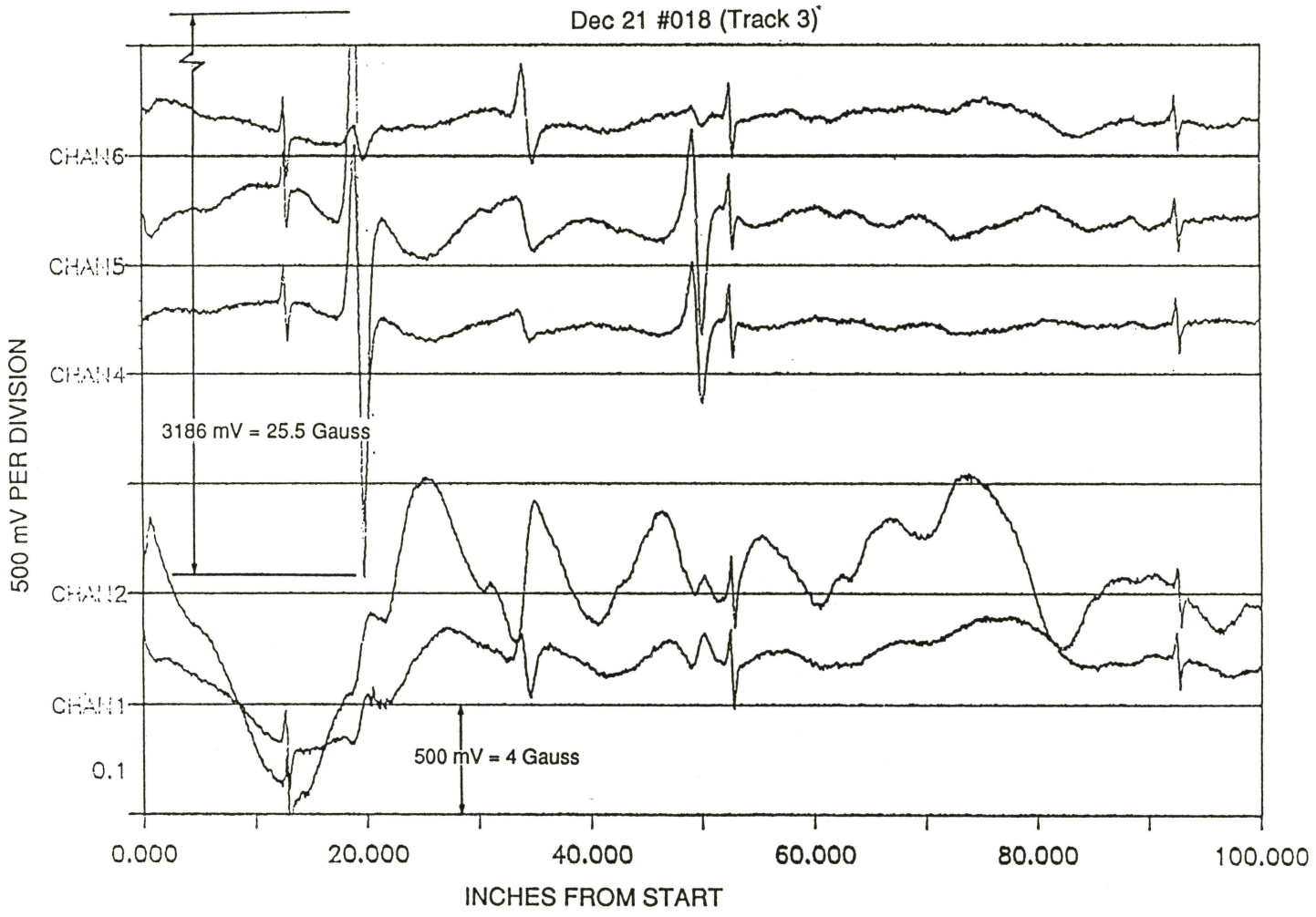

Figure 44. Prominant signatures from all flaws after subtracting CH3, modified laboratory specimen cable *(25 amp. 8500-9500 gauss; CH3 subtraction produces 3 reference signals which inverted polarity on all channels, also since CH2 was inoperative second record from bottom becomes inverted CH3, compare with CH3 lower records of Figure 43).*

now great enough to provide confidence in developing parametric relationships, and in particular in calculating the exponent for the equation relating signal amplitude to flaw depth. Before presenting these results a few further comments will help clarify the records of figure 44. Note that the reference signals now appear on all five channels and this is because channel 3 was subtracted from all other channels. Also by referring back to figure 43, it is observed that channel 2 is inoperative; accordingly, when channel 3 is subtracted from all other channels the channel 3 record appears on channel 2, unchanged except for inverted polarity. This feature is readily apparent by comparing channel 3 of figure 43 with channel 2 of figure 44 (increased gain). The fact that only a small amplitude signature is obtained from the flaw at 34 in is caused by subtracting the channel 3 signature from the other channels, and by referring to figure 43 it is apparent that signals from this flaw are approximately the same amplitude on all channels. The upward going part of the signal from the flaw at 20 in is completely offscale, and measurements have been corrected with the correct value indicated on the records.

The parametric relation describing maximum flaw signal amplitude was previously presented in figure 10, and a more comprehensive presentation is in appendix C. To investigate the relation of signal amplitude from identical flaws at different depths, equation (8) appendix C becomes:

$$\frac{S_1}{S_2} = \left[\frac{d_2}{d_1}\right]^n \qquad (1)$$

Experimental data from the flaw signals on CH 5 at 20 in and 50 inches in figure 44 can be used in the above equation to determine the value for the exponent n. Solving the above equation for n, a more convenient equation is obtained.

$$n = \frac{\ln \frac{S_1}{S_2}}{\ln \frac{d_2}{d_1}} \qquad (2)$$

Signal amplitudes measured from figure 43 and figure 44 and measured depths to the flaws are:

$S_1 = 3186$ mV; $S_2 = 996$ mV
$d_1 = 0.50$ in; $d_2 = 0.75$ in

Substitution in the equation 2 yields:

$$n = \frac{\ln \frac{3186}{996}}{\ln \frac{0.75}{0.50}} = \frac{1.163}{0.405} = 2.87 \qquad (3)$$

This value of 2.87 if somewhat higher than the value (2.22) calculated using the data of figure 33, and the signal decrease would be greater with increasing flaw depth; however, the theoretical value of 3.0 was used in the estimated capabilities of table 1, and the lower value of 2.87 would improve these estimates. Additional data are required to more precisely determine this important parameter.

Since the relation between flaw volume and signal amplitude is linear, and using the data (3186 mV) for the flaw at 20 in, it is estimated that a pit approximately 0.06-in diameter. by 0.06 in deep would produce a flaw signal of 80 mV. The small bipolar "signal" at 50 in on the CH 6 record of figure 44 is approximately 80 mV and is a "recognizable feature"; therefore, such a pit should be detectable at this flux density. Increasing the flux density would increase the signal and even smaller pits should be detected.

Software for the flaw algorithm and the correlation analyses were only developed shortly before the field trip, and it was not possible to complete the experiments for establishing the effectiveness of this method before the field demonstration. However, after returning from the field demonstration a very limited evaluation was completed. Figure 45 presents the results from one correlation analysis performed on the data of figure 43 after subtracting the channel 6 data. Very high correlation coefficients of 0.925 are obtained for the flaw near 20 in and 0.858 for the flaw near 50 in on the channel 5 record. Measured peak separation was approximately 0.7 in; however, the peak separation used in the correlation analysis was 1.0 in. It was not possible to investigate the correlation analysis other than on a limited basis and it is possible that the algorithm or the method of specifying peak separation is the cause for the lack of agreement inasmuch as peak separation of 0.7 in should have produced the highest correlation coefficient. When lower values of peak separation were used the correlation coefficient was significantly decreased from the 0.925 value to approximately 0.76 for a peak separation parameter of 0.7 in.

One of the main advantages of the correlation analysis is to provide a way of machine analysis of records to determine the locations of signatures in the data which correspond to the flaw algorithms stored in the computer. A further advantage is that this procedure can be effective when the signal to noise ratio is relatively low compared to visual analysis which usually requires a signal to noise ratio of 3/1 or greater for high confidence. Once the effectiveness of the algorithm and the correlation software have been confirmed, it would be possible to analyze all

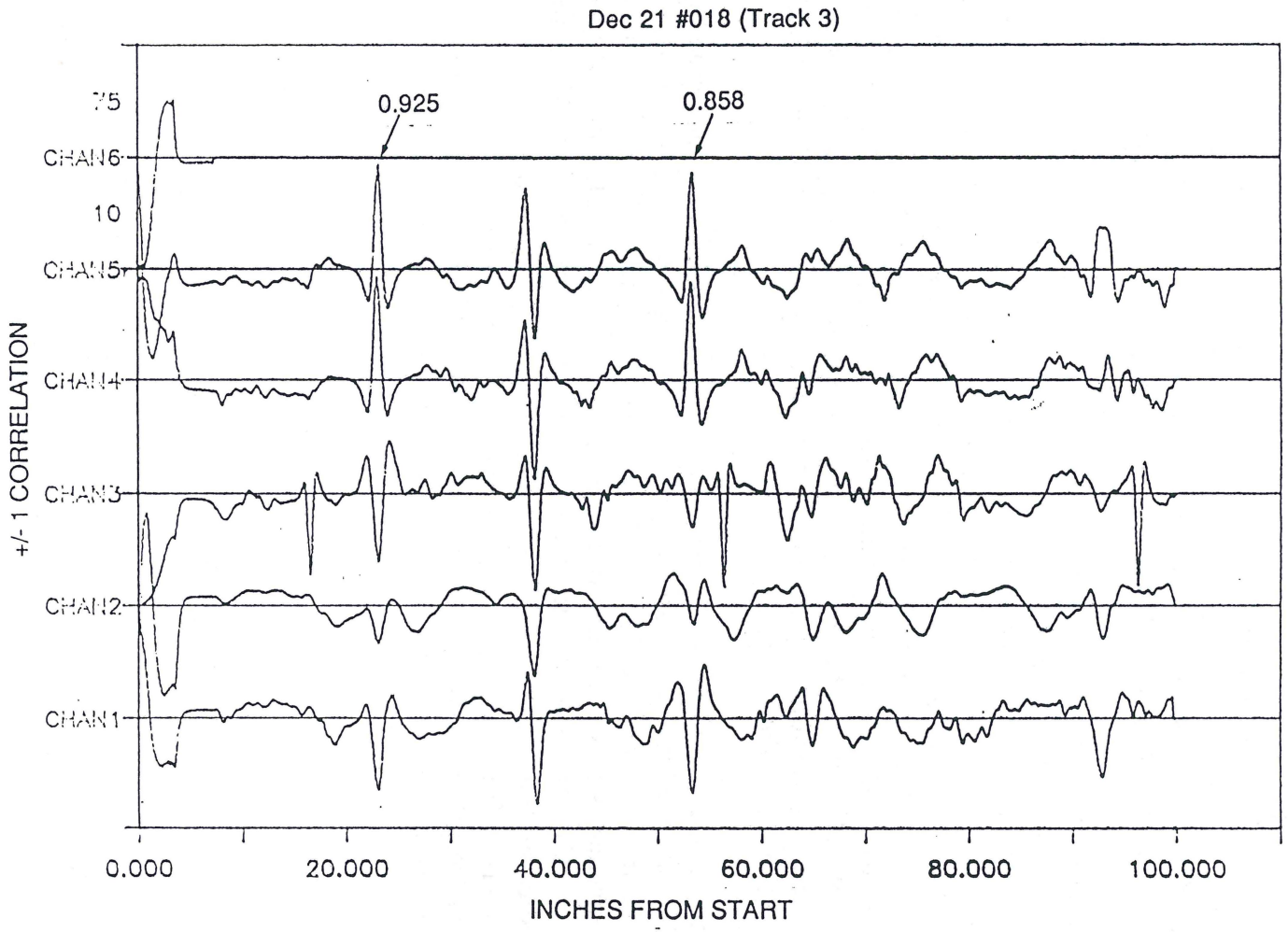

Figure 45. Correlation results using data from modified laboratory specimen after subtracting CH6 from all other channels; correlation parameters: 75 data points *(7.5 in)*; peak to peak separation 1.0 in *(Negative correlations obtained for flaws in CH1, 2, 3 because subtraction of CH6 inverted flaw signals; negative correlations for three reference signals on CH3 because the signals have polarity opposite to flaws, see Figure 43).*

data from cables and print out only those locations which are suspect on the basis of the machine or computer analysis. Data from these suspect locations could be retrieved and records reconstructed for further analyses.

The minimum size flaw that can be reliably detected is a primary consideration in judging the potential effectiveness of the MPC system for structural integrity assessment of bridge cables. The minimum amplitude signal that can be detected is directly influenced by the system and environment noise. Electronic noise during some of the early evaluations of the MPC system, but before the complete digital data system was operational, indicated a noise of approximately 3 mV peak to peak (see figure 11); however, it was necessary to have a large diameter grounding cable connecting the MPC structure and the moving electromagnet. Such a ground was inconvenient, and an alternative was to insulate or isolate the moving structure. Noise encountered in the system during the field demonstration varied from approximately 20 mV to 50 mV or even greater; after correction of a shorted insulating bushing, noise was consistently observed to be approximately 20 mV, and it should be possible by careful analysis to determine the component or components in the data system which contributes to this excess noise of 20 mV compared with approximately 3 mV. Minimum system noise is a primary factor influencing small fatigue crack detection as explained next.

During the program review on 26 January 1989, the importance of detecting fatigue cracks in cable wires and also possibly in welded joints of "steel pipe" protective enclosures was indicated. This presents somewhat conflicting magnetizing requirements since "earliest detection of tightly closed fatigue cracks" is optimized at relatively low flux densities while high flux density is required for detecting flaws such as pits and fracture separations.[13,14,15] Accordingly, multiple inspections at different flux densities may be required. Furthermore, since signal amplitudes will be very low from fatigue cracks, it is necessary to minimize noise to the greatest extent possible to enhance detection of such flaws (see appendix D).

VI. DISCUSSION OF INSPECTION RATES

The inspection rate for the prototype MPC system was relatively slow. Scan speed of the magnet assembly was 1 in/sec, therefore, a six channel 100-in data acquisition sequence was completed in 100 seconds. The magnet was returned to the initial starting position at a rate of 2 in per second. A complete five position data set plus a machine advance of 100 in to a new longitudinal inspection location required approximately 14 minutes which projects to approximately 15 hours for a 525-ft stay cable such as LN3. Including an installation and removal time of approximately 30 minutes each or a total of 1 hour would project to approximately 16 hours for inspecting these long cables. The shorter cables on the Luling Bridge could be inspected in approximately half this time or 8 hours. The estimated 27,000 linear ft of cable in the Luling Bridge would require approximately 823 hours total inspection time including set-up and removal of equipment. With a 10-hour work day approximately 15 to 16 weeks would be required assuming 5 days per week.

The limited experiments conducted at a inspection scan speed of 2.0 in per second offer promise that this inspection speed can be used without significant loss of flux penetration to the interior strands; however, additional effort is required to confirm this possibility. Assuming this higher inspection speed, inspection of all the cables on the Luling Bridge could be accomplished in approximately 7 to 8 weeks. With improvements in software routines and in particular machine analysis of records, an additional 2 to 3 weeks for data analysis would be required. Data acquisition time could be reduced further by using a scan sequence in which a 100-in scan is made in one direction and then the system is indexed to the next inspection track and data acquired during the reverse scan, and perhaps only 3 1/2 to 4 weeks would be required for acquiring data from all cables. Software for reconstructing records to correct for the alternate "forward" and "reverse" scans would be required, also the increased duty cycle could possibly cause excessive electromagnet temperatures.

Since stay cable diameters are in the range of 6 to 8 in, multiple magnets and probes arrayed around the entire circumference could provide significant advantages. The multiple magnets (possibly permanent magnets) could increase the flux density in the cable to very high values with only relatively moderate flux density (3000 to 4000 gauss) at the pole faces. Signal amplitude and flux in the interior regions would be greatly improved, thereby permitting detection of very small pits (perhaps approaching 0.02-in diameter and depth) at the exterior surfaces and possibly somewhat deeper. Only a single scan of the total cable length would be required, and at 1 in/sec a 525-ft long stay cable could be inspected in approximately 2.0 hours. Conceptually, design of such a single pass system is simple. However, power for electromagnets would increase several times; if permanent magnets are used means must be provided to shunt the magnets during attachment operations, additionally, it may be necessary to provide protective shields to prevent inadvertent injuries with such powerful magnets.

Appendix E presents a brief discussion of noise and approaches for noise reduction and also briefly discusses the influence of increased inspection speed and a single pass scan on data transmission requirements.

VII. EVOLUTION OF MPC PROTOTYPE SYSTEMS AND FUTURE POSSIBILITIES

Initial concepts and also preliminary designs for a magnetic perturbation system applicable to main cables included features for negotiating cable bands and for inspecting elements such as suspender cables and sockets. With the reduced scope authorized in May 1988 and selection of the cable stayed bridge at Luling, LA, the prototype system design objective was concentrated, primarily, to accommodate cables with features similar to stay cables of the Luling Bridge. Main cables and other elements of conventional suspension bridges would require different equipment designs, but much of the NDE data system and analysis foundation would be common to all cables. Accommodation of both type bridges by a single system has advantages and disadvantages; however, separate NDE systems would provide more advantages. For example, only a nominal range of cable diameters are used for existing and planned cable stayed bridges, and these can be accommodated by a single adjustable mechanism. However, the diameter range of main cables is so great and the attachments so varied that several mechanisms capable of complex motions would be required to accommodate existing suspension bridges. Also, existing suspension bridges would require a wide range of magnetizing assemblies, while cable stayed bridges would require only one adjustable assembly.

From these rather limited comparisons, the anticipated costs for developing a fully operational system adequate for routine inspection and monitoring of stay cables would be significantly less than for main cables. Nevertheless, even with these simplifying constraints, evolution of a fully operational system will require a major program, continuous for 3 or 4 years, and with realistic total funding in the range of $2 million. Continuing funding for maintaining a central archival data base, repeated inspections of cables, analyses of data and recommendations would require estimated funding in the range of $1 million each year. Continuing funding would be influenced by the number of bridges and cables, cable dimensions, inspection intervals, extent of familiarization with NDE data associated with specific cable anomalies, improvements in search and analyses routines, standardization of operational and reporting routines, etc. Such a program would be based on proven concepts for "structural life-time assurance" and "life cycle costs" which have been successfully applied to many high cost long life structures. A key element in all these programs is use of advanced NDE systems, such as the MPC System. Furthermore, the minimum flaw or anomaly that can be reliably detected, quantitatively sized, precisely located, and otherwise characteristically identified increases confidence in forecasts and is a major factor in specifying reinspection intervals and timely corrective or replacement actions. Since structural life-time assurance programs are usually most effective when they are initiated early in life, a high priority appears appropriate for applying this strategy to cable stayed bridges. Even though the present progress on the MPC system has not confirmed the Phase I quantitative estimates presented in table 1, these forecasts should be achieved or even exceeded with: refinements to minimize noise, significantly increased

magnetization, improvements in data processing, experience in correlating signatures associated with flaws and other cable details, etc.

VIII. CONCLUSIONS AND RECOMMENDATIONS

A. Conclusions

1. The magnetic perturbation method has the inherent sensitivity, resolution, repeatability, long-term stability, and other characteristics which are necessary and/or desirable in an NDE method for inspecting and monitoring structural cables and strands of suspension Bridges. (See figures 11, 12, 31, 33, 34, 40, 41, 43, 44 and tables 1 and 6.)

2. Flux densities significantly higher than could be provided by the 27,500 ampere turn electromagnet would be required for detecting very small flaws (0.01 percent cross-sectional area) such as corrosion pits even in the exterior regions of cables in the range greater than approximately 3 inches in diameter; this also applies to larger flaws (0.4 percent cross-sectional area and larger) in the deep interior regions beyond approximately 3 in.

3. The magnetic perturbation method has been successfully incorporated into a prototype Magnetic Perturbation NDE Cable System (MPC).

4. The prototype MPC System has been demonstrated to have excellent flaw detection performance on a specimen simulating a segment of the 6.3-in diameter stay cables used on the Luling Bridge; specimen instabilities caused background noise (undulations) that distorted signal shapes and reduced the confidence of parametric values used in forecasts of flaw detection capabilities; the higher flux density in the modified specimen and the greatly increased flaw signal amplitudes increased confidence in flaw detection capabilities.

5. The prototype MPC system was successfully demonstrated on stay cables of the Luling Bridge.

6. No signals indicative of fracture were observed in the 0.25-in diameter wires comprising the stay cables.

7. Comprehensive analyses of signals indicate nonuniform cement grout coverage with minimum thickness in the top regions of the cable.

8. Major background excursions (undulations) observed in several regions on top of cable LN3, and somewhat similar undulations observed in the ungrouted laboratory specimen (see figure 42) were attributed to wire movement in response to magnetic attraction (actually measured 3/16 in and flux density variations of approximately 12 gauss); therefore, the possibility must be considered that the grout is very thin or nonexistent and does not constrain movement nor provide protection for the wires in these regions of cable LN3.

9. Increasing the pole piece flux density by approximately a factor of 2 (from 4500 to 9000 gauss) produced an increase in flaw signal amplitude of approximately a factor of 10 with no increase of system noise (see figures 43 and 44).

10. The overall field operational capability of the prototype MPC system has been proven on the Luling Bridge, and results form stay cable LN1 and LN3 together with the results from laboratory specimens indicate that systems of this type (modifications/refinements and also advanced evolutionary models are anticipated) should be capable of providing the precise, stable, quantitative NDE data (heretofore unobtainable) that are essential for successful implementation of modern structural life time assurance strategies to suspension bridge cables.

The MPC System in the present configuration (or with a few modifications) can provide such NDE data from several cable stayed bridges; with major design changes the MPC System could accommodate the large diameter, aging main cables of the Golden Gate Bridge, the Williamsburg Bridge and other major suspension bridges.

B. Recommendations

1. Improved models of the MPC System should be developed and integrated into plans for structural life time assurance management of structural cables and strands of suspension bridges.

2. Since designs and costs of mechanisms that can accommodate and scan the cables is highly dependent on details of each cable design (size, outermost and intermediate coverings, attachments, accessibility, cable "makeup", etc.) several subdivisions should be established with priorities and funding assigned to each.

3. The prototype MPC System with minor modifications, primarily to increase the magnetization and refine software, should be used to quantitatively verify detection limits and parametric relationships using specimens that are mechanically stable.

(Reprinted from Public Works. Used by permission.)

Inspecting and Evaluating New York's East River Suspension Bridge Cables

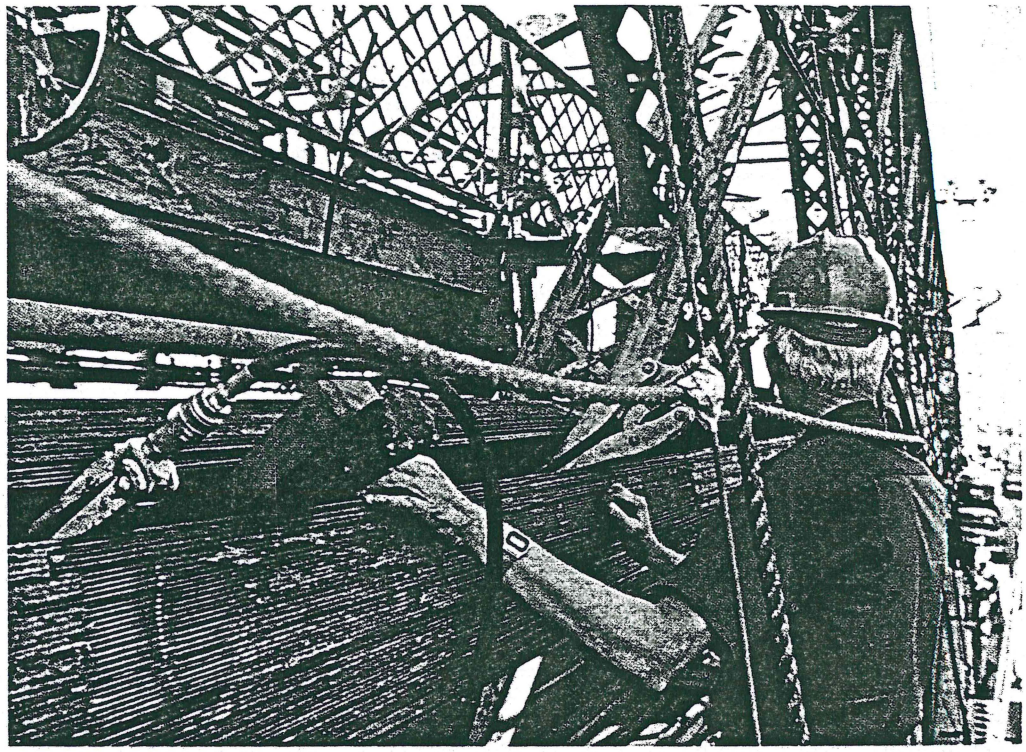

■ GROOVE is opened in the main cable of the Williamsburg Bridge to allow inspection of the interior wires.

FRANK J. MONDELLO, P.E.
Steinman, Boynton, Gronquist and Birdsall,
New York, New York

Reprinted from the Proceedings of the International Bridge Conference, Pittsburgh, Pennsylvania, U.S.A., June 13, 14, and 15, 1988.

THE inspection, evaluation and rehabilitation of New York City's East River bridges presented and continue to present engineers with unique and challenging problems. There are four major structures that cross the river:

The Brooklyn Bridge. John A. Roebling's last and greatest design, completed by his son, Washington, just celebrated its 105th Birthday last May. This combination suspension and cable stayed bridge has faithfully stood up to the ravages of the elements and traffic levels that surpassed even the Roeblings' vision.

The Williamsburg Bridge. This 85-year old single span suspension structure was the first all-steel bridge and the first to exceed the span length of the Brooklyn Bridge, but hardly its grace and beauty. The Williamsburg Bridge currently holds center stage due to the large number of severely corroded conditions found during its recent inspection; conditions that have caused the bridge to be completely closed for six weeks while emergency repairs were carried out. The bridge was re-opened in stages as repair work continued. With its eight roadway lanes and two rapid transit tracks, the Williamsburg Bridge surpasses the Brooklyn Bridge in functional usefulness.

The Manhattan Bridge. When opened 79 years ago, the Manhattan Bridge held the capacity record of the city's suspension bridges providing passage for four tracks of rapid transit trains, six tracks of trolley cars, and three lanes for vehicles. The trolley lanes have long been converted to truck lanes, however. The Manhattan Bridge contains many features proposed by the notable Gustav Lindenthal, then the city's commissioner of bridges. However, upon his dismissal from that position, certain design aspects were changed, and as a result, it was the first of New York City's bridges to be designed using the then new deflection theory of analysis.

The Queensboro Bridge. The only one of the four that is not a suspension bridge, but under the influence of Gustav Lindenthal, this double cantilever truss span was designed without the traditional simple span suspended from the cantilevers, and as a result, has the lines of a suspension bridge. The Queensboro was another high capacity structure when it opened in 1909 providing access to rapid transit trains, trolley cars, vehicles, and pedestrians. She currently carries ten lanes of car and truck traffic and, at about 145,000 vehicles per day, is the most heavily used toll free bridge in New York City.

Maintenance Problems

Since these bridges, like all bridges owned by the City of New York, are "toll free," maintenance is funded from general revenues. During the 1970s New York City was on the brink of fiscal collapse. Available financial resources were needed to fund the police, fire, and sanitation departments as well as a host of social and

welfare programs. Bridge maintenance was not viewed as an essential service and much work was deferred and staffing reduced. This occurred at a most unfortunate time since these four bridges had already served between 70 and 95 years and their roadway decks were between 25 and 50 years of age.

During the late 1970s the Federal government began funding bridge inspection and rehabilitation programs, administered through the states. The government mandated that bridges be inspected on a two year cycle. Since the East River bridges are owned by New York City, the city retained the services of local consulting engineering firms to perform inspections, prepare reports, and recommend rehabilitation. Having been long involved with inspecting, remodeling, and recommending maintenance on the Brooklyn and Queensboro bridges, Steinman, Boynton, Gronquist and Birdsall was retained to inspect those two structures. Similarly, the firm of Ammann and Whitney was assigned the Williamsburg Bridge as was Edwards and Kelcey, assisted by Weidlinger, and Steinman, for the Manhattan Bridge.

Each consulting firm had to familiarize itself with the respective bridges' unique history from original design and construction through subsequent modifications and repairs. Each bridge had main items of concern, or known deficient conditions, upon which the engineers needed to focus. For example, on the Brooklyn Bridge, the condition of the main cables within the anchorage chambers was a key concern as was the breakage of the short, solid rod type suspenders at the main span's center.

The Queensboro Bridge has been plagued by corrosion of its lower level floor steel and truss bottom chords due to a leaky roadway that allows water laden with deicing salts to contact the structure and deteriorate the deck itself. The Manhattan Bridge, designed by the deflection theory, does just that. From the beginning, the bridge has suffered through many instances of cracked floor and bracing members due to the effects of high torsional displacements caused by unsymmetrical rapid transit loadings. The Williamsburg Bridge was long ago observed to be suffering corrosion of its main cable wire.

In-Depth Inspections

During the late 1970s in-depth inspections were performed on the four bridges and their approach structures. Every element of each bridge received a close, "hands-on" inspection and observations were recorded on thousands of field notes, sketches, and photographs. Access to structural bridge members included walking on suspension cables, direct climbing of steel members, use of bridge maintenance travelers and rented lift vehicles, and rigging.

Perhaps the most unique and interesting aspect of the program was the inspection and evaluation of the suspension bridges' main cables. Suspension bridge cables, such as those found on the East River bridges are built-up of high-strength steel wire, spun from anchorage to anchorage until a desired cross section is attained. Groups of up to several hundred wires are spun into a strand. A specified number of strands are bundled to form the cable. There are several thousand wires in a typical bridge cable. The wire in each strand is spliced together during the spinning operation so that each strand is formed of one continuous wire several miles in length. The thousands of wires are compacted, or squeezed, into a solid cylindrical shape.

At this point, on a typical modern bridge, the cable bands that support the suspenders are installed and clamped tight. The exposed lengths of cable wire, between the bands are then wrapped, usually with a protective layer of soft steel wire embedded in a thick coating of red or white lead paste. This wrapping wire is caulked at the cable bands and painted to seal moisture out of the cable.

At the cables' anchorage, there is a special type of clamp known as a splay casting. The splay casting is a bell shaped cable band that allows the cable to change its shape from a solid cylinder, facing the bridge, to its individual strands diverging toward their respective anchorage points.

Usually the strands will split in half to wrap around a horse shoe shaped device called a strand shoe. The shoe is pinned to the end of a chain of eyebars that in turn is anchored beneath the huge mass of the anchorage structure.

A routine general inspection of main cables would usually involve walking on the cables and observing the condition of the paint on the wrapping wire and the wrapping wire itself. Breaks in the paint film or separations between turns of wire will allow water to enter into the cable itself and possibly cause corrosion. The exposed strands within the anchorage chambers would be observed for signs of corrosion and possible breaks, particularly in the vicinity of the strand shoes where they tightly turn to reverse direction.

Typically, main cable wire and wrapping wire are galvanized and the zinc layer serves to further protect the steel bridge wire. Normally this provides for a durable and long lasting cable system, if routine maintenance is provided.

Extraordinary Inspection

Because of their age, critical importance, and years of deferred maintenance, the 1978 and 1980 inspections included deeper levels of examination than described above. Steinman performed the in-depth inspection on the Brooklyn Bridge at

■ INSIDE anchorage chamber of the Williamsburg Bridge, engineers and iron workers move the location of a splay point for close inspection of the cable and broken wires.

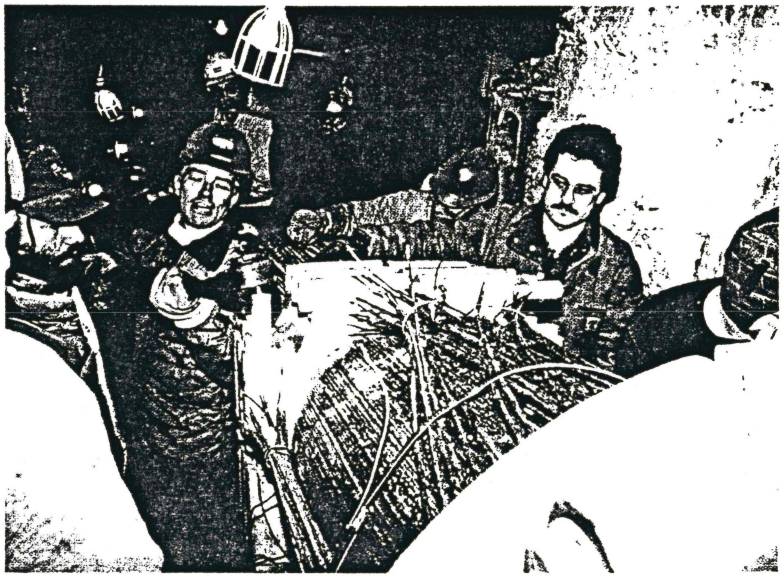

that time and developed procedures for further, deeper inspection techniques that were subsequently carried out as part of a rehabilitation contract. More recently, some of these techniques were used by the firm to perform an independent evaluation of the Williamsburg Bridge cables.

It is well-established that salt is a most effective deicing agent that keeps roadways passable during severe winter weather; and it is an agency's prime concern to keep the traffic moving safely. However, the very salt that works so well in attacking ice on the roadways, does an equally good job in attacking the steel floor members and reinforcing bars that support these roadways. This salty water on the roadway also gets splashed around by passing vehicles with the result that some steel members above the roadway level receive a showering of salt water.

On the Brooklyn Bridge, the four main cables sweep to within one foot of the roadway level at the center of the main span. On the side spans the cables actually pass below the roadway level to a degree that the roadway structure is supported by cable posts instead of wire rope suspenders. As the cables approach the anchorage structures they are nearly horizontal. The splay castings were originally located just inside the anchorage chambers. The exposed wires of the splaying cables inside the chambers are located just below roadway level.

Poor Chamber Conditions

It was noted that the original anchorage chambers on the Brooklyn Bridge were rather small and air did not freely circulate throughout the chamber. Roadway runoff was observed to leak through to the chambers' ceilings. In addition to the high humidity levels inside the chambers, salt laden water dripped through the ceilings, onto the exposed splaying strands and then flowed either downward toward the splay castings or down to the lower strand shoes. Despite these adverse conditions, most of the exposed wire was in good condition. The big unknown was the wire condition actually within the eight splay castings. Also, cement grout was placed over and around some of the eyebars and came in contact with some of the strand shoes. Some broken wires were observed in all eight chambers, but one interior cable at the Brooklyn Anchorage included over 100 breaks. With the above information, a program of in-depth inspection was advanced.

Between the anchorages, the main cables' galvanized wrapping wire was cut and removed for several panels at their low points. The outer layer wires were readily observed. Typically, only minor oxidation of the galvanizing was noted. The cable wire was generally in excellent condition. In a few locations minor surface rusting was observed on the wires with little in the way of section loss.

The next step was to look deeper into the cable to see the succeeding layers of wires. Wooden wedges were driven with hammers by hand between adjacent wires several inches into the cables. Below the surface the cables were generally in excellent condition.

Now that we knew the main cable between the anchorages was in good shape, our attention was focused on the splay areas within the anchorage chambers. It is possible, of course, to splice in a new length of wire to replace a corroded section of wire. This can be done to many wires as needed in a strand, but what if practically a whole strand or more than one was severely corroded? This seemed very possible within the splay castings as rusty water was in evidence dripping from the castings.

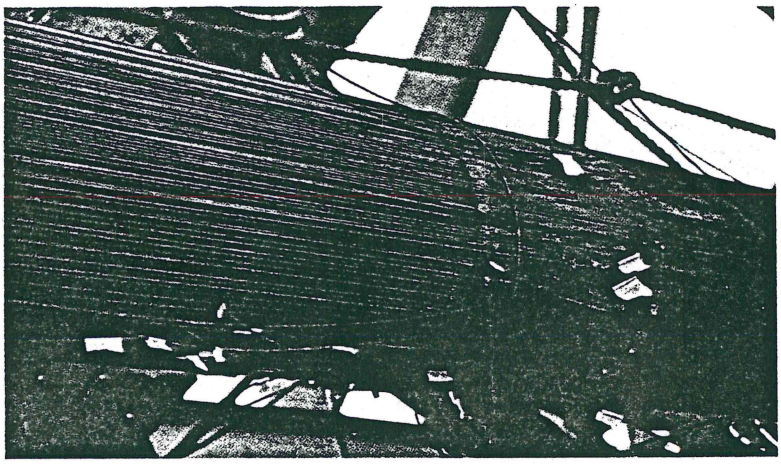

■ **CONDITION of the main cable of the Williamsburg Bridge after removal of wrapping materials and the cable band. Numerous broken exterior wires are identified by tabs.**

Research and Development

Our firm pursued a research and development program in conjunction with Columbia University's Carleton Laboratory in New York, with the goal of being able to examine the strands within the splay castings. In addition, procedures needed to be developed that would permit replacement of an entire strand of the cable should that become necessary.

A whole cause and effect scenario was studied, with the end result being that to examine this short portion of the cable, a major construction contract was required. The action took the following, rather complicated course:

- In order to see the strands within a splay casting, the splay casting had to be physically removed and relocated in a new position. Movement of the splay point would change the angles of the splay, the length of the splay, and stresses in the strands. It was decided to maintain the splay geometry by causing the strands to extend horizontally from the anchorage point for a length equal to the movement of the splay casting. This ensured that the existing strand stresses would be unchanged after the splay relocation was completed. A system of hydraulic jacks was employed to spread the strands apart to their desired positions and these positions were held by a permanent spreader frame mounted within the anchorage.
- The reconfigured cable splays took up significantly more space than the original splays and it became necessary to demolish and reconstruct the anchorage chambers to more generous proportions. It was also necessary to enlarge the openings at the face of the anchorages through which the cables pass.
- Because the spread strands extend beyond the anchorage faces and out into the bridge, several cable posts that support the roadway and stiffening trusses had to be eliminated.
- Because the posts were eliminated, the stiffening trusses needed to be strengthened to span a distance of five panels to support roadway loads.

All of this reconstruction work was carried out prior to any movement of the splay castings. We were pleased to find that there was no serious corrosion of any strand to the degree that

it would require replacement. All corroded or broken wires were replaced with spliced-in wire segments.

Successful Rehabilitation

The results of these efforts at the Brooklyn Bridge anchorages are cable strands that are now in good condition. Because of the reconstruction of the chambers, the ceilings are waterproofed, air can circulate more freely and there is more room to inspect and maintain the strands in the future.

Cable rehabilitation for the portions in between the anchorages includes replacement of cable bands, coating the cables with red lead paste, and rewrapping with galvanized steel wire.

If the Brooklyn Bridge is an example of a century old suspension bridge with main cables in generally good condition, the Williamsburg Bridge is one in which the main cables, the bridge's very lifeline, were suspect.

At the turn of the century it was the goal of Chief Engineer Lefferts L. Buck to construct a bridge of superior capacity at a cost lower than the Brooklyn Bridge. Among the cost saving items was one with regard to cable protection. The galvanizing process was not specified for this bridge. In its place, the cables, after erection were treated with linseed oil. In lieu of galvanized wire wrapping, the cables were wrapped with a fabric and the exposed lengths of cable, between cable bands, were covered with a sheet steel shell.

After the bridge had been in service for 15 years, an inspection revealed that the covering of sheet steel showed signs of corrosion. It was decided to replace the fabric and sheet steel covering with a wrapping of galvanized wire. It is noted that it was difficult to achieve a tight seal between the cable bands and the wrapping wire because the bands were not fabricated with a groove that would permit the wire to be wrapped under the edge of the bands and caulked into place. It is even more notable that no red lead paste was applied to the cable prior to rewrapping with wire.

Cable Concerns

Starting with the in-depth inspections and evaluations by other firms in the late 1970s, the condition of the cables, particularly within the anchorage chambers, was the focus of increasing concern. These evaluations concluded that the Williamsburg Bridge cables were deteriorated over their length and particularly within the anchorages, and that the cables would probably become nonfunctional by the mid-1990s.

Since suspension bridge main cables are non-redundant structural members, the loss of one cable causing catastrophic failure of the structure, they are designed with a generous factor of safety. In the case of Williamsburg Bridge, the ultimate strength of the main cables was designed to be four times greater than would be necessary to support maximum loading conditions.

It was recommended by others that the Williamsburg Bridge's main cables be replaced at a cost of about $250 million and the superstructure and approach structures rehabilitated. While the Federal government funds 80 percent of the cost of rehabilitation projects, there were indications that the FHWA might not consider funding the cable replacement project because the roadway structures were of substandard design. The FHWA did suggest that the city consider replacing the span. This triggered several actions:

- New York City and New York State Departments of Transportation assembled a Technical Advisory Committee to study the many aspects of the Williamsburg Bridge and recommend a long term solution. Possible choices included complete replacement, major reconfiguration, and rehabilitation.
- The city announced a request for proposals for design concepts concerning potential replacement of the span. Although it was not certain that the span would be replaced, the city considered it prudent to study various schemes and select for potential use, the most feasible. The competition was international in range.
- New York City and New York State Departments of Transportation retained the services of the Steinman firm to perform an independent evaluation of the main cables. In addition, the services of our firm were also retained to perform this current cycle of the Federally mandated biennial inspections.

It should be made clear that it was the conditions observed during the recently completed biennial inspection that caused the bridge to be closed for emergency repairs to the steel floor system, not the findings of the cable inspection. The Technical Advisory Committee considered the findings of the cable and biennial inspections in the process of determining the structure's eventual fate.

Evaluation Program

For the main cable evaluation, a program of in-depth inspection and testing was established for one exterior cable, known as Cable D, and one interior cable, known as Cable B. An investigation was also conducted on Cables A and B at the Manhattan Tower, an area that was affected by a fire during original construction. An in-depth investigation was conducted of the splay area of Cable D at the Manhattan anchorage where over 200 broken wires had been found. Finally, monitoring schemes were developed that would track any further deterioration of the cables by recording the strains of the individual eyebars that anchor the strands.

The main cable inspection at the mid-span low point was similar to but deeper than that conducted on the Brooklyn Bridge. The inspection consisted of opening the main cable at eight equally spaced radial positions. Hardwood wedges were driven deep into the cable, which allowed for about 15 percent of the cable wires to be viewed directly. Observations of corrosion and broken wires were recorded.

Four wire samples were removed from each of the eight groove openings at each location inspected. The wires within each groove opening were then cleaned with a wire brush. Samples of existing lubricant were removed for lab analysis. Before each groove was closed, the opening received a liberal coating of protective oil.

The condition of the cable splays within the anchorages appeared to be much worse than that of the wrapped cables. Cable D at the Manhattan anchorage was obviously in the worst shape with over 200 broken wires in evidence, all within a few feet of the splay casting. All upper layer strand wires displayed some signs of corrosion with several suffering major loss of section. Many repair splices were observed, particularly in the upper portion of the cable. Most of the damage was apparently caused by salt laden water leaking through the anchorage roof from the roadways. Again, it was the wire in the vicinity of the splay castings that aroused the greatest concern.

As on the Brooklyn Bridge, new splay castings were fabricated and installed, then the old one was removed. The splay was moved out from the anchorage in increments until the splay point was moved a total of 40 feet. A detailed inventory of broken wires was made and measurements of corroded wires were recorded.

Wire Samples Analyzed

Samples of wire taken from the wrapped portion of the cables were sent to Carleton Laboratory for analysis. The wires were labeled as to location and position in the cable and

broken wires obtained from the cables' surfaces were kept separate from those broken wires found deeper in the cables.

The wires were cleaned, measured, and photographed. Particular attention was given to the condition of the wires found broken in the field. Specimens were tested for tensile strength, elongation, and reduction of area. Stress-strain curves were developed by testing uncorroded samples. Hundreds of specimens were also tested for fatigue resistance.

Although results of the testing program are not fully complete, some generalizations can be made from the results so far available.

- Carbon content of the samples varies from 0.59 percent to 1.06 percent. This was somewhat surprising as bridge wire normally contains about 0.80 percent carbon.
- The average tensile strength of the wires agrees closely with original tests performed during construction.
- Fatigue endurance information is consistent and encouraging.
- Most specimens, tested to destruction, began to break near the center of the wire due to a coalescence of microvoids within the steel. The breaks were generally ductile.
- A typical ten foot segment of wrapped cable at mid-span appears to have retained at least 97 percent of its sectional area. The most corroded, randomly sampled wire retained 79 percent of its cross section. It is concluded that the cables are deteriorating at a slower rate than originally believed.

An interesting discovery that requires further investigation is that at least some of the broken wires found at the surface of the wrapped cable may have suffered from hydrogen embrittlement. The mode of failure was different from those that suffered heavy corrosion as in the anchorages. It is possible that in the presence of moisture the zinc coating of the galvanized wrapping is corroding to protect the outer layer of ungalvanized cable wire with which it is in contact. Hydrogen atoms are freed in this process and may be absorbed into the microstructure of the bridge wire.

Important Conclusions

All things considered, the results of the inspection and the preliminary test results have led us to come to some conclusions regarding the longevity of the Williamsburg Bridge cables. It was determined that the cables presently can support the bridge and its substantial live load. There is no immediate concern for the safety of the suspended span. Second, the existing cables should be able to function well into the future if a program of rehabilitation is advanced. Rehabilitation would include:

Unwrapping the cables.

Replacing broken segments of wire.

Installing new cable bands.

Applying corrosion inhibiting oil to the interior of the cables.

Applying a coating of red lead paste to the exterior cable wires.

Rewrapping the cables with either the proven wire wrapping, or a new system, depending upon further study.

Caulking at cable bands.

Painting the exterior of the wrapping.

Rehabilitation in the anchorage areas would include replacing broken and corroded wires with new ones spliced into place, and maintaining a coating of protective oils. Two strands (208 wires each) will probably require complete replacement between the splay casting and the strand shoes.

The above recommendations are included in the report to the city and the state.

In early June 1988, the Technical Advisory Committee's recommendations regarding the fate of the Williamsburg Bridge were presented to Mayor Ed Koch. These recommendations are summarized as follows:

- Rehabilitate the suspension bridge span by repairing and protecting the main cables, replacing the suspenders and cable bands, and rehabilitating the superstructure, towers, and roadways.
- Replace the approach spans in both Manhattan and Brooklyn because of their seriously deteriorated steel work and historically greater incidents of vehicular accidents.

Finally in July 1988, the city announced that three of the more than 20 entries in the Williamsburg Bridge Replacement Scheme Competition were worthy of serious consideration. Cash awards were presented to: T.Y. Lin International, San Francisco and Neil A. Bettigole, New York City; Schlaich & Partner, Stuttgart, West Germany; and Steinman, Boynton, Gronquist and Birdsall, New York City. □□□

Acknowledgment. Key project personnel on this project included William F. Geyer, partner-in-charge; Blair Birdsall, special cable consultant; Peter Sluszka, principal-in-charge; Terry Koglin, project manager, cable inspection; Kenneth Serzan, project manager, biennial inspection; John Nixon, cable specialist; Janusz Kupiec, cable specialist; Dyab Khazem, field engineer, cable inspection; and Hank Godfrey, bridge wire specialist. I wish to specially thank Ms. Nanci Buscemi of the firm for her assistance in obtaining and organizing the materials used to prepare this paper.

APPENDIX B

NDE OF BRIDGES

It is important to point out initially that most of the NDE methods used on bridges today have been applied primarily to the inspection and monitoring of structural members such as steel girders and not routinely to cables or strands with the few exceptions indicated below. Many of the methods in fact are not applicable at all to the inspection and monitoring of specialized cable structures and others are in a very primitive stage of development, but it is still useful to consider the NDE of bridges as practiced today to provide a perspective for more complete discussions of the methods which are most promising for cable inspection and monitoring at this time.

In general there are three types of nondestructive inspection methods applicable to bridges today: (1) surface, (2) subsurface, and (3) monitoring [16]. The first two entail either geometric defect sizing or scanning approaches to flaw detection or both. The third detects subcritical flaw growth activity.

Pertinent surface methods include dye penetrant and magnetic particle inspection (visible and fluorescent) and electromagnetic testing. Although relatively inexpensive in terms of equipment and investment in operator training, the first two require paint removal and cleaning to be effective. Cost increases when expendable materials are included. Electromagnetic testing may prove more effective than either dye-penetrant or magnetic-particle methods, and require less surface preparation. For weld inspections several eddy-current or magnetic field disturbance units are available. FHWA sponsored development of the Magnetic Crack Definer (MCD). This unit is designed to locate and measure surface cracks and can be used by relatively inexperienced personnel.

The two main subsurface methods are radiography and ultrasound although magnetic methods have been used, too. Transmission radiography has not been considered for routine NDE bridge surveillance because of high cost, low productivity and radiation safety requirements. Also, when taking radiographs of objects with great differences in thickness such as wire ropes and cables, the marginal zones are overexposed so that details can no longer be distinguished. However, both film and electronic, real-time detection are attractive since images present a great deal of information about variations in thickness and density. Most recently, computerized photon tomography which produces a cross-sectional image of the object inspected has shown promise for inspecting wires at end fitting locations and has the potential to inspect wrapped strands on suspension bridges since the radiation can penetrate superficial wrapping and permit observation of wire profiles; however, the cost of these systems is very high ($1 million or more) so as to be prohibitive.

Ultrasonics can be useful for both scanning and flaw evaluation. Generally, however, ultrasonics requires significant expenditures in equipment and personnel training and it is unproven on cables. Due to versatility, though, ultrasonics is now considered by some States to be an essential part of their routine NDE surveillance program on structural bridge girders if only to confirm indications by other NDE methods or to measure surface-crack depths. FHWA also sponsored development of the Acoustic Crack Detector (ACD) for subsurface crack detection on bridges. As with the MCD, this device is designed to minimize operator requirements.

A novel scanning magnetic method has found application to subsurface flaw detection and characterization in prestressed and post-tensioned concrete bridge members. The Magnetic Field Disturbance (MFD) system has proven to be an effective and reliable prototype system for detecting flaws in reinforcing steel of bridge beams in situ [8,9,10]. Recently, 1984, the capability of this MFD prototype system to reliably detect the fatigue fracture of two wires in a seven wire strand of pretensioned reinforcing cable was confirmed during fatigue cycling of a typical concrete bridge beam.

While it is commonly and mistakenly assumed that applications of the magnetic field method are limited to the detection of the surface breaking and near subsurface flaws, as will be shown later the method is capable of detecting flaws such as corrosion and loss of section at significant depths. For example, based on experimental results obtained on 1/2-in thick plates in which small drilled holes were used as test flaws, it is estimated that in a 36-in diameter cable, a 2 percent cross-sectional area loss could be detected at a depth of approximately 12 to 18 in provided a high flux density can be obtained in the cable cross section. Detailed analyses and capability forecasts are presented in appendix C.

As further evidence of the feasibility of the magnetic field method, a prototype magnetic instrument designed specifically for inspecting parallel wire suspender ropes was recently, 1985, described and results of actual use to successfully inspect 22 suspension ropes for a suspension roof were presented. This magnetic instrument used direct current in an electromagnet and two arrays of 36 hall elements for high resolution sensing of corrosion and other deficiencies [7].

Acoustic emission testing shows promise as a tool for monitoring bridges, especially steel girders. Importantly, however, acoustic emission testing cannot be used to geometrically size defects. Any acoustic emission source must be sized using some other NDE method. When traffic flow is relied on to drive cracks, extended monitoring may be required since acoustically "quiet" periods are often encountered in early or intermediate stages of fatigue crack growth. Also, AE investigations have encountered difficulties from background noise inherent in bridges. The ability of AE to monitor cables in the presence of high attenuation is questionable.

In summary, both film and real-time radiography have potential for the inspection of small to intermediate diameter cables containing bundles of strands for broken wires, thinning, corrosion and other anomalies because of the penetrating power of gamma- and x-radiation. However, cost, safety, speed and resolution constraints must be considered serious disadvantages. Computerized photon tomography also shows potential for inspecting wires, especially at end-fitting locations, but development must consider the very high cost and same safety and speed constraints as conventional radiography. Ultrasonic testing of wires using rod waves generated by magnetostriction excitation and pulse-echo testing using angle probes on accessible wires are possible. However, past attempts to apply ultrasonic pulse-echo techniques transverse to a wire rope were not successful [3]. The sound pulses were reflected at each single wire, and it was not possible to distinguish between broken and intact wires. No practical reports of velocity and attenuation measurement on cables and strands have been found in the NDE literature. On the other hand, magnetic field perturbation methods have been used effectively to detect cracks and other damage in, for example, mine and elevator wire rope [6]. Equipment of this type has been used for many years and may be of interest for tests of newly fabricated wires and structural strands and also for suspender strands and ropes. Typically, it has been limited to cable diameters less than 2 to 3 in. Importantly, the new MFD system has demonstrated the potential of magnetic methods to detect subsurface defects, as well as surface anomalies, and this successful development opens many possibilities for application to cables (see appendix C). Acoustic emission testing has been used to monitor cables on a lift bridge in California and also has been employed in wire rope tests; however, attenuation was a serious problem. Recent field work has demonstrated the potential of acoustic emission techniques for detecting cracking in steel girders in areas of high background noise. This work has shown that AE may also be applicable to cable locations difficult to monitor by visual examination, e.g., main cables under bands and on suspender ropes at end fittings.

Ultrasonic, acoustic emission, magnetic field perturbation and photon tomography have shown promise for solving some of the inspection and monitoring problems encountered in highway bridge inspections. While all of these methods may have potential useful application to smaller diameter suspender ropes and smaller diameter cables, only two methods, acoustic emission and magnetic field perturbation, offer significant practical potential for structural integrity interrogation of the larger diameter cables used in suspension bridges. Since the magnetic perturbation method is described in detail elsewhere in this report, a brief discussion of the acoustic emission method will be presented in the following paragraphs.

Acoustic emission methods are considered among the more prominent and promising advanced nondestructive evaluation approaches. Factors which contribute to this prominence are the flexibility in application of this method to a wide range of structural component configurations and processes together with the

capability for sensing or monitoring at a distance from the actual flaw or anomaly location. Furthermore, it has sometimes been possible to use, at least conceptually, the mature and well established techniques used in seismology for geologic and other types of investigations. Because of the foregoing and because of significant research and development activities relating to wire rope, bridge cables, steel bridges and other bridge elements under FHWA and other agency sponsorship since approximately 1972, a significant background base exists for assessing applicability of the acoustic emission approaches to bridge inspection and monitoring problems.

An essential element of all acoustic emission approaches is that the item being inspected either emits naturally or is caused to emit by appropriate stimuli mechanical vibrations, and that these vibrations result in sufficient amplitude or surface displacements at the sensor location to generate an output of the sensing element for recording and analysis. The material displacements at the source are often minute (microscopic) and abrupt, and produce near the source, at least, a step function change of displacement. This step function displacement propagates through the medium at essentially the velocity of sound as a mechanical stress wave. Since the material is elastic, the step displacement or abrupt displacement actually results in a series of approximately sinusoidal oscillations that propagate through the medium as a wave packet. A number of different wave fronts are propagated as shear, longitudinal, and other modes, and for ordinary crystalline material of finite dimensions there are complex interactions, for example, at grain boundaries, inclusions, and particularly at geometric boundary surfaces which cause other modes of wave propagation and other propagation paths to occur.

Most acoustic emission models for data interpretation make use of the first arrival or the sequence and relative amplitudes of the first few arrivals. For many applications on simple geometric configurations, the material is homogeneous as, for example, in a pressure vessel where data interpretation is relatively straightforward. Also, since a variety of frequencies ranging from a few kilohertz to more than a megahertz are propagated through the medium and since the higher frequencies are attenuated more rapidly than the lower frequencies, if is often the practice (similar to the practice of ultrasonic inspection methodology) to use lower frequencies in attempts to monitor sources at greater distances. Accordingly, selection of transducers is a critically important step in developing a practical system for acoustic monitoring of specific applications.

Usually the transducer is a ceramic piezoelectric device which is undamped and is caused to oscillate in response to the abrupt wave front or high frequency wave packet causing the surface displacement. In other cases, conventional accelerometers and low frequency piezoelectric devices in the kilohertz range of resonant frequencies have been used.

The above is by no means a complete or precise description of acoustic emission processes and sensing, but it illustrates the complexities of realistic

modeling for practical applications and the potential for significant and often serious errors in forecasts derived from such models. While the availability of sensors and microprocessors for data handling and analysis has been significantly improved during the last few years, and while progress has been made in modeling the input phenomena, this modeling has still not reached a state of maturity that forecasts can be accepted with reasonable confidence. Unfortunately, this is particularly true for complicated applications such as the suspension bridges.

Most NDE methods which are serious candidates for the inspection and monitoring of cable suspension bridge elements rely on modeling supported by limited experimental and empirical results extrapolated to the cable suspension bridge application and, as such, are deficient and cannot provide precise forecasts with high confidence. In the case of acoustic emission methodology these modeling deficiencies are particularly severe because of the complexities of the fundamental emission sources among other factors. Modifications to the primary emissions caused by the complexities of the medium (in this case the metal wire compressed into strands and cables) result in numerous geometrically complex interfaces, etc. Transmission paths from the medium through the wire wrap and/or other protective materials beneath the saddles and then through paint buildup and incrustations to the sensor itself are torturous at best. Experimental model investigations in the laboratory cannot be conveniently analytically scaled to the full-size configurations of the bridge. While remote monitoring possible with acoustic emission is a distinct advantage not shared by any other serious candidate, the extent of such remote monitoring in the practical case will be limited to at best a few feet; accordingly, it is apparent that a large number of transducers and associated electrical cabling complexes would be required. A few examples follow which provide a perspective assessment of the difficulties caused by attenuation of the propagating medium.

The use of acoustic emission monitoring was investigated for the cables on the lift span of the Dumbarton Bridge [4]. In this exploratory effort it was necessary to apply a load to the cables by transverse force to stimulate acoustic emission. Attenuation between strands of the cable was high with a value of 24 dB being measured for adjacent strands. Since a main cable is made up of many strands and with this high attenuation, several transducers spaced around the circumference of the cable at each monitoring location would be required. For example, in the George Washington Bridge which has 35-in diameter main cables, made up of 61 strands each approximately 4 1/2-in diameter, there are approximately 25 exterior strands. Assuming no attenuation through the overlays, a useful system gain of approximately 60 dB, and using only 20 dB as the attenuation between strands, it is estimated that a single transducer could perhaps monitor three adjacent strands in either direction from the strand on which the transducer was mounted; accordingly, a minimum of four transducers would be required to monitor the exterior strands of this main cables at any one station. Attenuation along the individual wires of the cable ranged from 1 to 5 dB/in. Using the lower (and probably optimistic) value of 1

dB per in and with a useful system gain of approximately 60 dB, a monitoring distance of 5 ft in each direction along the cable from the transducer is estimated. Assuming panel separation points of approximately 50 ft would require approximately 20 transducers, that is four at each 10-ft location.

While as indicated above, lower frequencies in the range of 5 to 20 khz in comparison to approximately 100 to 300 khz used in reference 4 could result in a somewhat greater monitoring distance along the cable, the improvement would not be dramatic since the lower figure of 1 dB per inch was already used, and furthermore the major contribution to the attenuation would be from scattering and mode conversion as the propagating beam intersects the cylindrical surface of the wire and also from pits and other surface anomalies encountered along the length of the wire.

Other recently reported research is particularly significant to the proposed program since they reported results obtained on tensile fatigue tests of wire rope [17]. The arrangement consisted of one AE sensor and one accelerometer attached to both upper and lower cable sockets of the test cable sections which were about 28 in long. Significantly, wires which broke in a socket were detected by both accelerometers but only by one AE sensor, the one attached to the socket in which the wire fracture occurred. Since the AE sensor mounted on the other socket did not detect the fracture and since the reported system gain was approximately 34 dB and the wire was 28 in long, the attenuation of the wire is estimated to be at least 1 dB per inch. This is also approximately the minimum attenuation observed in reference 5 and probably represents a reasonably reliable value for the lower end of attenuation.

The research describing acoustic emission monitoring on a large bridge on I-24 in which locations known to have fatigue cracks were monitored is also of significance [5]. This exploratory research used the ambient traffic as a "crack driving mechanism". It was indicated that high acoustic emission activity, over 1,000 AE events per hour, occurred from fretting noises and other noises apparently associated with the bolted connection and accordingly was representative of a relatively high noise background. It was also reported that in one test location where a 2-in long through-crack, at the toe of the web-to-flange fillet weld in addition to a second crack eminating from under the angle splice plate, was located, that a correlation of acoustic emission noise was detected coming from this specific site over a 2 1/2-hour long monitoring period. While these limited results were encouraging, it is not possible to extrapolate such results from a large, at least greater than 2-in long, through crack with a large plastic zone enclave at the crack tip, to the crack propagation and/or corrosion product fracture acoustic emission noise in a suspension cable or other suspension cable bridge elements. A novel feature of this experimental exploratory effort was also indicated in which a third, relatively high power sensor was intermittently pulsed to provide acoustic noise for the remaining sensors in order to test the entire system.

A recent report describes a new AE system employing a novel two-step approach for continuous monitoring of large structures [18]. The system uses small size, low cost surveillance units and contains a microprocessor which is software controlled to continuously monitor the structure and extract features of the AE activity.

An important and novel element in the two-step approach which is adopted in the new system is the preprogramming of the detection units, through the control unit, with failure parameters which are characteristic of the type of application to which the system is adapted. These failure parameters are determined with a research program which involves evaluation of the level of acoustic emission activity in the material(s) used in the structure, evaluation of the causes of failure and the nature of the sources of acoustic emission, and determination, with theoretical and experimental analysis, of the effect of material and geometry on the wave propagation characteristics of the structure including the extent of attenuation in the structure. Thus, concurrent with the development of the hardware and software components of the new system, this research program to determine the failure parameters also takes place.

In this research program, laboratory tests are performed to determine the level of activity that the material emits under conditions similar to those it is exposed in the actual application. For example, for steel used in off-shore structures, laboratory tests will determine the relationship between acoustic emission parameters including total count, count rate and energy, as well as the waveform of the signal, and fatigue and corrosion fatigue under the effect of a seawater environment. Thus, curve similar to those obtained in reference 19 relating acoustic emission total count N with the increase in stress intensity factor K are obtained. The mechanisms of emission may also be determined using microstructural examination with optical and electron microscopy.

Together with the laboratory tests, model tests are performed on a scaled-down model of the structure under consideration. The model tests are very important in determining the effect of geometry on the waveform of acoustic signal and in calculation of the attenuation characteristics of the particular structure. The results of these tests, together with those obtained form the laboratory test, determine parameters such as the type of transducer to be used in the real application, its frequency response, the bandpass of the filters used to discriminate the background extraneous noise, the gain of the system and most importantly, the spacing between transducers to maximize the efficiency of the system.

In summary, while significant progress has been achieved in acoustic emission technology applied to evaluating and monitoring deteriorating conditions associated with bridges, much additional effort is needed to define the specific responses, the propagating distances and other features and parameters that are important to reliable use of this detection methodology on suspension cable bridge

elements. To envision the NDE inspection and/or continuous long term or intermittent monitoring of a large cable suspended bridge at enough locations to provide reasonable confidence in the results would require possible 100 and more likely several hundred transducers. The difficulties of installing, maintaining the integrity of the coupling path, the integrity of the cable connections and in fact just management of the complex routing of the cables in the face of the environmental conditions such as high winds, thunderstorms, etc. is indeed a problem of sobering magnitude. Because of the complexities involved and the extensive effort required for reasonable precise results, several years of research and exploratory investigation will be required for confident use of this methodology.

APPENDIX C

THE MAGNETIC FIELD PERTURBATION METHOD

A. Introduction

Magnetic methods are one of the oldest nondestructive testing approaches, and perhaps are more widely used than any of the conventional nondestructive evaluation methods except visual inspection and radiography [20,21,22]. The most commonly used approach is the magnetic particle method which, essentially, consists of magnetizing a part or region and then flowing fine dry magnetic particles or particles suspended in a solution over the region to be examined [21,22,23]. Flaws or anomalies are indicated by the accumulation of particles attracted to the magnetic poles formed by the discontinuities and anomalies; often a fluorescent coating is added to the particles and an ultraviolet light source is used to illuminate the region being examined, thereby enhancing the visual indication. A number of specialized magnetic methods have been used for selected applications and the magnetic approaches offer potential for application to a wide range of specialized problems.

Early research and applications of magnetic fields for the inspection of wire ropes extends back to the 1930's. Since then and to the present, there has been almost continuous research and improvement in applications to wire ropes. A review of this area was presented in 1978, and this review also indicates the excellent and advanced development state of the analytical principles underlying the AC magnetic field inspection methods [24]. Extensive research and application of DC magnetic field inspection methods have also been reported [13,14,15,25]. The basic principles and potential of such methods for application to cable inspection will be reviewed in the following paragraphs.

B. Principles and Analyses

Assume a spheroidal region (void or hole) of constant permeability μ_0 embedded in an infinite ferromagnetic matrix of constant permeability μ and with a magnetic field H_0 applied along the x-axis as shown in the upper part of figure 46. An exact solution for the magnetostatic potential at any point P (x,y) outside the hole is given by equation 4: [26,27]

$$U(x,y) = \left[1 - \left(\frac{\mu_0 - \mu}{\mu_0 + 2\mu} \right) \frac{a^3}{(x^2 + y^2)^{3/2}} \right] H_0 x \qquad (4)$$

where U = magnetostatic potential, μ = permeability of matrix material, μ_0 = permeability of void or hole, a = radius of void or hole, and H_0 = applied magnetic field.

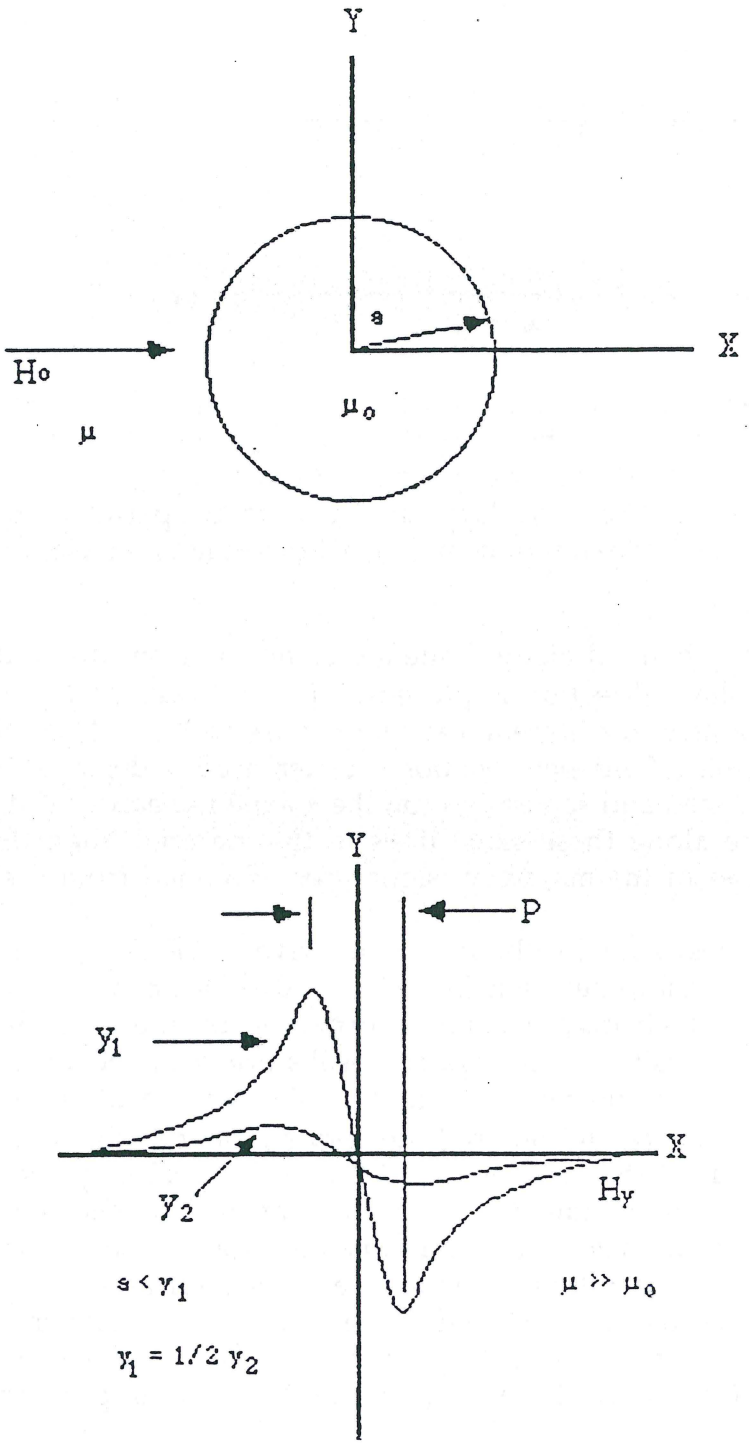

Figure 46. Sketch of spherical void or hole in an infinite magnetized ferromagnetic matrix and the resulting magnetic field perturbation in the Y direction.

The magnetic field components H_x and H_y can be obtained by taking the negative partial space derivatives along the x and y directions. Equations (5) and (6) are obtained:

$$H_x = \frac{-\delta U(x,y)}{\delta_x} = H_0 \left[1 - \left(\frac{\mu_0 - \mu}{\mu_0 + 2\mu}\right)\left(\frac{a^3}{(x^2 + y^2)^{3/2}}\right)\left(1 - \frac{3x^2}{x^2 + y^2}\right)\right] \qquad (5)$$

$$H_y = \frac{-\delta U(x,y)}{\delta_x} = 3H_0 \left[1 - \left(\frac{\mu_0 - \mu}{\mu_0 + 2\mu}\right)\left(\frac{a^3}{(x^2 + y^2)^{5/2}}\right) xy\right] \qquad (6)$$

Attention will be concentrated on equation (6) which is the magnetic field component, H_y, that would be obtained if a magnetometer probe were scanned parallel to the x-axis to detect the magnetic field component emerging out of the surface of the steel. (The boundary, assumed to be parallel with the x-axis, is neglected as a first approximation and can be partially accounted for by the μ^* correction [28,29].

A plot of H_y obtained along a line a distance, y, from the center of the sphere and extending in the x direction is presented in the lower part of figure 46; values obtained on a line at two different values of y are shown. Note the characteristic shape of the magnetic field perturbation, at increased y distance (depth) the peak amplitudes are reduced and separation (on the x axis) increases. If it were possible to scan a point probe along these same lines in the material, then this sketch would represent the shapes of the magnetic "signatures" obtained from the "flaw".

Since is is desirable to obtain quantitative NDE data, it is informative to determine the relationship between flaw size, a, distance beneath the surface, y, and signature features which may provide information on these factors. Accordingly, the locations of the positive and negative peaks are obtained by taking the partial derivative of H_y with respect to x and setting the result equal to zero. For conciseness the details are omitted, but the very simple relation $x=\pm 1/2y$ is obtained. The two peaks occur at the locations $x=\pm 1/2y$ or the peak-to-peak separation, p, in figure 46 is equal to the distance, y, from the scan path to the centroid of the flaw independent of the flaw size. This is a very important observation since for many practical cases the flaw depth is a primary parameter for assessing criticality. Also, the flaw size can be determined from the signature only after the depth has been estimated. The amplitude of the signature at this location can be obtained by substituting the values $x=\pm 1/2y$ into equation (6). After simplifying, equation (7) is obtained.

$$H_y\,(x = \pm 1/2\,y) = K\frac{\mu_0 - \mu}{\mu_0 + 2\mu}\,\frac{a^3}{y^3} \qquad (7)$$

Examining this equation, it is seen that the signature amplitude is directly proportional to the volume of the flaw, a^3, and inversely proportional to the cube of the distance, y, from the scan path to the centroid of the flaw. Furthermore, an examination of the factor containing the permeability terms shows that when μ is larger than μ_0, the polarity of the signature would reverse.

C. Experimental Results with Estimates for Cables and Ropes

The magnetic method as embodied in the magnetic field perturbation approach has been applied successfully to the detection of minute flaws as small as 0.001 inches in diameter in precision ball and roller bearing components and also for the detection of minute, tightly closed fatigue cracks in bearings and other components [13,14,25]. Of more interest to cable inspection is the fact that larger flaws can be detected at significant depths in steel components. An example indicating the potential for detecting anomalies at significant depths in the interior of cables will be described.

Experimental magnetic perturbation data were obtained from drilled holes in a steel plate specimen 18 in by 6 in long by 1/2 in thick. Signal data were obtained with the electromagnet and sensor probe scanned along the surface in which the holes had been drilled and also from the opposite surface. Graphs of the signal amplitude data are presented in figure 47. With the electromagnet poles and the probe separated from the steel plate surface by approximately 0.4 in (lift-off), a 10/1 signal-to-noise (S/N) ratio was obtained from the 1/4-in diameter by 1/4-in deep hole at a depth from the scanning surface to the centroid of the hole of approximately 0.38 in. At a liftoff of 0.0 in the S/N ratio was 45/1 (symbol ⊙ in plots of figure 47). Since equation (7) above indicates that the signal amplitude, H_y, decreases as the inverse cube of depth, y, the maximum depth for detection of a 1/4-in diameter cylindrical flaw, 1/4 in long, simulating a single broken wire of a strand can be estimated by:

$$\frac{\text{Signal at Depth 1}}{\text{Signal at Depth 2}} = \left(\frac{\text{Depth 2}}{\text{Depth 1}}\right)^3 \times \frac{\text{Vol 1}}{\text{Vol 2}} \qquad (8)$$

Assume a suspender cable with no covering and the magnet and probe on the cable surface, i.e., 0.0 inch lift-off; also assume Vol 1 = Vol 2. The, Signal at Depth 1 equals 45 (from the graphs in figure 47, symbol ⊙ at 0.0 lift off), Signal at Depth 2 equals 2 for a S/N ratio = 2/1, and Depth 1 is equal to 0.38 in. Solving for Depth 2 gives approximately 2.82 times 0.38 in or 1.07 in. This is equivalent to a cable diameter of approximately 2.14 in. Therefore, this estimate indicates that a single

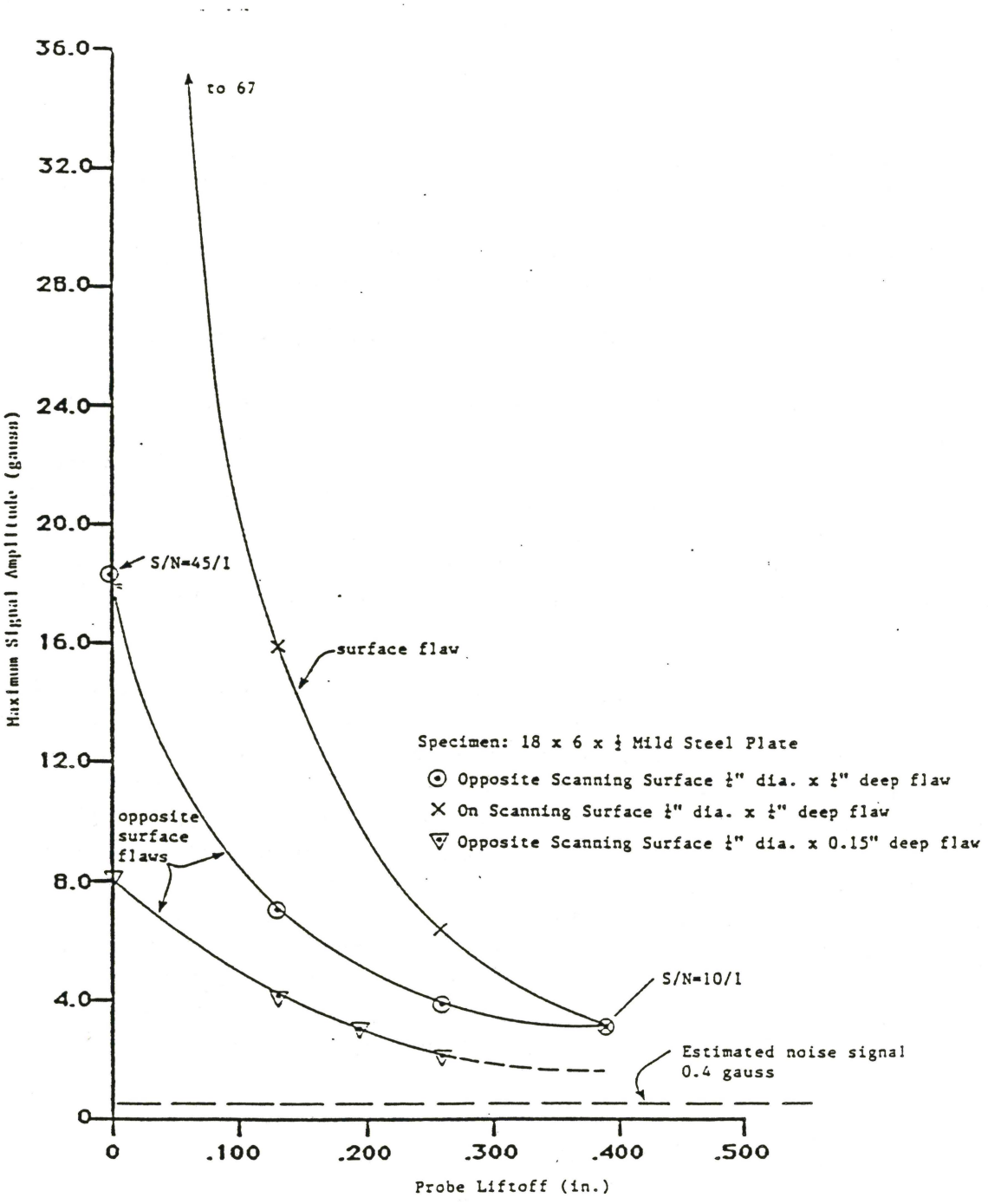

Figure 47. Graphs of magnetic perturbation signals.

broken wire with ends separated approximately 0.25 in could be detected near the middle of a suspender rope which would be comprised of approximately seventy-five 1/4-in diameter wires or detection would be approximately 1 percent to 2 percent of the suspender rope cross section. As another example, on the main cables for the George Washington Bridge which are approximately 36 inches in diameter and consist of 26,474 wires 0.196-in diameter, the detection limit is estimated to be approximately 460 wires (1 strand is 434 wires) with end separations of approximately 4 in (slightly less than one strand diameter) at the center of the cable. A cross section of this volume would represent a decrease in strength of the main cable of approximately 2 percent.

For cables 5 in and 15 inches in diameter with polyethylene or other type of nonmagnetic coating with a thickness of approximately 3/8 in, the following estimates are obtained. In this case the data for a liftoff of 0.38 in indicate a S/N ratio of 10/1 from figure 47. The estimated limit of detection capability at the center of a 5-in diameter cable is approximately 3.5 percent of the cross section if the wire ends are separated approximately 1.0 in and 7percent for 0.5 in separation. For a 15-in diameter cable the estimated detection limit is approximately 10 percent of the cable cross section at the center with wires separated 1.0 in.

Of even more interest are results from magnetic modeling of the main suspension cables for detection of fracture induced, wire end separations in the exterior strands of the Portsmouth Bridge over the Ohio River. The model is depicted in figure 48 and the detailed steps follow.

PORTSMOUTH BRIDGE:

wire wrap 0.2 in dia.
cable approx. 7 in dia. (19 strands)
wire approx. 0.12 i dia.
tie bands separation 70 in (assumes two tie bands between each 17.5-ft spaced cable bands)
Magnetizer and Probe separated from cable by 0.25 in for clearance of bumps, wrappings, paint buildup, etc.

From equation (8)

1. Set minimum S/N ratio = 2 (assumes only 1/5 max. flux density in the plate can be produced in the cable)
   Depth 2 = 0.2 in; i.e., exterior of wire in strand but beneath spiral wire wrap
   Vol 1 = 0.25-in dia. by 0.25-in deep hole in 0.5-in thick plate from flaw ⊙ in figure 47
   Depth 1 = 0.375 in mean depth to Centroid (0.25 + 0.125) in
   Vol. 2 = Δ x cross-sectional area = Δ x $\pi/4$ $(0.12\ in)^2$

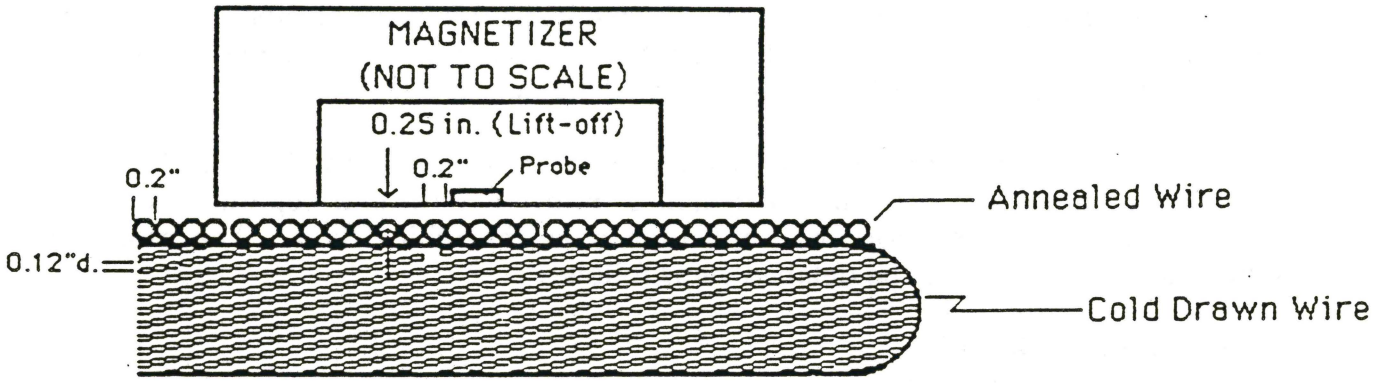

Figure 48. Magnetic modeling of flaw detection in main suspension cables.

2. Δ = end separation after fracture
   assume two tie bands between cables bands @ 17.5 ft
   therefore distance between anchor points = 17.5 ft/3 = 70 in = L

$$\Delta = eL = \left(\frac{\text{stress}}{\text{modulus}}\right) L = \left(\frac{\text{stress}}{\text{modulus}}\right) 70 = \left(\frac{\text{stress}}{24 \times 10^6}\right) 70 \qquad (9)$$

(see page 23 of reference 30)

3. Solve for stress by rearranging equation (8)

$$\text{Vol}_2 = \frac{\text{Signal 2}}{\text{Signal 1}} \times \left(\frac{\text{Depth 2}}{\text{Depth 1}}\right)^3 \times \text{Vol}_1 \qquad (10)$$

$$\text{Vol}_2 = 2\left(\frac{x0.2}{0.375}\right)^{3.89*} \times 0.25 \times \frac{\pi}{4}(0.25)^2 \qquad (11)$$

$$\text{also, Vol}_2 = \Delta \times \frac{\pi}{4}(0.12 \text{ in})^2 = \text{Stress}\,\frac{70}{24 \times 10^6} \times \frac{\pi}{4}(0.12 \text{ in})^2 \qquad (12)$$

(Substitute value of Δ from Step 2 for Δ in Step 1)

4. $$\text{Stress} = \frac{2\left(\frac{0.2}{0.375}\right)^{3.89} \times 0.25 \times \frac{\pi}{4}(0.25)^2}{70 \times \frac{\pi}{2}(0.12 \text{ in.})^2}\,(24 \times 10^6) \qquad (13)$$

(Equate Vol_2 expressions in Step 3 and solve for stress)

$$\text{Stress} = 64500 \text{ psi and } \Delta = \frac{64500}{24 \times 10^6} \times 70 \text{ in} = 0.188 \text{ in} \qquad (14)$$

Maximum Design Service Stress on the Portsmouth Bridge = 76,400 PSI (see page 31 of reference 31)

In summary since the operating stresses are <u>in the range</u> adequate to produce fractured wire end separations of approximately 0.2 in or greater, there is <u>very high confidence</u> of detecting one fractured exterior wire without removal of paint, protective grouting, and wrapping wires. One wire is <u>only</u> approximately 0.03 percent of the total cross-sectional area of the cable!

*experimental value calculated from figure 47 graphs rather than theoretical value = 3.0

The magnetic flux density estimate is probably conservative and deep pitting of exterior wires may also be detectable.

A summary of estimated detection limits is presented in table 5.

Table 5. Estimated detection limits of magnetic method.

Cable Dia. (in)	Flaw Cross-Sect. Area	Covering Thick. (in)	Wire Size Dia.(in)	Broken End Sep. (in)	Depth** (in)
2-1/2	1%	None	1/4	1/4	1-1/4
5	7%	3/8 Plastic	1/4	1/4	2-1/2
5	3.5%	3/8 Plastic	1/4	1	2-1/2
15	10%	3/8 Plastic	1/4	1	7-1/2
36	2%	3/8 Wire Wrap	0.196	4	18
7	0.03%*	0.2 Wire Wrap	0.12	0.2	Exterior Wire

* (Portsmouth Bridge)
**By inspecting at several different azimuthal locations the total cross section could be inspected

Actual minimum detection capabilities should be approximately two to three times the indicated cross-sectional areas (except for the Portsmouth Bridge cable) since estimates in the table are based on a uniform magnetic flux density throughout the cable cross section. For small diameter ropes this correction would be near two, and for larger diameters, perhaps three or four.

Although information on broken wire end-separation distances is not available, the numbers which have been used are reasonable approximations, and in any event detection capability is such that near the exterior regions, adequate sensitivity is anticipated even if separation distances are considerably less. It is also pointed out that grouting of the strands and other protective coatings such as red lead, zinc paste, etc. will have little or no effect on the magnetic field detection method.

D. Significant Attributes

While the preceding discussions and examples have provided specific and general information on capabilities of the magnetic method, significant attributes of the method which are helpful in assessing applicability to the inspection problem are presented in Table 6.

Table 6. Significant attributes of the magnetic field perturbation NDE method.

- Minimal surface preparation - removal of paint and protective coverings (wire or plastic wrapping, grouting, etc.) is not required
- No physical contact of sensors
- No installation of sensor arrays or cabling complexes
- Quantitative - Proven linear response with section loss
- Flaw detection, approximate sizing, and location (including depth)
- High sensitivity and resolution (particularly for near surface region)
- Not affected by dirt, paint, repainting, etc., nor moisture or grease (crawler excepted)
- Long term stability adequate for reliable long term (years) monitoring
- No influence from T.V., FM/AM radio, radar, (aircraft, police, ship)
- Previously proven in the field [7,8,9,10]

APPENDIX D

RESULTS OF SIGNAL ANALYSIS INVESTIGATIONS

Correlation analysis is a mathematical process which quantitatively assesses the goodness of fit (or the degree of shape matching) between two signals or signatures. The quantifying number describing the fit is called the sample correlation coefficient, R. The correlation coefficient can be computed automatically, using the logic processing subsystem according to the following equation:

$$R = \frac{\sum_{i}^{n} x_i y_i - n\overline{X}\,\overline{Y}}{\left[\left(\sum_{i}^{n} x_i^2 - n\overline{X}^2\right)\left(\sum_{i}^{n} y_i^2 - n\overline{Y}^2\right)\right]^{1/2}} \qquad (15)$$

where R is the sample correlation coefficient for signatures "a" and "b"

x_i is the set of n data points describing the amplitude of the digital samples for signature "a"

y_i is the set of n data points describing the amplitude of the digital samples for signature "b"

$\overline{X}$ is the mean of the x data points

$\overline{Y}$ is the mean of the y data points

n is the number of data points in each set

The range of values possible for R is ±1. Correlation of two identically shaped signatures yields R = ±1. Correlation of two signatures identical in shape but with reversed polarities yields R = -1. An important property of the correlation function above is that it is independent of the absolute amplitudes of the signatures being correlated.

The above correlation computation consists of the multiplication of two matrices, each matrix consisting of a set of numbers representing the location and amplitude of the digitized data points from a signal or signature. One axis in each matrix represents the location of each spatial sampling interval and the other axis represents the digital signal amplitude at each sampling interval. For the problem at hand, a 101-point matrix representing a typical flaw signal is correlated against a 590-point matrix which represents an entire scan signature (such as record A in

figure 49). The calculation is carried out by computing the correlation coefficient for the 101-point matrix representing the flaw signal with the first 101-data points in the scan signature starting from the left, i.e. starting at data point 1 and extending through data point 101. Subsequently, the 101-point matrix representing the flaw signal is correlated with the next 101 data points from the signature starting with data point 2 and extending through data point 102. This process is continued point by point along the record and results in 490 correlation coefficients which are then plotted. An example of the correlation coefficient plot is shown by record D in figure 49. The greater the correlation value, the better the match between the flaw signal being used to interrogate the scan track and that segment of the scan signature which corresponds to the location of the correlation peak, and the higher the confidence that a flaw exists. The maximum correlation coefficient value in a correlation plot is indicated by the cursor (an inverted V) near the baseline pointing out the peak, such as that associated with peak 2 in record D of figure 49. The present processing program prints out the value of all peaks greater than 0.700.

In the case of figure 49, notice that the correlation peak corresponding to the flaw location, 0.861, is slightly less than that from the maximum peak 2, 0.881, which corresponds to stirrup. Next, examine the correlation coefficient plot associated with the differenced record using the normalizing procedure as illustrated in record E of figure 49. The correlation coefficient plot associated with this differenced record is shown at the bottom of the figure, and in this case, the correlation peak associated with the flaw has the greatest value in the plot, but is less than the unflawed coefficient maximum, 0.871. This second differencing procedure (using normalization) would, therefore, not have detected the flaw unambiguously. The correlation analysis of the differenced plot in figure 50 (the Channel 1 - Channel 4) results in the unambiguous detection of the flaw.

Up to this point, a typical flaw signal has been considered for use as the interrogating, correlation function. It is possible, however, to use an algorithm to represent the flaw signal and such a procedure facilitates modification in the flaw signal shape which can be shown to be related to certain flaw properties and to the depth of the flaw within the beam. Figure 51 presents graphs of a typical flaw signal, an algorithm (and its equation), and a plot of the correlation coefficient for the two signals. The similarity between a graphical presentation of the algorithm equation and that of a typical flaw signal (from a 1/4-in (0.63 cm) gap in 6 wires of 7-wire strand) is obvious. The mathematical relationship for the algorithm in figure 51 was selected from an extensive background in magnetics analyses and is based on theoretical model for the magnetic field perturbance from a sphere of permeability, μ_o, buried in an infinite volume of different permeability material, μ. The two constants in the algorithm equation are, A, which is related to amplitude and, B, which is a shape factor, usually referred to as peak separation. Peak separation is a parameter that is associated with the distance between the sensor and the source or flaw; the greater the sensor-flaw distance, the greater the value of B. The value of B

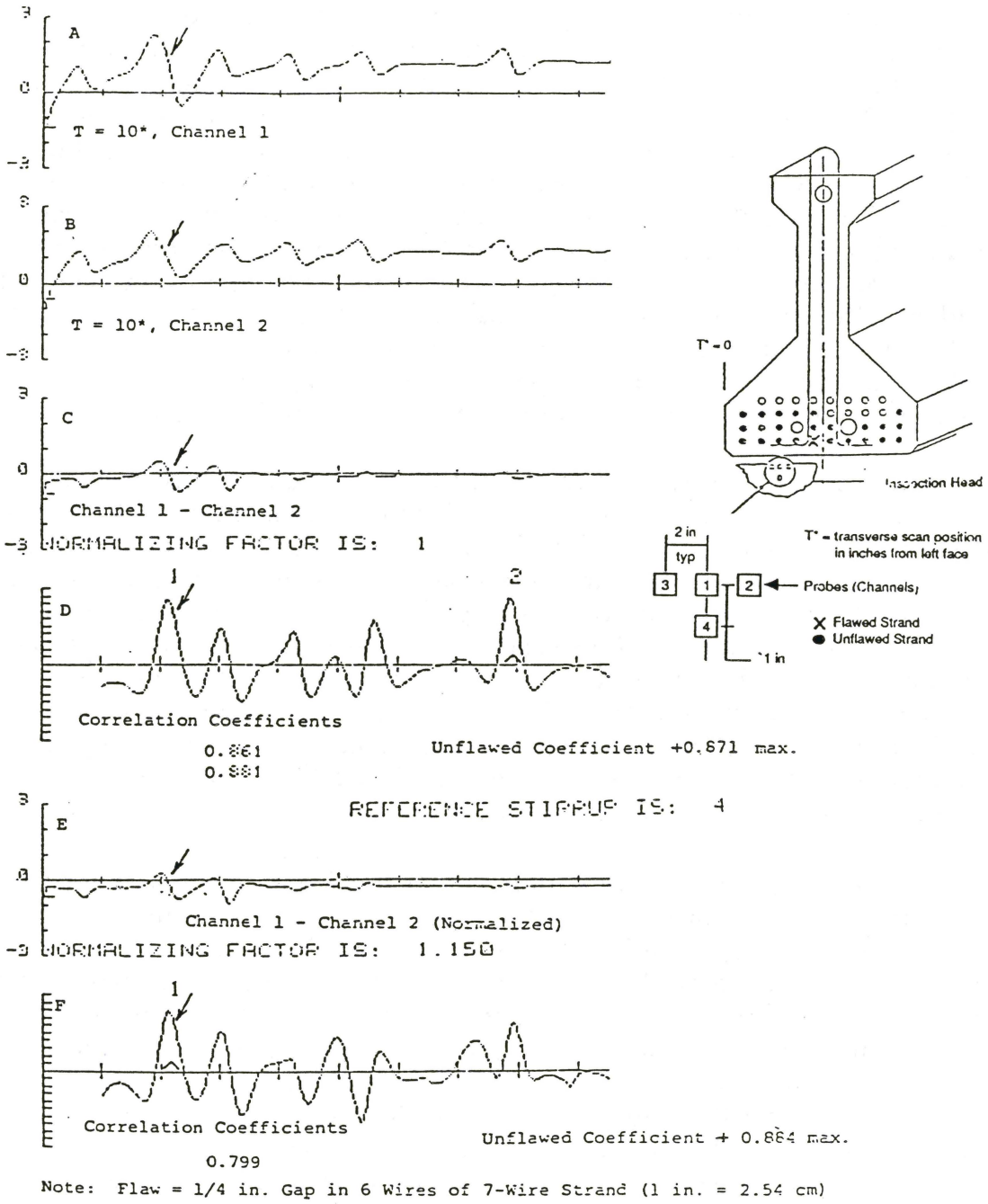

Figure 49. Reconstructed digitized magnetic signatures before and after enhancement and correlation for strand with medium flaw in first row, near stirrup *(B=16)*.

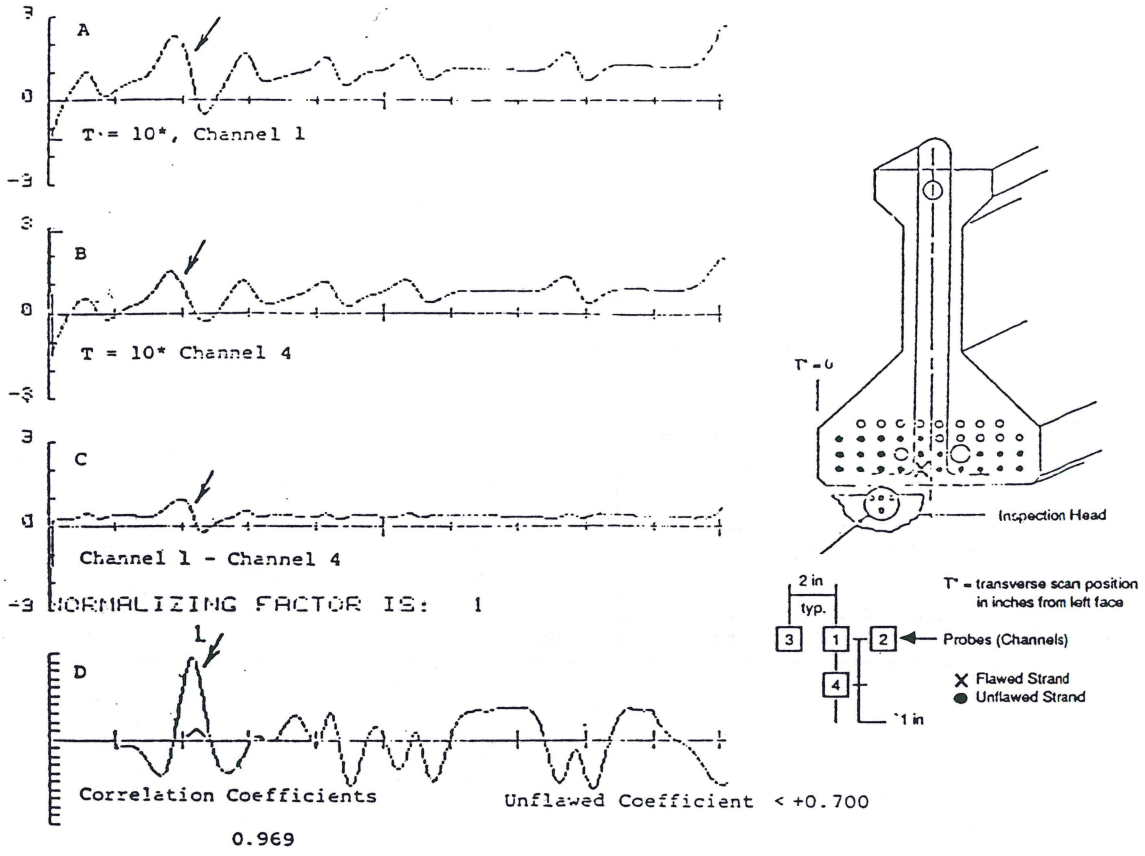

Note: Flaw = 1/4 in.. Gap in 6 wires of 7-wire strand (1 in. = 2.54cm)

Figure 50. Reconstructed display of digitized magnetic signatures before and after enhancement and correlation for strand with medium flaw in first row, near stirrup *(B=16)*.

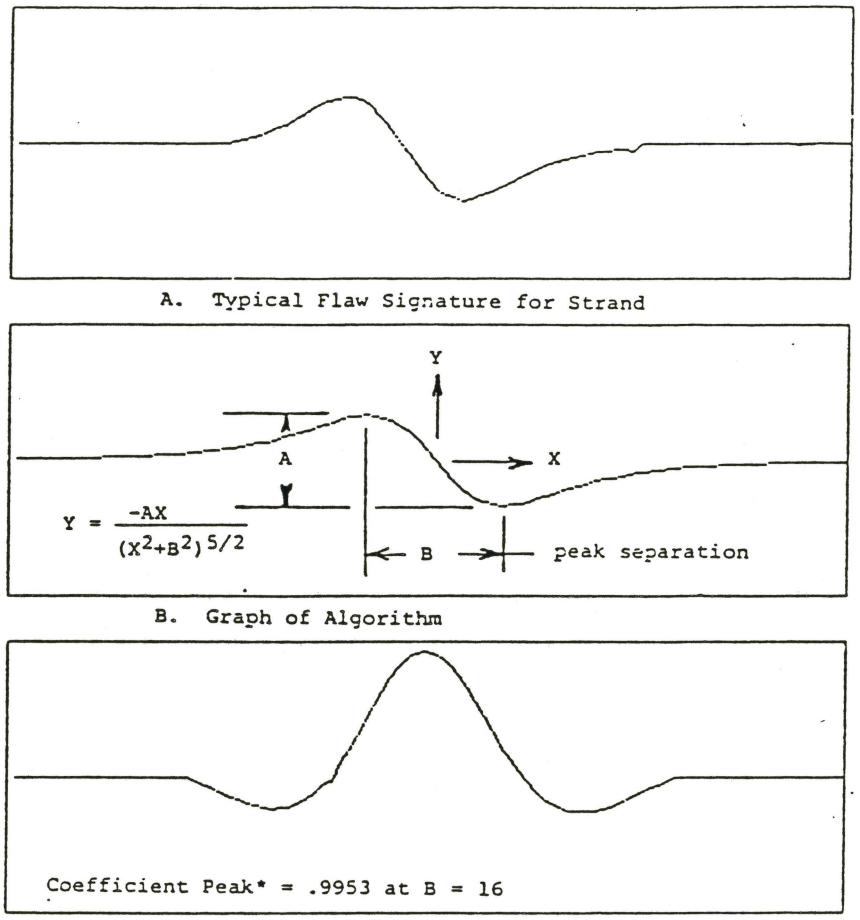

Figure 51. Goodness of fit between a typical strand flaw and the algorithm based on a theoretical model.

may also be influences by the distribution of the flaw if the distance over which the flaw is distributed is significant compared to the sensor-flaw spacing, (e.g. distributed over a distance equal to or greater than the sensor-to-flaw spacing). The goodness-of-fit between the algorithm and a typical flaw signature is confirmed in the fact that a peak correlation value of 0.995 is obtained for a peak separation of B = 16. All correlation results presented in this report were obtained using the algorithm of figure 51; the value of B is indicated in each case. The graphs of correlation value as a function of B in figure 52 for typical flaws in strand and in a bar were obtained by varying the B value of the algorithm when correlated against a flaw signal having a peak separation of B ≅ 32 for the bar flaw.

An important property of the correlation function, i.e. that inversion of polarity between the interrogating or flaw signal and a signal in the scan signature will result in a negative value of the correlation coefficient, makes it possible to eliminate the influence of disturbing elements such as the "wire scrap" near the lower surface of the beam from further consideration. For example, the top two records in figure 53 show the influence of a 1 1/2-in (3.81 cm) long piece of 16-ga. iron "tie" wire on the magnetic signature from Channels 1 and 4 when scanned directly beneath the wire scrap on transverse track location, T = 16. Because of proximity of the wire scrap to the sensor, the signal amplitude is greatly reduced on Channel 4 (see arrows in figure 53). In addition notice that the signal from the wire scrap is inverted in polarity; that is, the wire signal is first downward then upward going as viewed from left to right while the signal from a stirrup is upward going and then downward going. Flaw signals have the same polarity as stirrup signals, upward going and then downward going as viewed from left to right (see the third signature form the top in figure 53, where the flaw signal is pointed out by the arrow). Again, referring to figure 53, the third signature from the top shows the result of differencing Channel 1 and Channel 4 - a prominent "opposite polarity" signal is obtained from the piece of wire mounted on the lower surface of the beam. The fourth record from the top is a plot of the correlation coefficient (without regard for sign) corresponds to peak 2, from the wire scrap, but is negative in sign. It is also pointed out that this wire scrap correlation was obtained for B = 8, indicating it is very near the lower surface of the beam. The lower two records in figure 53 show a progressively smaller value for the corresponding correlation peak (pointed out by the arrows) for values of B = 16 and B = 32. Accordingly, it is possible to discriminate between surface and near surface artifacts and other structural elements deeper within the beam as well as to detect the presence of flaws.

With the above background, it is now pertinent to briefly review selected examples of flaw correlations, some in which the flaw signals are visually obvious and others in which the presence of the flaw can only be confirmed through the use of logic processing analyses.

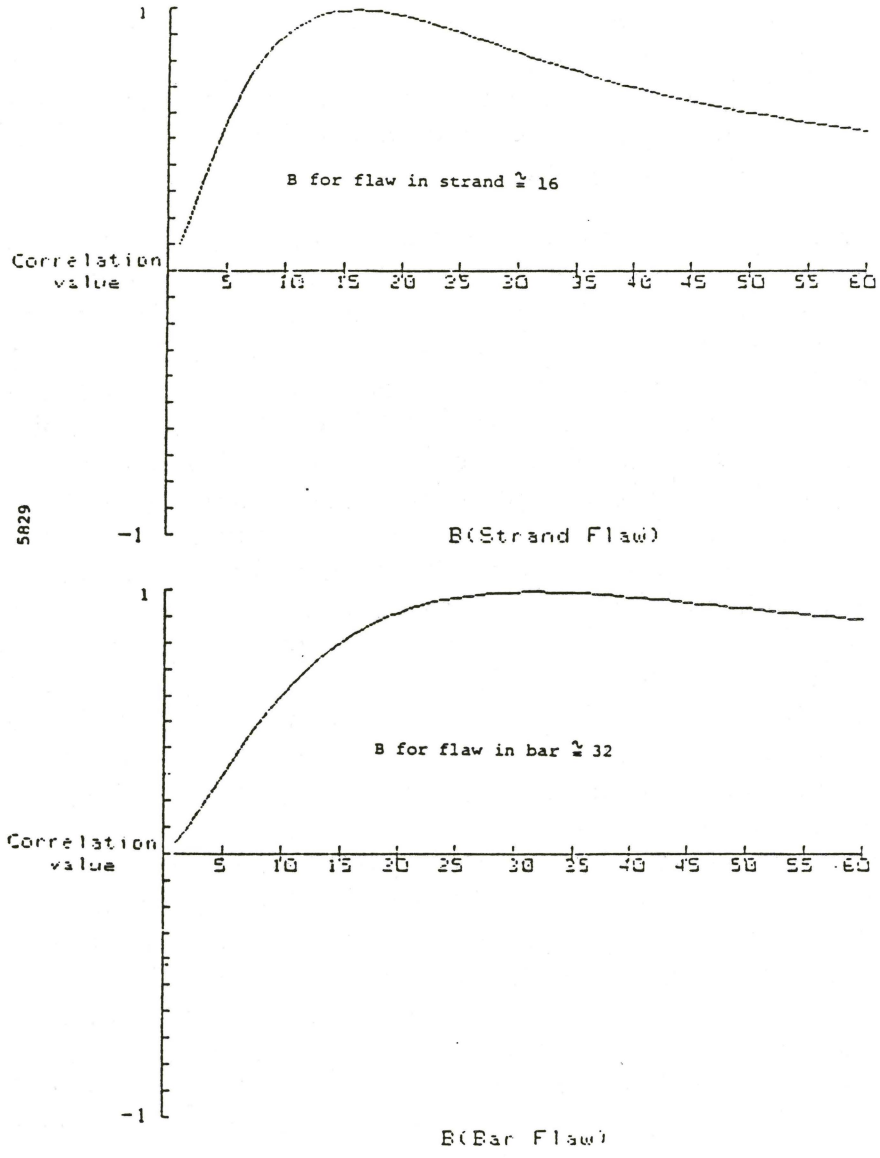

Figure 52. Graph of correlation value between algorithm and typical flaws in strand and bar as a function of B *(peak separation)*.

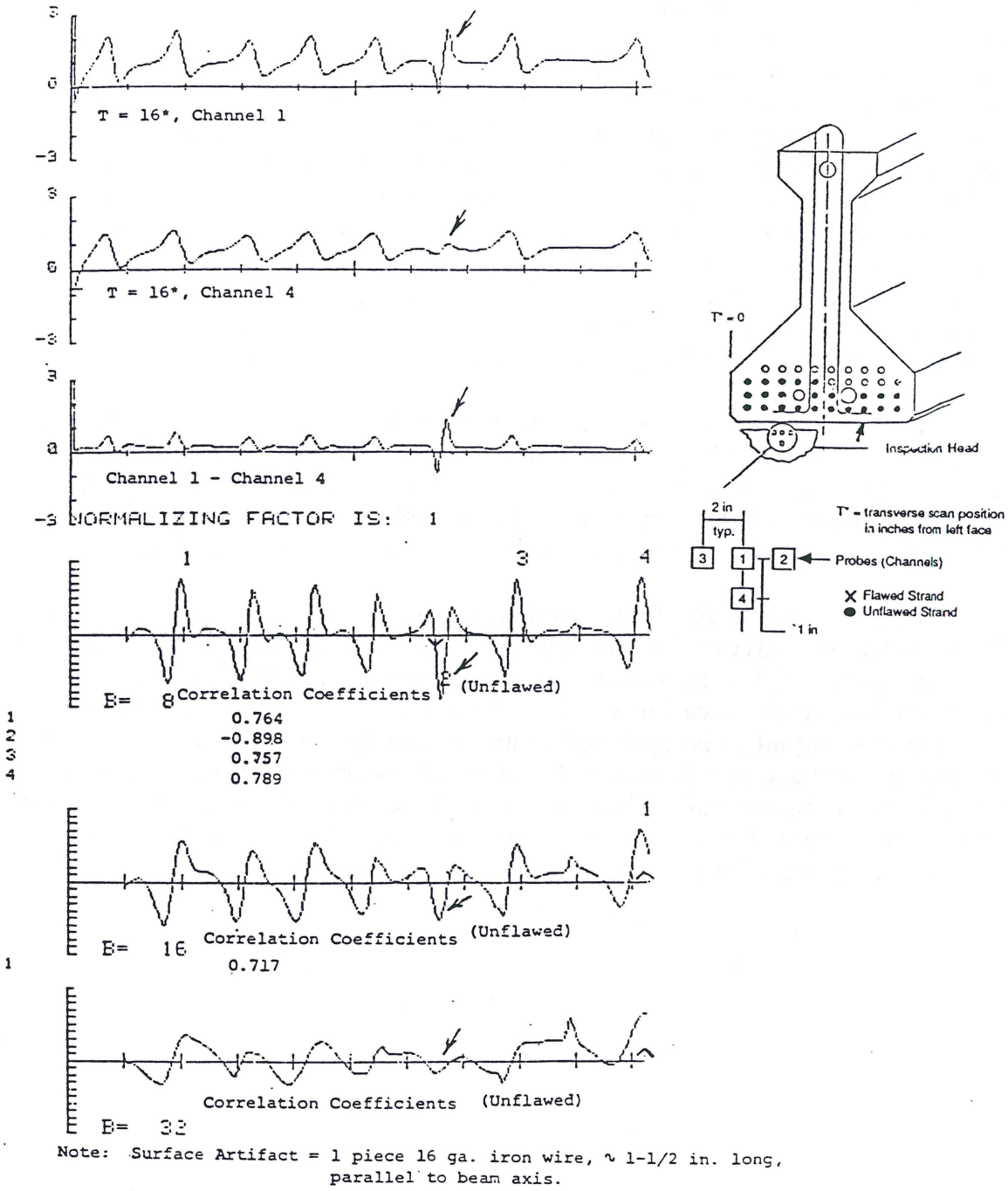

Figure 53. Reconstructed display of digitized magnetic signatures before and after enhancement and correlation for surface artifact *(B=8, 16,32)*.

Figure 54 presents the results of applying differencing and correlation procedures for a very small flaw (1/4-in (0.63 cm) gap in 1 wire of 7-wire strand) placed in the first row of the outermost strand position in the beam, (see sketch in figure for strand location). The location of the flaw is pointed out by the arrow in the upper two signatures, however, the signal does not appear visually different from the surrounding stirrup signals. Notice for the third signature from the top in the figure that the flaw signal is much more evident after differencing Channels 1 and 4. Examination of the correlation coefficient plot at the bottom of figure 54 shows an outstanding correlation peak value of 0.862 at the flaw location; all other significant correlation peaks (those having a value greater than 0.700) are negative. For the case illustrated in figure 54, the flaw was placed in a longitudinal location coincident with a stirrup location. A value of B = 16 was used in the algorithm (typical of the depths of stirrups and first row steel elements).

Figure 55 shows results from the same flaw previously described in figure 54 except that the longitudinal position of the flaw has been placed midway between two stirrups. Again note the visually evident flaw signal after differencing Channels 1 and 4 and the very outstanding correlation peak with a value of 0.969; all other correlation peaks of significance are negative and less than this value.

A more difficult detection problem is now considered. A medium sized flaw placed between stirrups in the first row of strands, but in the third column transverse position, T = 16, was analyzed and the results are shown in figure 56 (see sketch for transverse location of flawed strand). The upper two scan signatures show the flaw signal to be approximately the same magnitude as the stirrup signals (see arrows for flaw signal location). After differencing Channels 1 and 4, the flaw signal is more recognizable but would still be difficult to point out with high confidence. Again, the correlation coefficient plot show the maximum correlation peak to correspond with the flaw.

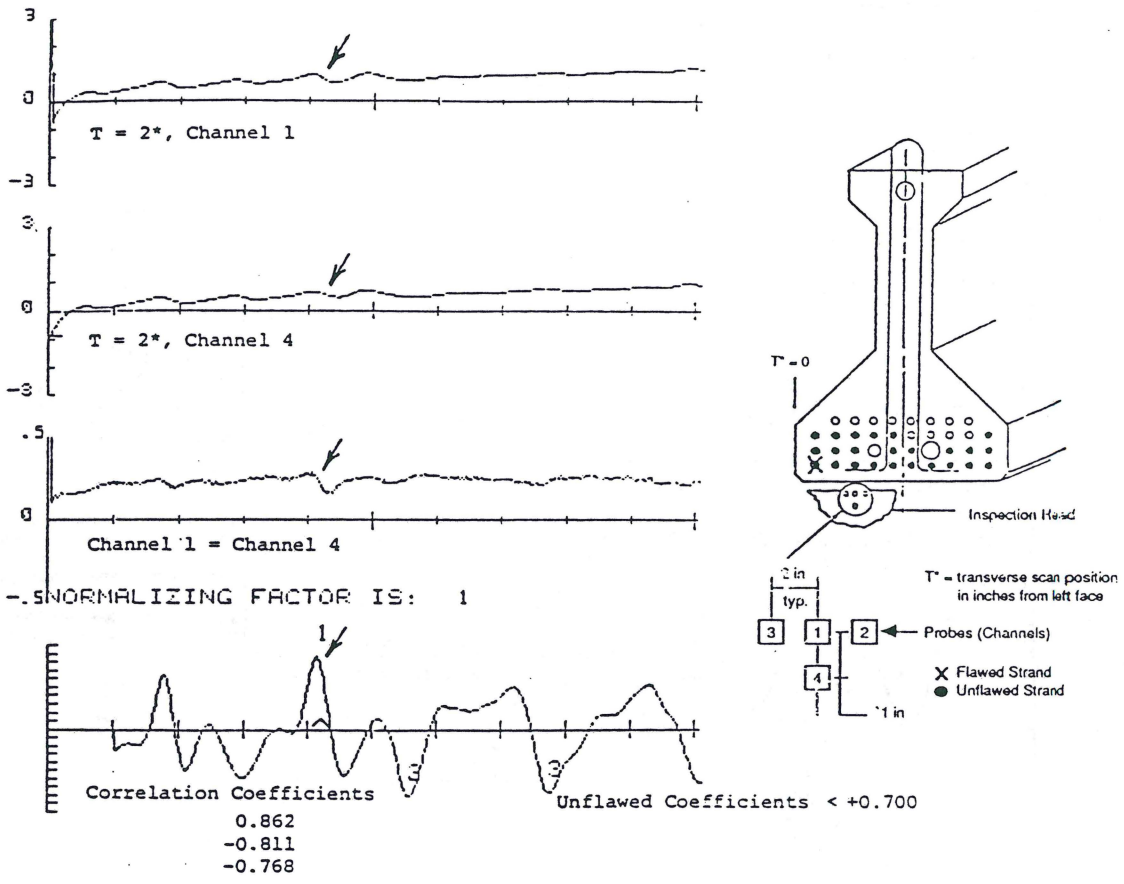

Note: Flaw = 1/4 in. Gap in 1 wire of 7-wire strand (1 in. = 2.54 cm)

Figure 54. Reconstructed display of digitized magnetic signatures before and after enhancement and correlation for strand with small flaw in first row, over stirrup *(B=16)*.

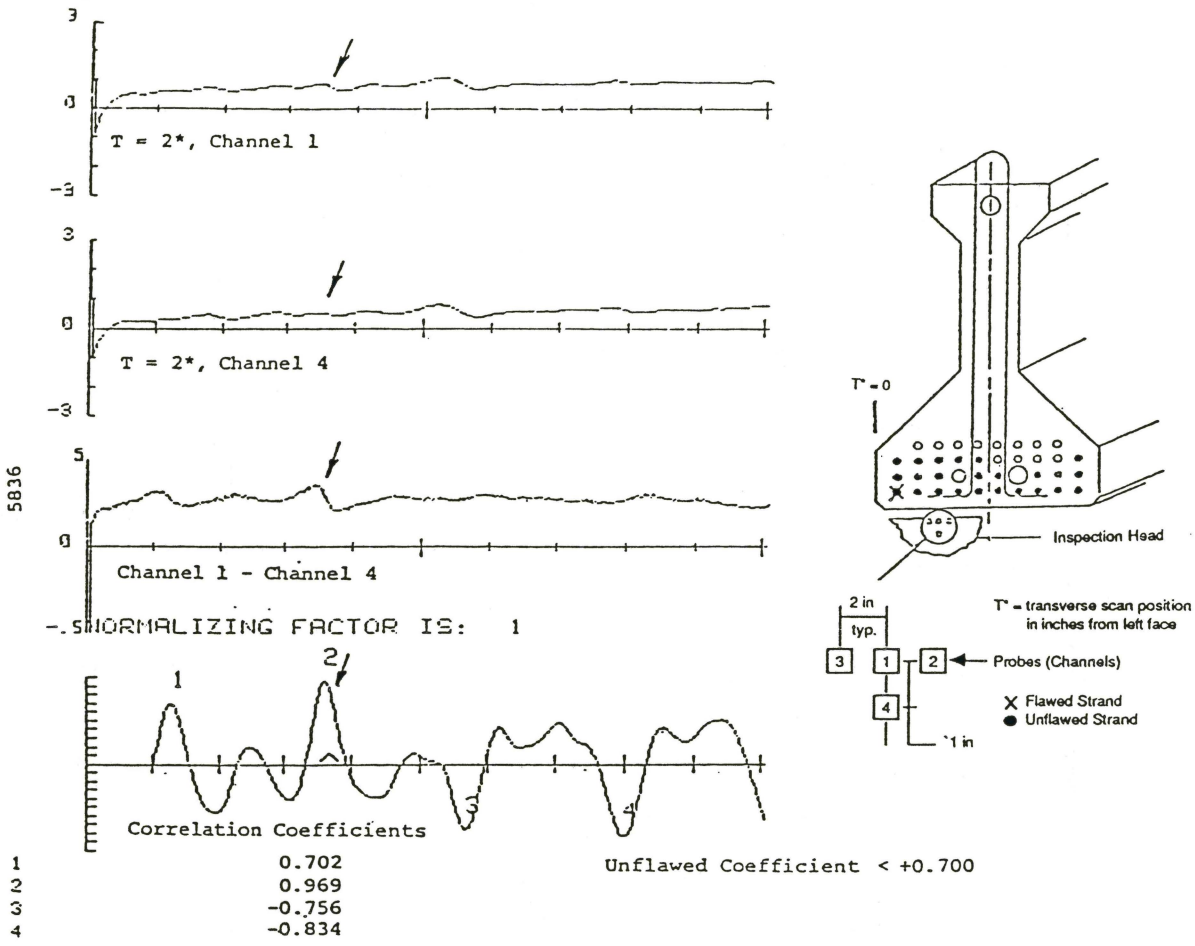

Note: Flaw = 1/4 in Gap in 1 wire of 7-wire strand (1 in. = 2.54 cm)

Figure 55. Reconstructed display of digitized magnetic signatures before and after enhancement and correlation for strand with small flaw in first row, between stirrups *(B=16)*.

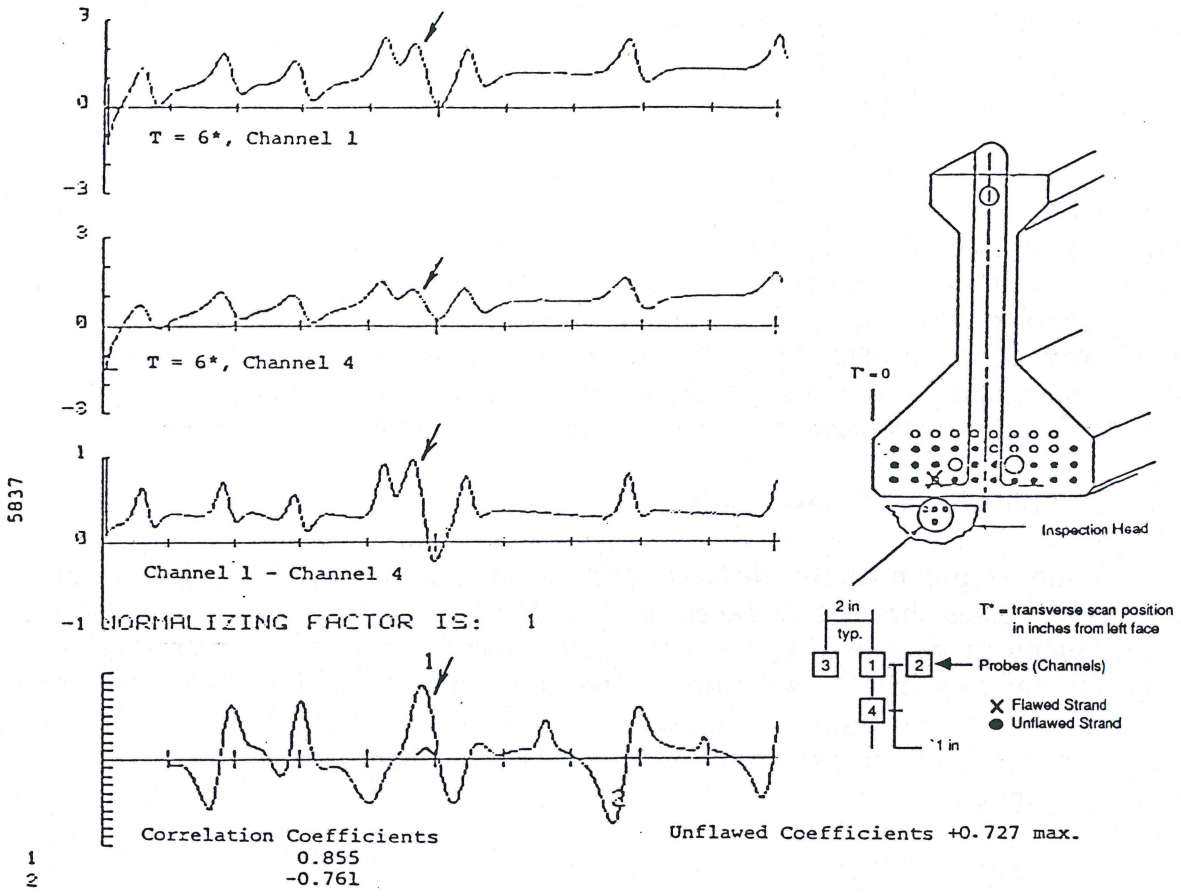

Note: Flaw = 1/4 in. Gap in 6 wires of 7-wire strand (1 in. = 2.54 cm)

Figure 56. Reconstructed display of digitized magnetic signatures before and after enhancement and correlation for strand with medium flaw in first row, between stirrups *(B=16)*.

APPENDIX E

POTENTIAL MPC SYSTEM IMPROVEMENTS

A. Electronic Noise Considerations

In this discussion noise is considered to be any undesirable or extraneous signals appearing at the output terminals of any or all of the signal amplifiers. The sources of this noise and possible remedies are discussed below.

1. Magnetic Signals

Magnetic signals introduced by the cable under test which have no relationship to flaws may be considered noise. Corrosion pitting can cause high frequency signals that may have a bearing on the condition of the cable whereas magnetic anomalies and geometric effects may produce large signals completely unrelated to the condition of the cable. Gradients and other low spatial frequency signals can be minimized by judicious frequency domain filtering and the use of differential magnetic sensors (gradiometers). Care must be taken that signals from deep flaws are not attenuated or distorted by these methods.

2. Transducer "Excess" Noise

Some semiconductor devices and other transducer components produce broadband noises that are in excess of the "Johnson" noise. Johnson noise is well known; being proportional to the element resistance, absolute temperature, and the frequency bandwidth of observation. The Johnson noise in the MPC application is very small and is negligible. The excess noise in the Hall effect devices (small) and in the first stage of the preamplifier (significant) is fixed for a given material and frequency range.

The only practical method of dealing with this phenomena is to select "low noise" amplifiers and to avoid the low frequencies (D.C. to 10 Hz) at which the "1/F" noise dominates. The preamplifier selected for the MPC are OP-227's by PMI. By employing a carrier system, i.e., exciting the transducers with a 5 kHz current, the frequency of the preamplifier is set at 5 kHz ± 500 Hz. At this frequency and bandwidth (1000 Hz), the source and amplifier noise referred to the input of the amplifier is approximately 0.1uV (0.1×10^6 volts). The level of noise at the system output after amplification of 2500 would be 0.25 mV. Since the measured noise is much greater than this, the sensor noise and the preamplifier noise is apparently not a major contributing factor.

A possible source of electronic noise is through the 5 kHz sensor excitation source. Although the mode of noise injection at this point is not clear, the possible source of noise should be investigated. Any noise entering via the 5 kHz oscillator

should be coherent from channel to channel and could be minimized by subtraction techniques.

3. Variable and Fixed Common Impedances

In a complex electro-mechanical system such as the MPC, it is quite difficult to maintain a design free of common impedance paths (commonly called "ground loops"). These ground loops develop when signal channels share ground or common leads with D.C. power supplies or with 60 Hz power lines. Often supplying separate wires is not adequate if there is any remote common connection between these conductors.

The most serious effects noted in the MPC were 60 Hz pick-up in the signal channels and sharp spike-like noise in the signal channels related to movement of the magnet/sensor module. The 60 Hz signals were reduced by the bandwidth limiting effect of a 60 Hz "notch" filter in each signal channel. Increasing the size of grounding conductors, careful electrical bonding of the various structural parts of the frame, and other ground isolation techniques could be employed to further reduce the power line frequency interference.

The spike-like noise present during data acquisition scans was the result of the varying impedance of the magnet structure to the machine frame through the linear bearing on the rails and other moving and sliding contacts. Although a separate bonding wire was included in the moving cable between the system frame and the magnet structure, this variable impedance produced large noise spikes in the analog outputs essentially the same in all channels.

This noise was minimized by electrically insulating the magnet bearings and other moving contacts leaving only the fixed bonding wire resistance. The noise can also be reduced by the channel to channel subtraction technique. This technique would be more effective if simultaneous sampling of all channels were employed. This change would involve significant modifications in the microcontroller hardware and software. Further consideration of this problem is desirable.

4. The measured noise at the system output is approximately 20 mV peak to peak (7.14 mV rms). Referred to the sensor input terminals, this is 2.8 μV rms. The sensitivity of the Hall effect detector is 50 μV per gauss at the excitation level of 0.2 amperes. The calculated equivalent noise level is therefore 0.056 gauss. It is estimated that this level can be reduced by approximately a factor of 10 if the improvements noted above are implemented.

B. Data Transmission

Communication between the host computer and the inspection module is via a 9600 baud serial interface. During data acquisition scans, sensor position and 6

digitized signal levels are transmitted to the computer 10 times per second (1 in per second, 0.1-in data intervals). With control and other required bits, the number of bits to be transmitted each second approaches four thousand. Thus, with the 9600 baud communications line, the maximum scan rate is about 2.5 in per second for 0.1-in data intervals.

If a higher data rate were desired, the communications elements of the micro-controller would have to be modified and some of the functions of the micro-controller changed from software to hardware. The serial line baud rate could be doubled to 19,200 baud without changing the communications cable.

In the event that it be advantageous to receive the inspection data at a remote location, standard telephone lines would support the present 9600 baud transmission rate. For example, real time inspection data could be received in Baton Rouge from the Luling Bridge near New Orleans over standard telephone lines. For higher data rates, improved phone lines or a rented microwave link would be required.

Very high data acquisition rates could be supported by special communications circuits and either a coaxial cable, fiber-optic cable or a radio frequency link between the inspection module and the host computer. Data acquisition rates of this magnitude would be encountered in a single pass cable inspection system in which up to 30 channels of data would be available simultaneously.

REFERENCES

1. Hopwood II, T., and Haven, J.H., "Corrosion of Cable Suspension Bridge," Research Report UKTRP-84-14, University of Kentucky, Lexington, KY, May 1984.

2. Hopwood II, T., and Havens, J.H., "Inspection, Prevention and Remedy of Suspension Bridge Cable Corrosion Problems," Research Report UKTRP-84-15, University of Kentucky, Lexington, KY, May 1984.

3. Hubertus Babel, K., "Destructive and Nondestructive Test Methods to Determine the Life of Wire Ropes - Part II," WIRE 28(1980) 1, pp. 38-44.

4. Harris, D.O., "Acoustic Emission Monitoring of Life Span Cables on Dunbarton Bridge," Report DC-72-TM11, Dunegan Division of Physical Acoustics Corporation, San Juan Capistrano, CA, December 1972.

5. Prine, D.W., and Hopwood, T., "Improved Structural Monitoring with Acoustic Emission Pattern Recognition," 14th Annual Symposium on Nondestructive Testing, Southwest Research Institute, San Antionio, TX, April 1983.

6. Weischidel, H.R., "The Inspection of Wire Ropes in Service: A Critical Review," Materials Evaluation, 43, December 1985, pp. 1592-1605.

7. Fujinaka, Y., et al, "Magnetic Inspection of P.W.S. Ropes," Proceedings of the 11th World Conference on Nondestructive Testing, held Nov. 3-8, 1985, Las Vegas, Nevada, Vol. 1, pp. 154-161.

8. Kusenberger, F.N., et al, "Development of Magnetic Field Disturbance (MFD) System for Detecting Deteoriation in the Reinforcement of Prestressed Concrete Bridge Members," FHWA Contract No. DOT-FH-11-8999, 1977.

9. Kusenberger, F.N., and Birkelbach, R.S., "Signal Enhancement Interpretation for the Detectionof Flaws in Reinforcing Steel and Prestressed Concrete Bridge Members," Final Report, Contract DTFH61-80-C-00002, Feb. 1981.

10. Beissner, R.E., and Barton, J.R., "Laboratory Test of Magnetic Field Disturbance (MFD) System for Detection of Flaws in Reinforcing Steel in Prestressed Concrete Bridge Members," Final Report, Contract DTFH61-C-00002, May 1984.

11. Proposal 6040 dated 6 June 1986 submitted in response to RFP DTFH61-86-00090.

12. Personal discussions (during visit - 15 March 1988) of C.M. Teller and J.R. Barton with Richard Maitino, Director of Project Coordination New York State Dept. of Transportation, and others from Steinman Boynton Bronquist and Birdsall.

13. Barton, J.R., and Kusenberger, F.N., "Magnetic Perturbation Inspection to Improve Reliability of High Strength Steel Components," Paper 69-DE-58, Design Engineering Conf. of ASME, New York, NY, May 1969.

14. Barton, J.R., and Kusenberger, F.N., "Fatigue Damage in Gas Turbine Engine Materials," Chapter on Fatigue Damage Detection, ASTM STP 495 (1971), 193-208.

15. Barton, J.R., et al, "Advanced Quantitative Magnetic Nondestructive Evaluation Methods - Theory and Experiment," Nondestructive Evaluation of Materials, 23rd Sagamore Army Materials Research Conference Proceedings, 1979.

16. Hopwood II, T., and Deen, R.C., "Periodic Nondestructive Evaluation of In-Service Metal Bridges," Research Report UKTRP-84-4, University of Kentucky, Lexington, KY, March 1984.

17. Toda, Y., Yokota, H., and Hanzawa, M., "Detection of Wire Breakage During Tensile Fatigue Tests of Wire Rope," Proc. 10th World Conference on NDT, Vol 5, 23-27 Aug. 1982, Moscow, USSR, Paper 2-29, pp. 174-181.

18. Bassim, M.N., "A Two-Step Approach for Continuous Monitoring Using Acoustic Emission," Proceedings of the 11th World Conference on Nondestructive Testing, held Nov. 3-8, 1985, Las Vegas, Nevada, Vol. 1, pp. 91-95.

19. Hamel, F., Bailon, J.P., and Bassim, M.N., "Acoustic Emission Mechanisms During Fatigue," Eng. Fracture Mechanics, 14 (1981), 853-860.

20. McMasters, R.C., ed., Nondestructive Testing Handbook, Vols. I and II, Soc. for Nondestructive Testing, Roland Press, 1963.

21. Betz, C.E., Principles of Magnetic Particle Testing, Magnaflux Corp., 1963.

22. Gardner, C.G., Nondestructive Testing - A Survey, NASA SP-5115, 1973.

23. Doane, F.B., and Betz, C.E., Principles of Magnaflux, Magnaflux Corp., 1941.

24. Wait, J.R., "Review of Electromagnetic Methods in Nondestructive Testing of Wire Ropes," Proc. of the IEEE, Vol. 67, No. 6, June 1979.

25. Barton, J.R., "Quantitative Correlation Between Magnetic Perturbation Signatures and Inclusions," ASTM Intl. Symposium on Rating of Non-metallic Inclusions on Bearing Steels, Boston, MA, May 1974.

26. Harnwell, G.P., Principles of Electricity and Electromagnetism, McGraw-Hill, New York, pp. 406-407.

27. Kraus, J.D., Electromagnetics, McGraw-Hill, New York, 1953, pp. 538-41.

28. Kittel, C., "Physical Theory of Ferromagnetic Domains," Reviews of Mod. Physics, Vol. 21, No. 4, October, 1949.

29. Craik, D.J., and Tebble, R.S., Ferromagnetism and Ferromagnetic Domains, John Wiley & Sons, Inc., 1965.

30. Hopwood II, T., Havens J.H., Introduction to Cable and Suspension Bridges, UKT RP-84-12 May 1984.

31. Transportation Cabinet Commonwealth of Kentucky and FHWA, U.S. Department of Transporation.